

Duquesne University

Duquesne Scholarship Collection

Electronic Theses and Dissertations

Fall 12-18-2020

Pharmacological Characterization of Novel Serotonin Transporter Inhibitors Identified Through Computational Structure-Based Virtual Screening

Michael Wasko

Follow this and additional works at: <https://dsc.duq.edu/etd>



Part of the [Medicinal and Pharmaceutical Chemistry Commons](#), [Other Pharmacy and Pharmaceutical Sciences Commons](#), and the [Pharmaceutics and Drug Design Commons](#)

Recommended Citation

Wasko, M. (2020). Pharmacological Characterization of Novel Serotonin Transporter Inhibitors Identified Through Computational Structure-Based Virtual Screening (Doctoral dissertation, Duquesne University). Retrieved from <https://dsc.duq.edu/etd/1954>

This One-year Embargo is brought to you for free and open access by Duquesne Scholarship Collection. It has been accepted for inclusion in Electronic Theses and Dissertations by an authorized administrator of Duquesne Scholarship Collection.

PHARMACOLOGICAL CHARACTERIZATION OF NOVEL SEROTONIN
TRANSPORTER INHIBITORS IDENTIFIED THROUGH COMPUTATIONAL
STRUCTURE-BASED VIRTUAL SCREENING

A Dissertation

Submitted to the Graduate School of Pharmaceutical Sciences

Duquesne University School of Pharmacy

Duquesne University

In partial fulfillment of the requirements for
the degree of Doctor of Philosophy

By

Michael J. Wasko

December 2020

Copyright by
Michael J. Wasko

2020

PHARMACOLOGICAL CHARACTERIZATION OF NOVEL SEROTONIN
TRANSPORTER INHIBITORS IDENTIFIED THROUGH COMPUTATIONAL
STRUCTURE-BASED VIRTUAL SCREENING

By

Michael J. Wasko

Approved September 29, 2020

Paula A. Witt-Enderby, Ph.D.
Committee Chair and Professor of
Pharmacology
School of Pharmacy and Graduate
School of Pharmaceutical Sciences
Duquesne University, Pittsburgh, PA

Rehana K. Leak, Ph.D.
Committee member and Associate
Professor of Pharmacology
School of Pharmacy and Graduate
School of Pharmaceutical Sciences
Duquesne University, Pittsburgh, PA

David A. Johnson, Ph.D.
Committee Member and Associate
Professor of Pharmacology
School of Pharmacy and Graduate
School of Pharmaceutical Sciences
Duquesne University, Pittsburgh, PA

Kevin Tidgewell, Ph.D.
Committee Member and Associate
Professor of Medicinal Chemistry
School of Pharmacy and Graduate
School of Pharmaceutical Sciences
Duquesne University, Pittsburgh, PA

Antonio Ferreira, Ph.D.
Committee Member, Chief
Information Officer and Chief
Information Security Officer
National Energy Technology Laboratory,
Pittsburgh, PA
Scholar in Residence
Duquesne University. Pittsburgh, PA

James. K. Drennen, III, Ph.D.
Dean, School of Pharmacy and Graduate
School of Pharmaceutical Sciences
Duquesne University, Pittsburgh, PA

Marc W. Harrold, Ph.D.
Representative and Professor of
Medicinal Chemistry
School of Pharmacy and Graduate
School of Pharmaceutical Sciences
Duquesne University, Pittsburgh, PA

ABSTRACT

PHARMACOLOGICAL CHARACTERIZATION OF NOVEL SEROTONIN TRANSPORTER INHIBITORS IDENTIFIED THROUGH COMPUTATIONAL STRUCTURE-BASED VIRTUAL SCREENING

By

Michael J. Wasko

December 2020

Dissertation supervised by Dr. Paula A. Witt-Enderby

Depression is a mental health disorder affecting greater than 350 million people worldwide with roughly 7% of the United States population diagnosed as of 2017. The selective serotonin reuptake inhibitors (SSRIs) have been the mainstay of pharmacotherapies for depression for the last 40 years. The SSRIs target the serotonin transporter (SERT), a monoamine transporter (MAT) responsible for terminating serotonergic neurotransmission. The SSRIs are not perfect therapeutics and suffer from delayed response times, inconsistent efficacy among patients, and often produce intolerable side effects. Therefore, a strong need exists to develop new antidepressants that are more efficacious and have fewer adverse effects. The Surratt and Madura laboratories approached this problem through the application of computational chemistry and classical pharmacology to rationally identify novel MAT inhibitors and ligands. The work within

this doctoral thesis encompasses a structure-based virtual screen targeting SERT and the pharmacological analysis of the compounds identified from the screen.

Previous virtual screens utilized SERT homology models based on a bacterial leucine transporter as the structural template (Manepalli *et al.*, 2011; Kortagere *et al.*, 2013; Gabrielsen *et al.*, 2014; Nolan *et al.*, 2014). More recently, the human SERT crystal structure was published by the Eric Gouaux laboratory (Coleman *et al.*, 2016) and used as the template for the present study. The Molecular Operating Environment software was chosen to target the orthosteric binding pocket S1 due to performance during benchmarking evaluations of the scoring function parameters. The HitDiscoverer chemical library was screened with the SERT computational model, and SERT ligand candidates were evaluated by predicted binding affinity, the Lipinski Rule of 5, and chemical uniqueness. Nine compounds were purchased and subjected to pharmacological analysis for binding, inhibition efficacy, and release potential. One compound bound to SERT with reasonable affinity; two compounds inhibited serotonin transport in *in vitro* assays. None of the compounds promoted the release of internal serotonin (*i.e.*, efflux). In conclusion, computational modeling was successfully used to identify novel inhibitors of the human SERT in a time and cost-efficient manner demonstrating the applicability to academic research.

DEDICATION

This thesis is dedicated to my family. To my parents, who supported and encouraged me to pursue this degree. To my brother, who reminded me at every moment to complete this thesis. To Catherine, who provided me with unconditional love.

ACKNOWLEDGEMENT

There are many people who I wish to acknowledge during my scientific journey leading to this degree. First, I wish to acknowledge Drs. Michael E. Rhodes, Jennifer Koehl, and Matt Fisher, who encouraged and guided me during my initial scientific journey as an undergraduate at Saint Vincent College. The *in vivo* pharmacology research completed with Arrissa Trulick was the catalyst toward pursuing graduate education. I will be forever grateful to Dr. Christopher K. Surratt for giving me an opportunity within his laboratory at Duquesne University. His mentorship helped guide me into becoming a critical scientist. Likewise, I would like to thank Dr. Jeffry D. Madura for his mentorship in computational chemistry, which formed the cornerstone of this thesis. Jeff is a person who is truly missed. During this journey, I have met many great people who have accepted me as a friend and colleague including the Madura lab (Kendy, Riley, Matt, Bern, Emily, Shiv, and Amanda), the O'Donnell lab (Apruva and Priya), the Cavanaugh lab (Thomas), the Leak lab (Dan), and the Janjic lab (Eric, Sherlock, and Michelle). I am grateful for the lessons and personal advice from professors Drs. Rehana Leak, Jane Cavanaugh, Lauren O'Donnell, David Johnson, Jelena Janjic, James Drennen, Patrick Flaherty, and Kevin Tidgewell. In addition, I would like to thank Scott Boesch, Alain Deschenes, Drs. Emilio Esposito, Antonio Ferreira, Martin Indarte, and Jeff Evanseck for their discussions and mentorship with computational chemistry. Lastly, I would like to thank Dr. Paula Witt-Enderby and her lab (Fahima and Mahmud) for helping me complete the pharmacological portion of my research. It was a wonderful end to my journey at Duquesne University.

TABLE OF CONTENTS

Copyright Page.....	ii
Committee Approval.....	iii
Abstract.....	iv-v
Dedication.....	vi
Acknowledgement.....	vii
Table of Contents.....	viii-ix
List of Figures.....	x
List of Tables.....	xi
List of Abbreviations.....	xii
Chapter 1: Introduction.....	1
Depression.....	1
Pharmacological Antidepressants Leading to the SSRIs.....	2
Monoamine Oxidase Inhibitors (MAOIs).....	2-3
Biogenic Amines: Serotonin.....	4-6
Tricyclic Antidepressants (TCAs).....	6
Serotonin Selective Reuptake Inhibitors (SSRIs).....	7
Monoamine Transport Proteins: Serotonin Transporter.....	8-14
Premise of this Research.....	14
Computational Drug Discovery.....	15-17
Structural Biology of the MATs.....	17-19
Structural Templates of the MATs.....	19
LeuT.....	19-21
LeuBAT.....	21-22
dDAT.....	22-24
hSERT.....	24-26
Chapter 2: Computational Modeling to Identify Inhibitors of the Human SERT.....	27
Computational Virtual Screening.....	27
Computational Approach.....	28
Methodology.....	29
SERT Crystal Structure Preparation.....	29
Virtual Screening (Docking) Protocol.....	30
Chemical Library.....	30-31
Analysis of Virtual Screen.....	31
Results.....	32-38
Docking Software Benchmarking.....	39
Virtual Screen.....	40
Discussion.....	41-46
Chapter 3: Pharmacological Analysis of the Candidate Compounds.....	47
Background.....	47-48
SERT Virtual Screens.....	48-51
Pharmacological Approach.....	51

Methodology.....	52
Candidate Compound Preparation.....	52
Cell Culture.....	52
Total Binding Assay.....	52-53
Competition Binding Assay.....	53-54
Total [³ H]-Serotonin Uptake Inhibition.....	54-55
Concentration-Response [³ H]-Serotonin Uptake Inhibition.....	55
[³ H]-Serotonin Release Assay.....	55-56
GPCR Screen from the PDSP.....	56
Results.....	57-65
Total Binding Assay.....	66
Competition Binding Assays.....	66
Total [³ H]-Serotonin Uptake Inhibition.....	67
Concentration-Response [³ H]-Serotonin Uptake Inhibition.....	67
[³ H]-Serotonin Release Assay.....	67-68
Discussion.....	69-77
Chapter 4: Strengths and Limitations.....	78
Strengths.....	78
Weaknesses.....	78-79
Chapter 5: Conclusions.....	80-81
Chapter 6: References.....	82-88
Appendix.....	89 -
	100

LIST OF FIGURES

Figures

Figure 1.1: Structural Overview of the MATs.....	9
Figure 1.2: Alternating Access Mechanism of Monoamine Transport.....	10
Figure 1.3: Vestibule Leading into the S1 Binding Pocket.....	11
Figure 1.4: Neurogenesis Pathway.....	14
Figure 1.5: Comparison of Ligand-Based and Structure-Based Drug Design.....	16
Figure 1.6: Electron Density of the DAT (4XP1).....	17
Figure 1.7: LeuT Crystal Structure.....	19
Figure 1.8: External Gate of LeuT.....	19
Figure 1.9: LeuT Fold.....	20
Figure 1.10: S1 Binding Pocket TM Domains.....	20
Figure 1.11: LeuBAT Crystal Structure (PDB id. 4MM5).....	21
Figure 1.12: dDAT Crystal Structure (PDB id. 4M48).....	22
Figure 1.13: DAT Binding Pocket.....	23
Figure 1.14: SERT S2 Binding Site.....	24
Figure 1.15: SERT S1 Binding Site.....	25
Figure 2.1: Serotonin Transporter Structure.....	32
Figure 2.2: Virtual Screening Protocol.....	37
Figure 3.1: LeuT S1 and S2 Occupied.....	48
Figure 3.2: dDAT S1 Occupied.....	49
Figure 3.3: Total Binding Analyses of Candidate Compounds to SERT.....	57
Figure 3.4: Competition of Sertraline for [³ H]-Citalopram Binding to SERT.....	58
Figure 3.5: Competition of Compound 4 for [³ H]-Citalopram Binding to SERT.....	59
Figure 3.6: Single Point Substrate Uptake Inhibition of Candidate Compounds to SERT.....	60
Figure 3.7: Concentration Response Substrate Uptake Inhibition with Citalopram, Compound 1, and Compound 4 for SERT.....	61
Figure 3.8: Release Assay with the 9 Compounds.....	62
Figure 3.9: Binding Interactions Between Compound 1 and the S1 Binding Pocket of SERT.....	64
Figure 3.10: Binding Interactions Between Compound 4 and the S1 Binding Pocket of SERT.....	65
Figure 3.11: Overlay of Compound 1 and Compound 4 within the S1 Binding Pocket.....	76
Figure 3.10: Comparison Between Compound 4 with Citalopram.....	77

LIST OF TABLES

Tables

Table 1.1: Chemical Structure of the Monoamine Neurotransmitters.....	3
Table 1.2: Chemical Structures of the MAOIs.....	4
Table 1.3: Chemical Structures of the TCAs.....	7
Table 1.4: Chemical Structures of the SSRIs.....	8
Table 1.5: Guide to Protein Crystal Structure Resolution.....	18
Table 2.1: Computational Testset for Docking Benchmarking.....	33
Table 2.2: SERT Correlation Testing without Ions.....	34
Table 2.3: SERT Correlation Testing with Ions.....	35
Table 2.4: Final Validation of the Docking Protocol with the Structural Pharmacophore.....	36
Table 2.5: Candidate Compounds Identified for Pharmacological Analysis.....	38
Table 3.1 Comparison between Virtual Screening Analysis and Pharmacology.....	63
Table 3.2: Comparison of Pharmacology from SERT Virtual Screens.....	73

LIST OF ABBREVIATIONS

1-palmitoyl-2-oleoylphosphatidylcholine (POPC)
3,4-methylenedioxy-N-methylamphetamine (MDMA; ecstasy)
Aromatic L-amino acid decarboxylase (AADC)
Biogenic amine transporter (BAT)
Brain-derived neurotrophic factor (BDNF)
Central nervous system (CNS)
cAMP response element binding protein (CREBP)
cGMP-dependent protein kinase (PKG)
Dopamine transporter (DAT)
Drosophila dopamine transporter (dDAT)
G protein-coupled receptors (GPCRs)
High-throughput screening (HTS)
Human DAT (hDAT)
Human SERT (hSERT)
Inward-facing (IF)
Kinetic off-rate (K_{off})
Leucine transporter (LeuT)
Major depressive disorder (MDD)
MOE database (MDB)
Molecular Operating Environment (MOE)
Monoamine oxidase (MAO)
Monoamine oxidase inhibitors (MAOIs)
Monoamine transport protein (MAT)
National Institute of Mental Health (NIMH)
Nuclear magnetic resonance spectroscopy (NMR)
Norepinephrine transporter (NET)
Outward-facing (OF)
p38 mitogen-activated protein kinase (MAPK)
Peripheral nervous system (PNS)
Protein Data Bank (PDB)
Protein kinase C (PKC)
Selective serotonin reuptake inhibitor (SSRI)
Sequenced Treatment Alternatives to Relieve Depression (STAR*D)
Serotonin-norepinephrine reuptake inhibitor (SNRI)
Serotonin transporter (SERT)
Solute carrier 6 (SLC6)
Structure-activity relationships (SARs),
Structure database file (sdf)
Thermostability (TS)
Tricyclic antidepressants (TCAs)
Tryptophan hydroxylase 2 (TH2)
United States Center for Disease Control (CDC)
Vesicular monoamine transporter 2 (vMAT2)
Virtual screening (VS)

Chapter 1: Introduction

Depression

Depression is a disorder that affects a person's mental integrity, resulting in a period of prolonged sadness that interrupts normal functioning (Akil *et al.*, 2018). It is characterized by a spectrum of clinical symptoms including anhedonia, depressed mood, sleep imbalances, fatigue, suicidal tendencies, deflated self-esteem, and sexual dysfunction (Wong and Licinio, 2001; Nestler *et al.*, 2002). Although depression is widely underdiagnosed, it is estimated that more than 350 million people are diagnosed worldwide (Smith, 2014). Additionally, depression has been classified as the leading cause of worldwide disability with over 76.4 million work-years lost per year (Smith, 2014). The National Institute of Mental Health (NIMH) reported that 7.1% of adults in the United States, roughly 17.3 million people, experienced a depressive episode of at least two weeks during 2017 (National Institute of Mental Health). The American Psychiatric Association further classified individuals that display more than five depressive symptoms per day over two weeks as having major depressive disorder (MDD) (Hillhouse and Porter, 2015). MDD is typically seen as an adult-onset disease, and women are 2 - 3 times more likely to be diagnosed with MDD (Kessler *et al.*, 2012; Hillhouse and Porter, 2015).

The currently available antidepressant medications are not without their limitations. Alarming, a large percentage of MDD patients (34-46%) do not respond to current antidepressant treatments, a condition classified as treatment resistance (Fava and Davidson, 1996; Hillhouse and Porter, 2015; Akil *et al.*, 2018). The Sequenced Treatment Alternatives to Relieve Depression (STAR*D) clinical trial by the NIMH showed that 28% of patients obtained remission of their depression using citalopram after 14 weeks (Insel and Wang, 2009). Beyond the issue of effectiveness, this study also highlighted another issue regarding the slow onset of remission from the symptoms of depression. It is common for antidepressants to have a latency period of weeks

to months before remission occurs (Insel and Wang, 2009; Scheuing *et al.*, 2015). Regardless of efficacy, a variety of side effects from the medication can occur including gastrointestinal distress, headaches, sexual dysfunction, insomnia, weight gain, dry mouth, anxiety, and fatigue (Santarsieri and Schwartz, 2015; Cartwright *et al.*, 2016). Adherence to prescribed antidepressant treatments is another problem with some studies reporting around 50% of patients ending treatments prematurely (Sansone and Sansone, 2012).

Pharmacological Antidepressants Leading to SSRIs:

Monoamine Oxidase Inhibitors (MAOIs)

The identification of modern antidepressants is linked with the development of tuberculosis treatments during the late 1940s and early 1950s. Isoniazid (isonicotinyl hydrazide) was first synthesized by Hoffmann - La Roche and proved to be an effective anti-tubercular agent (Figure 1.1) (Hillhouse and Porter, 2015). This led to the synthesis of derivative molecules based on isoniazid in an attempt to develop active analogs resulting in iproniazid (isopropyl-isonicotinyl hydrazide; Figure 1.1) (Hillhouse and Porter, 2015). Clinical trials in 1952 at the Sea View Hospital on Staten Island, NY identified the antidepressant potential of iproniazid and initially classified CNS activation as a side effect (López-Muñoz and Alamo, 2009). Tuberculosis patients receiving iproniazid at Sea View were reported to experience strikingly increased energy and social behavior. Iproniazid was shown by the Ernst Albert Zeller lab in 1952 to be an inhibitor of the enzyme monoamine oxidase (MAO) that breaks down monoamine neurotransmitters including serotonin, dopamine, and norepinephrine (Table 1.1) (Zeller *et al.*, 1952; López-Muñoz and Alamo, 2009).

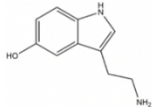
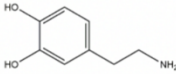
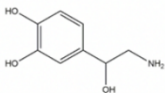
Name of Compound	Structure
Serotonin	
Dopamine	
Norepinephrine	

Table 1.1: Chemical Structure of the Monoamine Neurotransmitters.

Iproniazid hepatotoxicity led to its withdrawal from the U.S. market, but it was replaced by more potent MAO inhibitors (MAOIs) including phenelzine, isocarboxazid, and tranylcypromine (Figure 1.1) (Shulman *et al.*, 2013). MAOIs can be classified by their selectivity and binding mode to the MAO enzymes (Shulman *et al.*, 2013). Two isoforms of MOA – MAO_A and MAO_B – differ based on their substrates; MOA_A oxidizes serotonin, while dopamine and norepinephrine are broken down by both MAO_A and MAO_B (Youdim *et al.*, 2006). Selective inhibition of the MAO isoforms can be achieved with low doses of moclobemide (MAO_A-selective), pargyline (MAO_B-selective), or selegiline (MAO_B-selective) (Figure 1.1) (Shulman *et al.*, 2013). Additionally, nonselective MAO inhibitors exist including phenelzine and high doses of selegiline (Figure 1.1) (Shulman *et al.*, 2013).

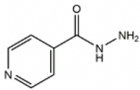
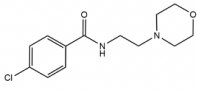
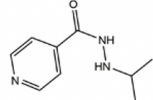
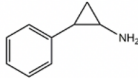
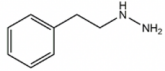
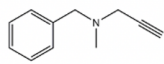
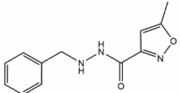
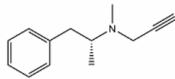
Name of Compound	Structure	Name of Compound	Structure
Isoniazid		Moclobemide	
Iproniazid		Tranylcypromine	
Phenelzine		Pargyline	
Isocarboxazid		Selegiline	

Table 1.2: Chemical Structures of the MAOIs.

Biogenic Amines: Serotonin

The MAOIs modulate the signaling of the biogenic amines including serotonin, dopamine, and norepinephrine (Figure 1.2) by preventing the destruction of the neurotransmitters, leading to increased signaling via their respective receptors (Shulman *et al.*, 2013). With respect to current antidepressant therapies, the serotonergic system plays a greater role than the other biogenic amines (Yohn *et al.*, 2017). Serotonin is derived from the essential amino acid tryptophan, of which approximately 2% in the body is converted into serotonin and enters the CNS through the L-amino acid transport proteins (Best *et al.*, 2010; Chen and Miller, 2013). L-tryptophan is converted into serotonin by the sequential actions of the aromatic L-amino acid decarboxylase (AADC) enzyme and the tryptophan hydroxylase 2 (TH2) enzyme, the latter being the rate limiting step within serotonergic neurons (Lovenberg *et al.*, 1962; Best *et al.*, 2010; Chen and Miller, 2013). Serotonin is collected and recycled into vesicles within the neuron through the

vesicular monoamine transporter 2 (vMAT2) (Kroeze *et al.*, 2012). Once serotonin is released from the neuron, it binds to and activates one of 14 serotonin receptor types consisting of 13 G protein-coupled receptors (GPCRs) and one ligand-gated ion channel (Nichols and Nichols, 2008). The 14 receptors are grouped into 7 families (5HT1-7) based upon the coupling G protein and genetic similarity; the 5HT3 receptor is the ion channel.

The 5HT_{1A}, 5HT_{1B}, 5HT₄, 5HT₆ and 5HT₇ receptors have been associated with clinical depression (Yohn *et al.*, 2017). The 5HT_{1A} is both a presynaptic autoreceptor and a postsynaptic receptor. Presynaptic 5HT_{1A} receptors inhibit firing of serotonergic neurons and are thought to contribute to the latency period of antidepressant activity, although sustained receptor occupancy leads to desensitization (Chilmonczyk *et al.*, 2015). The postsynaptic 5HT_{1A} found in the dentate gyrus has been implicated in adult hippocampal neurogenesis in response to antidepressants (Samuels *et al.*, 2015). Mice specifically lacking the 5HT_{1A} receptor in the dentate gyrus do not exhibit neurogenesis from treatment with the antidepressant fluoxetine (Samuels *et al.*, 2015). The 5HT_{1B} receptor is a widely-distributed inhibitory GPCR found on presynaptic neurons (Tiger *et al.*, 2018). The 5HT_{1B} shares 43% of the amino acid sequence of the 5HT_{1A} and can function as an autoreceptor that inhibits serotonin release (Tiger *et al.*, 2018). Mice lacking the 5HT_{1B} display antidepressant- and antianxiety-like properties in rodent models of depression (Tiger *et al.*, 2018). The 5HT₄ has been implicated in both anxiety and depression, with activation of the receptor producing short-term anxiolytic properties in mice and long-term promotion of adult hippocampal neurogenesis (Mendez-David *et al.*, 2014). The 5HT₆ receptor involvement in depression needs more study, as both agonists and antagonists of the receptor have been identified to have anxiolytic and antidepressant-like effects in rodent models (Yohn *et al.*, 2017). The 5HT₇ receptors are expressed in the limbic and cortical regions of the brain and interact with the hypothalamus-

pituitary-adrenal axis (Yohn *et al.*, 2017). Because the SERT-inhibiting antidepressant drugs need time to downregulate the 5-HT receptor, a direct antagonist yields a faster antidepressant response in rats (Yohn *et al.*, 2017).

Tricyclic Antidepressants (TCAs)

As with the MAOIs, the mood-altering properties of the tricyclic antidepressants (TCAs) were also discovered through serendipity. In the 1950s, the phenothiazine compound chlorpromazine was established to elicit antipsychotic effects while in clinical trials (Kuhn, 1958; López-Muñoz *et al.*, 2004). This resulted in a flurry of clinical trials to test the potential of prior synthesized compounds with similar chemical structures, which led to the identification of the TCA imipramine in 1956 (López-Muñoz and Alamo, 2009). Ironically, initial testing of imipramine with schizophrenics showed worsening of symptoms but it was noted that depressed schizophrenics appeared to have a positive mood change after a couple weeks of treatment (López-Muñoz and Alamo, 2009). Imipramine was the first TCA approved by the FDA to treat depression in 1959 (Hillhouse and Porter, 2015).

The TCAs currently approved for depression by the FDA include amitriptyline, amoxapine, desipramine, doxepin, imipramine, nortriptyline, protriptyline, and trimipramine (Figure 1.3) (Food and Drug Administration; Chockalingam *et al.*, 2019). The TCAs inhibit the SERT and the norepinephrine transporter (NET), and to a lesser extent the dopamine transporter (DAT) (Tatsumi *et al.*, 1997; Penmatsa *et al.*, 2013; Yohn *et al.*, 2017). Their antidepressant effects are thought to be primarily a result of the SERT and NET blockage, acting similar to later-identified serotonin-norepinephrine reuptake inhibitor (SNRI) antidepressants (Gillman, 2007). The TCA drug class is plagued by safety concerns including potentially fatal cardiovascular effects

and CNS toxicity, which are observed at high plasma concentrations due to off-target receptor promiscuity. Nortriptyline is thought to be the safest TCA (Gillman, 2007).

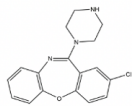
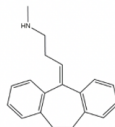
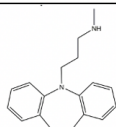
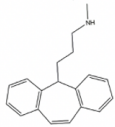
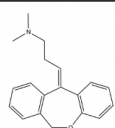
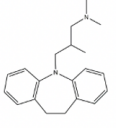
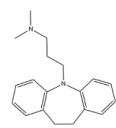
Name of Compound	Structure	Name of Compound	Structure
Amoxapine		Nortriptyline	
Desipramine		Protriptyline	
Doxepin		Trimipramine	
Imipramine			

Table 1.3: Chemical structures of the TCAs.

Serotonin Selective Reuptake Inhibitors (SSRIs)

The MAOIs and the TCAs elevate monoamine levels through inhibition of enzymatic degradation (MAOIs) or reuptake into the neuron (TCAs). Further support of the involvement of the monoamines came from reserpine, a VMAT2 inhibitor that depletes monoamine neurotransmitter levels, resulting in behavioral effects similar to depression (Pletscher *et al.*, 1955; Chessin *et al.*, 1957; López-Muñoz and Alamo, 2009). It was speculated in the early 1970s that selective inhibition of SERT would be an effective antidepressant strategy and led to the discovery of the selective serotonin reuptake inhibitor (SSRI) fluoxetine (ProzacTM) by researchers at Eli Lilly in 1975 before receiving FDA approval in 1987 (Tatsumi *et al.*, 1997; Wong *et al.*, 2005).

The success of the SSRIs proved that serotonin was the primary monoamine neurotransmitter responsible for the alleviation of depression. In addition, the SSRIs were found to have a safer pharmacological profile, lacking the norepinephrine-based cardiovascular side effects commonly found with the TCAs (Ferguson, 2001). Not surprisingly, SSRIs became the first-line pharmacological treatment for depression. The SSRIs currently approved by the FDA to treat depression include citalopram, escitalopram, paroxetine, fluoxetine, fluvoxamine and sertraline (Figure 1.4) (Food and Drug Administration).

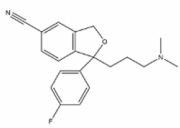
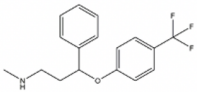
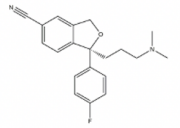
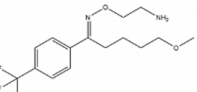
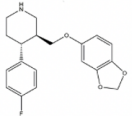
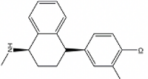
Name of Compound	Structure	Name of Compound	Structure
Citalopram		Fluoxetine	
Escitalopram		Fluvoxamine	
Paroxetine		Sertraline	

Table 1.4: Chemical Structures of the SSRIs.

Monoamine Transport Proteins: Serotonin Transporter

The SSRIs are competitive inhibitors of the SERT protein, one of the monoamine transport proteins (MATs) that includes the DAT and NET. The MATs are plasma membrane-bound transporters responsible for terminating neuronal signaling of their endogenous substrate (Aggarwal and Mortensen, 2017). The MATs belong to the solute carrier 6 (SLC6) family of 20 genes. This family encodes secondary active transporters that couple movement of

neurotransmitters with Na^+ down their concentration gradients (Kristensen *et al.*, 2011). The SLC6A4 gene encodes the 630 amino acid SERT protein expressed in the CNS, peripheral nervous system (PNS), placenta, epithelium, and blood platelets (Kristensen *et al.*, 2011; Iurescia *et al.*, 2017). The MAT proteins are expressed on the presynaptic terminal of their respective neurons (Lin *et al.*, 2011; Aggarwal and Mortensen, 2017).

Structurally, the MATs are composed of 12 transmembrane domains (TM) that are interconnected by a series of extracellular and intracellular loops as well as extended intracellular amino (N-) and carboxyl (C-) terminal tails (Figure 1.1) (Penmatsa *et al.*, 2013; Coleman *et al.*, 2016; Coleman and Gouaux, 2018). The substrate transport mechanism is characterized by alternating access of the substrate/ion pore to the intracellular and extracellular sides of the cell membrane. This is achieved with a progression of structural conformations that make

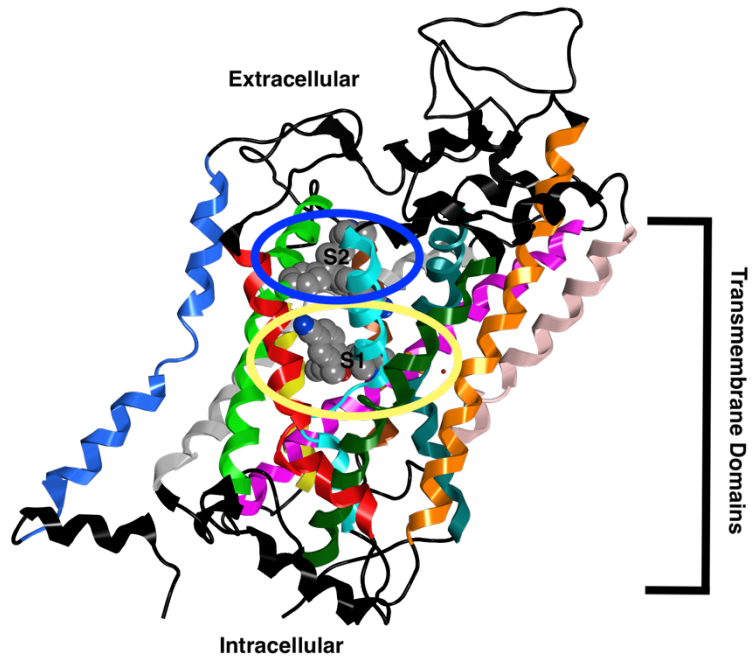


Figure 1.1: Structural Overview of the MATs. The 12 transmembrane domains (TMs) that define the MAT structure are color coded [TM1 (teal), TM2 (dark green), TM3 (silver), TM4 (dark orange), TM5 (pink), TM6 (light blue), TM7 (light orange), TM8 (magenta), TM9 (yellow), TM10 (light green), TM11 (red), TM12 (dark blue)]. Intracellular (bottom) and extracellular (top) loops (black) connect the TMs and indicate orientation of the protein within the lipid bilayer. Midway through the bilayer is the S1 binding site occupied by citalopram (yellow oval). The allosteric/S2 site (blue oval), also occupied by citalopram, is in the vestibule that leads into the S1 site.

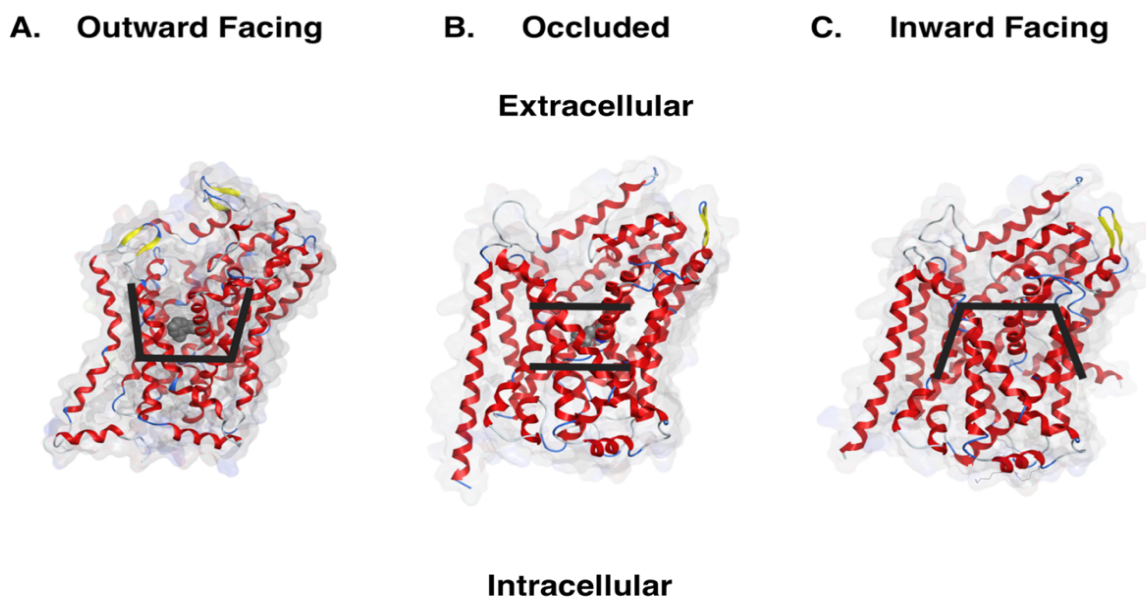


Figure 1.2: Alternating Access Mechanism of Monoamine Transport. The MATs undergo a conformational change during substrate transport with initial binding occurring with an outward-facing conformation open to the extracellular side of the membrane (A; dDAT protein, PDB id. 4M48). Substrate and ion cofactor binding trigger a conformational change to an occluded state (B; LeuT protein, PDB id. 2A65) before adopting an inward-facing structure (C; LeuT protein, PDB id. 3TT3) and release of the substrate into the cell. The reset transition back to the outward facing conformation is the rate-limiting step of transport.

up the transport cycle (Figure 1.2) (Forrest *et al.*, 2008). Per the alternating access mechanism, one of the conformations is an “outward-facing” (OF) structure that is open to the extracellular side of the lipid bilayer (Wang *et al.*, 2015). The substrate enters the OF structure through a vestibule (Figure 1.3) that leads into the orthosteric binding pocket (S1 site) located roughly midway through the protein (Figure 1.1) (Cheng and Bahar, 2015). An allosteric binding pocket has been proposed to reside within the vestibule that would affect the binding kinetics of the molecule within the S1 site (Coleman *et al.*, 2016). While the MATs display both the S1 and S2 site, the specific residues that make up the sites differ by each protein and will be further discussed in later sections. Entry of the substrate into the primary binding pocket triggers a conformational change of the protein to an occluded structure (closed to both extracellular and intracellular sides)

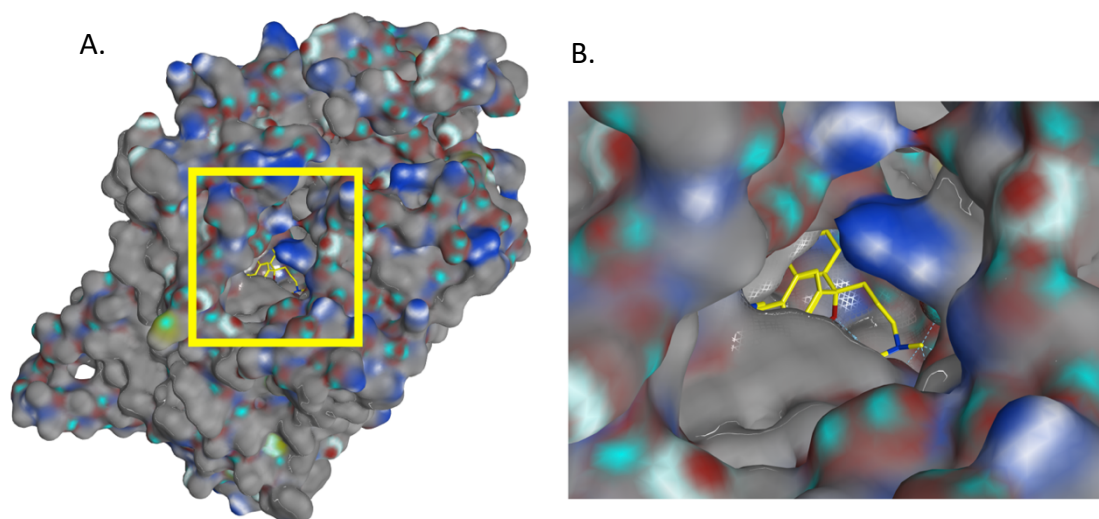


Figure 1.3: Vestibule Leading into the S1 Binding Pocket. A top-down view from the extracellular side of the SERT protein (PDB id. 5I73) using a surface map (Panel A). Outlined by a yellow box is the vestibule that leads into the S1 or orthosteric binding pocket. A close-up of the vestibule (Panel B) has citalopram (yellow) bound in the S1 pocket.

before opening to the intracellular side (“inward-facing” structure; IF) and releasing substrate and Na^+ (Coleman *et al.*, 2019). A K^+ ion is exported potentially through a channel-like mechanism during the reset of the SERT protein from the IF to OF conformation, although it is unclear why the K^+ ion is unnecessary for the DAT and NET proteins (Adams and DeFelice, 2002; Aggarwal and Mortensen, 2017). The SSRIs bind to the orthosteric binding pocket and typically lock the transporter in the OF conformation, although some SSRIs including citalopram also occupy the allosteric site and prevent the inhibitor in the S1 pocket from dissociating from the protein (Coleman *et al.*, 2016).

Surface expression of the SERT protein can be downregulated by chronic exposure to its substrate serotonin, which could be effected by the activity of protein kinase C (PKC), cGMP-dependent protein kinase (PKG) or p38 mitogen-activated protein kinase (MAPK) (Jørgensen *et*

al., 2014). Changes in SERT surface expression due to serotonin exposure were blocked by the antagonist citalopram (Jørgensen *et al.*, 2014). Dimerization of the SERT protein can occur and is an important regulator for trafficking the protein into Golgi vesicles for storage (Kilic and Rudnick, 2000; Sitte *et al.*, 2004). Although the SERT exists as dimers and oligomeric complexes of up to 8 subunits in the plasma membrane that are stable for up to 10 minutes, its impact is currently unknown and the monomeric form of the protein appears to be the functionally active one (Anderluh *et al.*, 2014; Coleman *et al.*, 2016; Cheng and Bahar, 2019). The relative expression of the oligomers in the plasma membrane is not affected by the SSRI antidepressants or cocaine analogs (Schmid *et al.*, 2001). The oligomeric complexes do not exchange subunits between complexes, which could suggest that they are the result of the initial placement within the membrane (Anderluh *et al.*, 2014). Additionally, the depletion of bilayer cholesterol, a molecule necessary for the functional activity of transport, did not alter the distribution of the oligomers in the membrane (Anderluh *et al.*, 2014). SERT molecules in dimers found during crystallization were inverted positioning relative to each other, but this is believed to be an artifact of the crystallographic conditions (supplementary material of Coleman *et al.*, 2016). Computational modeling of SERT dimers suggests that TM 12 is the likely subunit connection point (Periole *et al.*, 2018).

The SSRI antidepressants are antagonists of the SERT protein and prolong serotonergic signaling within the CNS (Immadisetty *et al.*, 2013). An early attempt to explain the mechanism behind the antidepressant effects of the SSRIs and the TCAs is the monoamine hypothesis of depression, which posits that depression is a result of a deficit of the monoamine neurotransmitters including serotonin in the brain (Krishnan and Nestler, 2008; Haase and Brown, 2015). It was noted that some violent suicide victims were reported to have low serotonin levels at the time of

death (Shaw *et al.*, 1967; Bourne *et al.*, 1968; Immadisetty *et al.*, 2013). The monoamine hypothesis is too simplistic of a model, however, to entirely encompass the mechanism behind the antidepressant effects shown by the SSRIs. One criticism of the hypothesis is the latency period of weeks to months of MAT inhibitor antidepressant treatment required before relief from the depressive symptoms occurs, even though these drugs cause an immediate increase in synaptic serotonin levels (Insel and Wang, 2009). A rationale offered for this latency period has been that the activation of inhibitory serotonergic autoreceptors (5HT₁ family) in response to the increased serotonin levels depresses serotonergic signaling (Yohn *et al.*, 2017). Long term SSRI treatment causes desensitization of these autoreceptors and changes in receptor expression that would eventually promote increased serotonergic signaling. This explanation ignores the fact that several postsynaptic 5-HT receptor types associated with antidepressive effects would still be immediately activated by the serotonin surge upon first taking the SSRI and is a desperate attempt to rationalize the monoamine hypothesis. The currently favored mechanism for the antidepressant effects shown by the SSRIs is the neurotrophic hypothesis and its role in adult hippocampal neurogenesis (Jacobs, 2002). Some postmortem studies have reported reductions in the volume of the prefrontal cortex and hippocampus of depressed patients (Krishnan and Nestler, 2008). The SSRIs are thought to elicit adult hippocampal neurogenesis through an increase in the expression of brain-derived neurotrophic factor (BDNF) in the hippocampus, which is regulated by the transcription factor cAMP response element binding protein (CREBP), altering gene transcription (Figure 1.4) (Haase and Brown, 2015). The activation of both the 5HT_{1A} and the 5HT₄ receptors has been found to increase neurogenesis in the dentate gyrus over weeks, and play a role in the antidepressant response found in rodent models (Mendez-David *et al.*, 2014; Samuels *et al.*, 2015). The recently FDA-approved fast acting antidepressant ketamine, a repurposed anesthetic, is thought to increase

neurogenesis through similar pathways downstream of the serotonin receptors, although ketamine has potential for abuse and can cause cognitive decline (Clarke *et al.*, 2017).

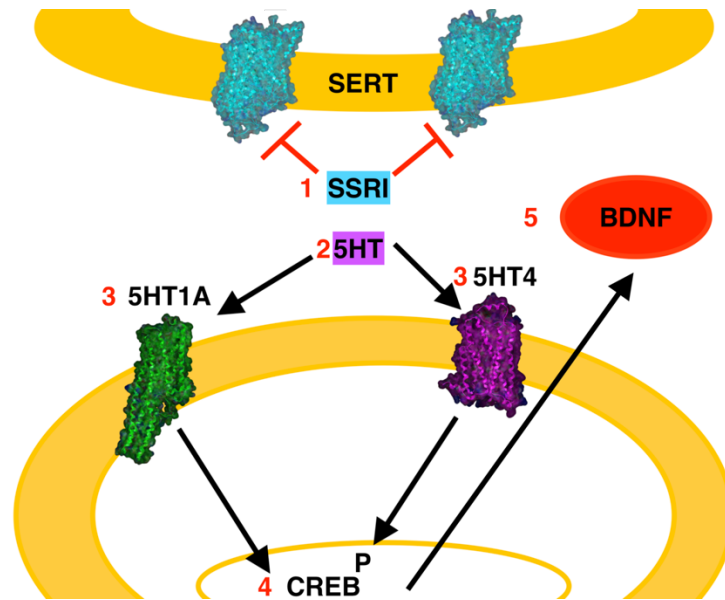


Figure 1.4: Neurogenesis Pathway. The SSRI antidepressants inhibit SERT on the presynaptic neuron (1), which leads to an increase in 5HT (2) within the synapse. Activation of postsynaptic 5HT_{1A} and 5HT₄ receptors (3) lead to the phosphorylation of CREB (4) within the nucleus and promote the synthesis of BDNF (5) ultimately leading to hippocampal neurogenesis.

Premise of this Research

The United States Center for Disease Control (CDC) depression data from 2011-2014 suggests that over 12% of people over the age of 12 have used antidepressants within the last month, an increase of 5% since the 1999-2012 survey (Pratt *et al.*, 2017). Additionally, roughly 25% of people that used antidepressants have been taking them for more than 10 years (Pratt *et al.*, 2017). The side effects of the first line SSRI antidepressants, including lack of efficacy and prolonged latency periods with many adverse effects before therapeutic relief, often make medication adherence a problem. This establishes the necessity for the identification of novel

inhibitors that offer the possibility of alternative therapeutic profiles compared to the SSRIs. Some design strategies have included the serotonin-norepinephrine reuptake inhibitors, and multimodal antidepressants such as vortioxetine and vilazodone, which modulate other serotonergic receptors in addition to SERT (Gillman, 2007; Andersen *et al.*, 2015; Wang *et al.*, 2016). The Surratt and Madura laboratories have approached antidepressant drug discovery by combining computational chemistry modeling of drug targets in the brain with classical pharmacological methods to identify potential inhibitors of the SERT protein (Manepalli *et al.*, 2011; Nolan *et al.*, 2011; Nolan *et al.*, 2014).

Computational Drug Discovery

The drug discovery process is focused on identifying pharmacologically active compounds with novel chemical structures that can be developed into potential candidates for clinical trials. The development of drug candidates is exceedingly expensive with an average cost over 2 billion dollars as of 2010 (Nicolaou, 2014; Mohs and Greig, 2017). Successful candidates take roughly 13.5 years to receive FDA approval, with under 10% of small molecules being approved (Nicolaou, 2014; Mohs and Greig, 2017). Roughly a third of the cost is spent on the preclinical development including target identification (initial decision of potential targets), target validation (confirmation of the target's involvement in the disease state), initial molecule discovery, structure-activity relationships (SARs), *in vitro* and *in vivo* pharmacological testing, toxicity and pharmacokinetics testing (Nicolaou, 2014; Dahlin *et al.*, 2015). One established strategy to identify potential candidates is high-throughput screening (HTS), which utilizes automation to screen chemical libraries, curated collections containing thousands of compounds with diverse structures, against a target protein to identify compounds that meet the set criteria of the assay (Saha *et al.*, 2018). HTS generally allows for 10,000 to 100,000 compounds to be screened per day due to the

miniaturization of assays, allowing more compounds to be screened in parallel through continuing advancement of robotics (Inglese *et al.*, 2007). Processing the data is a common problem associated with HTS due to the vast amount of data generated, and common approaches to handle this include grouping compounds by chemical diversity and unique biological profiling, which is determined by performance in cell-based assays looking at attributes such as gene expression or cell morphology (Wawer *et al.*, 2014; Saha *et al.*, 2018). In addition, the sheer cost of HTS is considered to be well beyond the capabilities of typical academic researchers, a compelling reason to incorporate computational modeling into the drug discovery process (Wasko *et al.*, 2015).

The major computational approaches to drug discovery are ligand-based or structure-based (Figure 1.5). The ligand-based method, the only choice when the structure of the drug's target is unknown, employs established ligands of the target receptor as templates that guide the design and synthesis of a SAR series of analogs, and in this way identifies common structural elements that are essential to their functional activity (Badalà *et al.*, 2008). Typically, the active compounds are superimposed and a pharmacophore is created. A pharmacophore is a model of the chemical interactions between ligand and receptor necessary

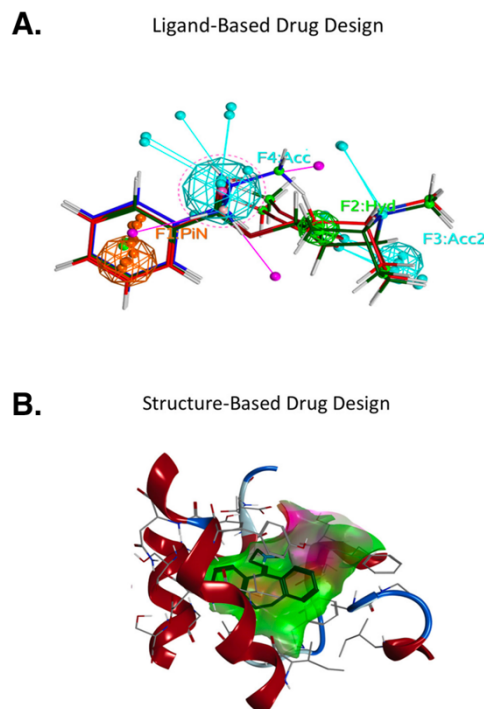


Figure 1.5: Comparison of Ligand-Based and Structure-Based Drug Design. Ligand-based approaches utilize known ligands to build a pharmacophore based on key chemical features (A). The created pharmacophore is highlighted by spheres indicating aromaticity, hydrogen bond donors, and hydrogen bond acceptors. Structure-based approaches utilize the receptor's structure (backbone displayed in red) to evaluate the compound's interactions within the binding pocket (green) (B). Figure adapted from Wasko *et al.*, 2015.

for the desired efficacy, which can be computationally modeled by combining common chemical attributes such as hydrogen bond donor / acceptor potential and hydrophobicity based on known ligands, and can be used to screen for molecules that match the pharmacophore's criteria (Ferreira *et al.*, 2015). Creating a pharmacophore is useful for both methods, but critical for the ligand-based search strategy. The structure-based approach utilizes a computational model of the target, usually a protein, to guide drug discovery.

Structural Biology of the MATs

The three-dimensional structure of a receptor protein can be elucidated using x-ray crystallography, nuclear magnetic resonance spectroscopy (NMR), and cryogenic electron microscopy (cryo-EM) (Yee *et al.*, 2005; Doerr, 2017). Crystal structures solved by x-ray diffraction are the most common structure-based ligand screening tools, and are curated by the Protein Data Bank (Berman *et al.*, 2000). These structures are considered “snapshots” of receptor conformations, rigid structures obtained under non-physiological conditions. These proteins often have site-directed amino acid sequence mutations introduced to aid crystallization with the goal of not appreciably affecting ligand binding sites or protein expression (Piscitelli *et al.*, 2015). This is not always the case; one mutation (T439S) located within the S1 binding pocket of SERT (PDB id. 5I6X) altered the binding of paroxetine (Coleman and Gouaux, 2018). An electron density map of the crystalized

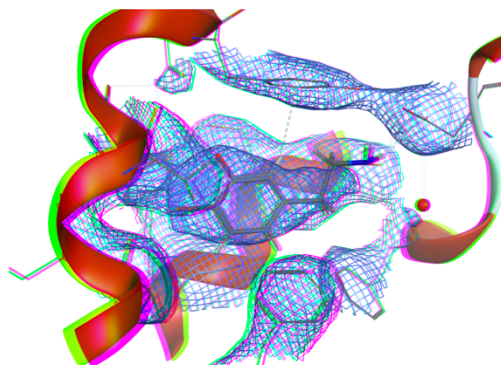


Figure 1.6: Electron Density of the DAT (4XP1). The electron density is displayed as blue mesh for the DAT structure. The crystallographer fits the side chains and ligand dopamine to the electron density. Figure adapted from Madura, 2016.

protein is determined based on the diffraction pattern of the x-ray beam, which is used by the crystallographer to position

the elemental structure of

the protein based on the

known amino acid sequence

(Figure 1.6) (Lang *et al.*,

2014). The resolution of the

model is determined by the

confidence and probability

of the structure's fit to the

electron density map, with

lower Ångstrom structures

Resolution (Å)	Description
> 4.0	Individual coordinates meaningless. Secondary structure elements can be determined.
3.0 – 4.0	Fold possibly correct, but errors are very likely. Many sidechains placed with wrong rotamer.
2.5 – 3.0	Fold likely correct except that some surface loops might be mismodelled. Several long, thin sidechains (lys, glu, gln, etc.) and small sidechains (ser, val, thr, etc.) likely to have wrong rotamers.
2.0 – 2.5	Same as 2.5 – 3.0, but number of sidechains in wrong rotamer is considerably less. Many small errors can normally be detected. Fold normally correct and number of errors in surface loops is small. Water molecules and small ligands become visible.
1.5 – 2.0	Few residues have wrong rotamer. Many small errors can normally be detected. Folds are rarely incorrect, even in surface loops.
0.5 – 1.5	In general, structures have almost no errors at this resolution. Individual atoms in a structure can be resolved. Rotamer libraries and geometry studies are made from these structures.

Table 1.5: Guide to protein crystal structure resolution.
Table is adapted from Madura, 2016.

representing a better fit (see Table 1.5; (Madura, 2016)) (Piscitelli *et al.*, 2015). Proteins are

inherently fluid molecules, and membrane-bound proteins like the MATs are difficult to crystalize

because of the absence of a lipid bilayer to stabilize the protein's physiological 3D structure. The

recently crystalized *Drosophila* DAT and the *human* SERT crystal structures have a resolution

around 3 Å, which would allow the crystallographer to successfully orient the backbone of the

protein structure (Wang *et al.*, 2015; Coleman and Gouaux, 2018). In comparison, many of the

GPCRs, specifically the adrenergic receptors, have a resolution under 2 Å, in which case the side

chains within the binding pocket can be accurately positioned. To achieve this resolution, the

external loops are often truncated (Zhang *et al.*, 2015). Until the *human* SERT crystal structures

were published in 2016, structure-based studies relied on building homology models of the protein,

using an evolutionarily-related protein as a structural template (Fiser and Šali, 2003). To build a

homology model, the amino acid sequences of the target protein and the template structure are aligned and compared using sequence identity (percent of amino acids conserved) and sequence similarity (percent of amino acids within the same class) (Hillisch *et al.*, 2004; Wasko *et al.*, 2015). The higher degree of similarity between the target protein and the template is indicative of a better structural template for a homology model. The first credible crystal structure available as a template for the MATs was that of the LeuT bacterial leucine transporter (Yamashita *et al.*, 2005).

Structural Templates of the MATs

LeuT

Although LeuT only shares 20-25% of its amino acid sequence (sequence identity) with MAT proteins, the first deposited LeuT structure (2A65) within the PDB confirmed the existence of the 12 TM domains (Figure 1.7) (Yamashita *et al.*, 2005). The 2A65 structure was defined as being in an occluded state by the closure of an external gate partially comprised of R30 (TM 1) and D404 (TM 10) (Figure 1.8). Co-crystallized were the endogenous substrate leucine along with the two Na⁺ ions required for substrate transport within the S1 binding pocket, buttressed by TMs 1, 3, 6 and 8 and an enclave formed by kinks within TM domains 1 and 6, located roughly 6 Å from the extracellular border of the lipid bilayer (Figure 1.10) (Yamashita *et al.*, 2005). Unexpectedly, the LeuT

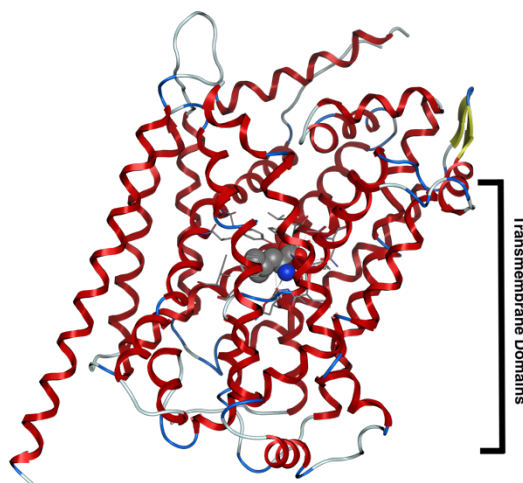


Figure 1.7: LeuT crystal structure. LeuT (red; PDB id. 2A65) is shown with the substrate leucine (grey) within the S1 binding pocket.

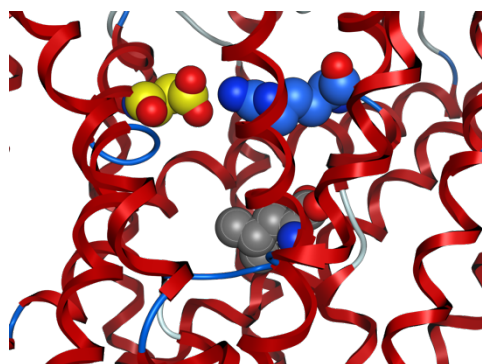


Figure 1.8: External Gate of LeuT. R30 (yellow) and D404 (blue) define the external gate above the S1 binding site occupied by leucine (grey).

structure revealed a tertiary motif known as the “LeuT fold”, which identified that TM 1-5 and 6-10 form a pseudo repeat that could be superimposed when rotated by 176.5°, with the remaining TM domains (11-12) not being essential for transport of the substrate (Figure 1.9) (Yamashita *et al.*, 2005). Interest in LeuT substantially increased in 2007 with the publication of LeuT structures that were co-crystalized with the tricyclic antidepressant clomipramine (Singh *et al.*, 2007). Clomipramine acted as a non-competitive allosteric modulator that sat approximately 11 Å above the S1 binding pocket and

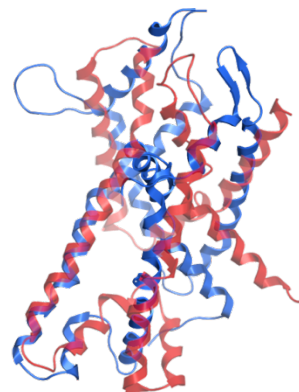


Figure 1.9: LeuT Fold. The LeuT fold is comprised of an inverted repeat consisting of transmembrane domains 1-5 (blue) and 6-10 (red).

altered the kinetic rates of the leucine molecule by stabilizing the extracellular gate (Singh *et al.*, 2007). Separately, Shi *et al.* argued for the existence of a secondary substrate (S2) site in the same vicinity. Using steered molecular dynamics simulations, they postulated that substrate occupation of the S2 site was necessary to trigger the conformational transitions for transport (Shi *et al.*, 2008). This view was contested by Gouaux and colleagues, who argued for only

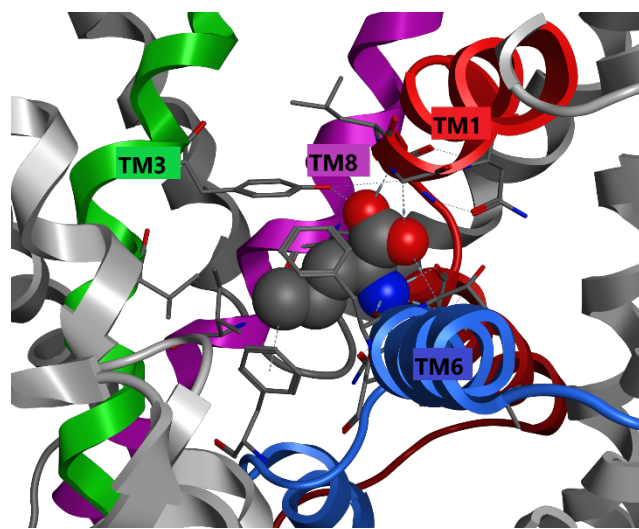


Figure 1.10: S1 Binding Pocket TM Domains. TM1 (red), TM3 (green), TM6 (blue) and TM8 (purple) form the S1 binding pocket co-crystalized with leucine (grey) within the LeuT crystal structure (PDB id. 2A65).

one high affinity binding pocket on LeuT (Piscitelli *et al.*, 2010). Using isothermal titration calorimetry to measure the thermodynamic response and stoichiometry of L-leucine binding to

LeuT, only a single high affinity site (S1) was detected. They acknowledged that the allosteric site may have lower affinity to lead the leucine substrate into the high affinity site, but stopped short of agreeing that a secondary leucine site was needed to trigger release of the substrate (Piscitelli *et al.*, 2010).

The alternating access transporter mechanism is based on the adoption of at least three distinct conformational states of the protein during the substrate translocation cycle (Forrest *et al.*, 2008). An outward-facing (OF) transporter structure open to the extracellular side would allow the substrate and necessary ions to bind in the S1 pocket, triggering conversion to the S1-occluded structure identified in the 2005 LeuT crystal structure (PDB id. 2A65), before shifting again to adopt an inward-facing (IF) structure to release the substrate and ion cofactors into the cytoplasm (Yamashita *et al.*, 2005; Piscitelli *et al.*, 2010). In 2012, crystal structures of LeuT in substrate-free (apo) OF and IF conformations provided more insight into the translocation cycle (Krishnamurthy and Gouaux, 2012). The OF structure (PDB id. 3TT1) appeared to rely on a hinge-like mechanism pivoting on V23 (TM1), G55 (TM2), and L257 (TM6) to adopt an OF structure compared to the occluded structure (Krishnamurthy and Gouaux, 2012).

LeuBAT

TCAs, SSRIs, and serotonin-norepinephrine reuptake inhibitors (SNRIs) bind non-competitively to the extracellular vestibule in the LeuT protein, but this is now thought to be artifactual and not reflective of the competitive binding of these compounds to the human MATs (Rudnick, 2007; Wang *et al.*, 2013).

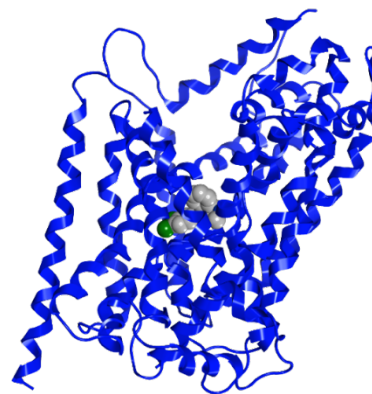


Figure 1.11: LeuBAT Crystal Structure (PDB id. 4MM5). LeuBAT (dark blue) was crystalized with the SSRI sertraline (grey) within the S1 binding pocket. The amino acids within the S1 binding pocket were mutated to those of SERT, which shifted the antidepressant binding site on LeuT from S2 to S1.

To identify key S1 pocket residues for BAT (biogenic amine transporter; *i.e.*, MAT) ligand recognition, MAT residues believed to be important for ligand binding systematically replaced the corresponding LeuT residues to form LeuBAT in hopes of simulating the competitive binding of known MAT ligands. The LeuT and hSERT amino acid residues within the S1 binding pocket were compared to identify probable residues imparting SERT selectivity. In total, 20 amino acids were mutated to result in 12 LeuBAT crystal structures that bound TCAs, SSRIs, and SNRIs within the S1 binding pocket (Figure 1.11) (Wang *et al.*, 2013). While the LeuBAT structures were an improvement over LeuT as templates to study the SERT protein, they were rapidly overshadowed by the publication of a fruit fly DAT structure (Penmatsa *et al.*, 2013).

dDAT

The 2013 *Drosophila* dopamine transporter (dDAT; PDB id. 4M48) was co-crystallized with the tricyclic antidepressant nortriptyline bound in the S1 binding pocket formed from TMs 1, 3, 6 and 8 (Figure 1.12) (Penmatsa *et al.*, 2013). The dDAT structure shares more than 50% of its amino acid sequence with the human MATs and was solved at a resolution of 3.0 Å through use of five stabilizing mutations (Penmatsa *et al.*, 2013). Overall, the structure was locked in an OF conformation with the TCA inhibitor blocking substrate access to the central binding pocket. The crystal structure displayed the LeuT fold motif, but notably deviated with a kink at P572

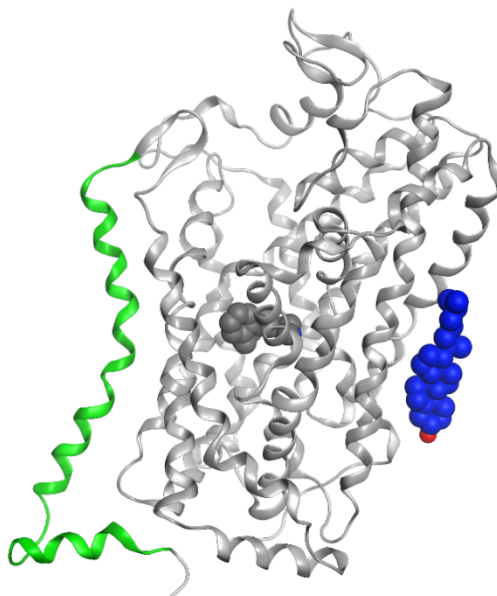


Figure 1.12: dDAT Crystal Structure (PDB id. 4M48). dDAT co-crystallized with the TCA nortriptyline within the S1 binding pocket (dark grey). Differing from the LeuT structures is a kink in TM12 highlighted in green. A cholesterol molecule (blue) is located near TM 1, 5, and 7.

in TM 12 that forced the second half of the TM away from the protein (Penmatsa *et al.*, 2013). This kink in TM 12 was later seen in the structures of the human serotonin transporters, which was co-crystallized with a cholesterol molecule within the kink of TM12 (Coleman *et al.*, 2016). A cholesterol molecule was identified on dDAT within a pocket comprised of TMs 1, 5, and 7 and is speculated to play a role in stabilizing the OF structure. Consistent with this idea, increased cholesterol concentrations in lipid membranes stabilize OF structures (Hong and Amara, 2010; Penmatsa *et al.*, 2013).

Later efforts in 2015 led to the crystallization of dDAT complexed with substrates, their analogs, and inhibitors including dopamine, its analog 3,4-dichlorophenethylamine (DCP), and psychostimulants (D-amphetamine, methamphetamine, cocaine, B-CFT, and RTI-55) (Wang *et al.*, 2015). Functional transport of dopamine was regained by reintroducing three of the thermostability mutations (V275A, V311A, and G538L) and extracellular loop 2 in the new dDAT construct (Wang *et al.*, 2015). In addition, mutations within the binding pocket at TM 3 (D121G) and TM 8 (S425M) were introduced to mimic the human DAT structure (hDAT) (Wang *et al.*, 2015). All of the ligands were co-crystallized while within the orthosteric binding pocket of the dDAT structures. The substrate dopamine was crystallized in an OF DAT structure with the charged amine interacting with the TM 1 D46 (equivalent of D79 in hDAT), the catechol group hydrogens bonding with A117, and the remainder sitting in a hydrophobic

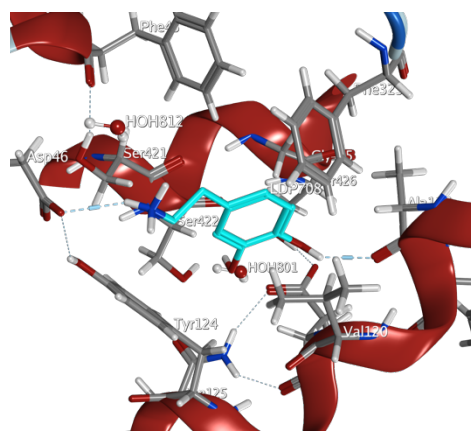


Figure 1.13: DAT Binding Pocket. DAT (PDB id. 4XP1) with dopamine within the S1 binding site.

pocket consisting of A121, Y124, S422, and F325 (Figure 1.13). Interestingly, two water molecules were observed within the binding pocket with dopamine but were not observed with

DCP bound, which formed a partially occluded OF structure with F319 rotating to occlude the binding pocket. The amine group of DCP formed a hydrogen bond with D46 while the dichlorophenyl ring interacted with V120 and F325. Both D-amphetamine and methamphetamine stabilized OF conformations from within the S1 binding pocket. Cocaine was crystalized within the S1 binding pocket, forming a salt bridge with D46 and aromatic interactions with F325 (Wang *et al.*, 2015).

hSERT

After multiple attempts to crystalize the human SERT (hSERT) protein were unsuccessful, two site-directed mutations (I291A and T439S) were added to enhance thermostability (TS2 construct) and structures were crystalized at a resolution of 4.5 Å (Green *et al.*, 2015; Coleman *et al.*, 2016). A third thermo-stability mutation (T110A) was necessary to enhance the resolution of the structures to 3.15 Å (TS3 construct). Unfortunately, the TS3 construct was locked in the OF conformation and was functionally inactive by failing to transport serotonin. Six hSERT crystal structures are deposited within the PDB

with the reference codes 5I6X, 5I67, 5I73, 5I74, and 5I75. The initial crystal structures were co-crystalized with citalopram and paroxetine within the binding pocket. Additionally, a Br-citalopram molecule was found within an allosteric site directly above the S1 site, similar to the LeuT structure with the TCA

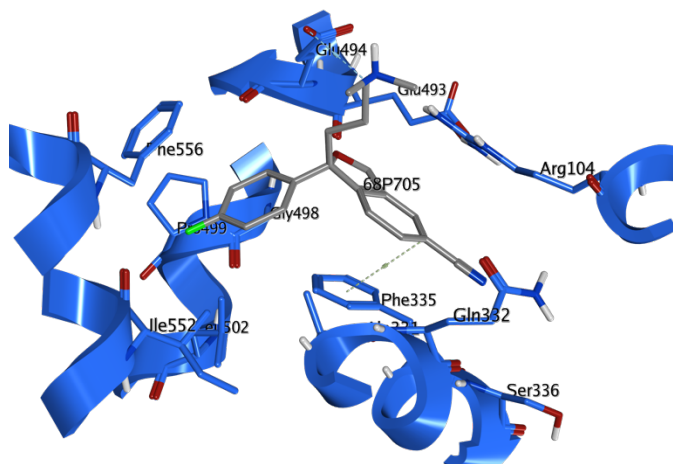


Figure 1.14: SERT S2 Binding Site. Citalopram (grey) is shown within the S2 binding site of SERT (PDB id. 5I73).

clomipramine (PDB id. 2Q6H) (Singh *et al.*, 2007). This allosteric site is thought to affect the

kinetic off-rate (K_{off}) of the citalopram molecule within the S1 site and extend the time bound to SERT (Coleman *et al.*, 2016). The S2 site sits above two external gates formed by amino acids Y176 / F335 and R104/E494 (Coleman *et al.*, 2016). Citalopram within the S2 site forms an aromatic interaction with F335 and an ionic interaction with E494 (Figure 1.14). Additionally, residues R104, D328, A331, and Y556 were reported to make up the S2 site (Coleman *et al.*, 2016). The TS3 construct contained the T439S mutation within the S1 binding pocket altered the binding of some antidepressants. Later efforts to crystallize SERT with the wild type T439 residue resulted in structures cocrystallized with the SSRIs paroxetine, fluvoxamine, sertraline, or S-citalopram (Coleman and Gouaux, 2018). Each antagonist interacted with Y95, D98, I172, Y176, F335, F341, and T439 within the binding pocket (Coleman and Gouaux, 2018). The S1 site is sometimes broken down into three subsites: A (Y95, D98, S336, S438), B (A173, Y176, N177, T439, G442) and C (I172, F334, F341, T497, V507) (Zeppelin *et al.*, 2019).

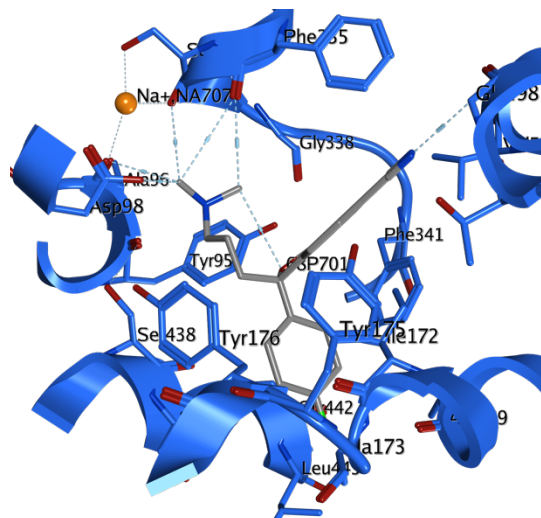


Figure 1.15: SERT S1 Binding Site. Citalopram (grey) is shown within the S1 binding site of SERT (PDB id. 5I73). An Na^+ ion is displayed in orange.

Moving beyond SERT crystal structures locked in the OF conformation, cryo-electron microscopy was used to study the conformational changes of the protein (Coleman *et al.*, 2019). Ibogaine, a purported anti-addiction drug with low affinity to many receptors including SERT, was utilized to establish changes from the OF conformation through the occluded structure before adopting an IF conformation (Wasko *et al.*, 2018; Coleman *et al.*, 2019). Ibogaine is a non-competitive inhibitor of serotonin transport but is a competitive inhibitor against antidepressants

for the primary binding site. At the functional TS2 SERT construct, ibogaine had a K_d of 400nM, while the OF-locked TS2 variant had a reduced K_d of 5-8 μ M (Coleman *et al.*, 2019). This fits with the proposed model allowing ibogaine to enter the S1 site through the OF structure before adopting the preferred IF conformation.

The work in this dissertation utilizes the crystal structure of the hSERT protein for virtual (*in silico*) screening for new compounds with affinity for the S1 (orthosteric) binding pocket (Coleman *et al.*, 2016). It was hypothesized that inhibitors with novel chemical scaffolds could be identified through the computational modeling. Chapter 2 details the computational modeling used to successfully identify inhibitors of the SERT protein. The *in vitro* pharmacological analysis of the compounds that were purchased is contained in Chapter 3.

Chapter 2: Computational Modeling to Identify Inhibitors of the Human SERT

Computational Virtual Screening

Computational drug discovery methods are utilized to identify interesting compounds before pharmacological testing is completed (Sliwoski *et al.*, 2014). With structure-based methods, virtual screening (VS) is a widely used technique once a protein target has been established and a three-dimensional model created. VS is analogous to HTS, but uses ligand docking, a computational technique that predicts the placement of the compound within the binding pocket and estimates affinity to the receptor. Virtual chemical libraries of a million molecules can be quickly screened for high affinity to the binding site of the target protein (Lionta *et al.*, 2014; Sliwoski *et al.*, 2014). The enormous equipment and chemical compound costs with HTS are not seen with virtual screening, and the latter provides a significant cost advantage by filtering out unlikely compounds before purchase / synthesis. The predictive accuracy of the virtual screen hinges on the docking software.

Docking software is available as open-source academic programs (Autodock suite), and from commercial vendors including Chemical Computing Group (Molecular Operating Environment; MOE), Schrödinger (Glide), and BioSolveIT (FlexX) (Pagadala *et al.*, 2017). Ligand-protein docking is classified based on the flexibility of both the ligand and protein side chains: “rigid-rigid” (both inflexible), “rigid receptor” (ligand flexibility alone), and “flexible receptor” (allowing both ligand and protein to be flexible) (Pagadala *et al.*, 2017). Rigid receptor docking is considered a standard approach by many pharmaceutical companies due to the additional computational resources necessary for flexible receptor docking (Andrusier *et al.*, 2008).

In order to sample the binding event in a time-effective manner, the docking programs do not account for the higher-order physics such as quantum or statistical mechanics, but rather rely on using approximations called scoring functions to place and rank the binding of ligands to the receptor. Scoring functions are classified into four categories: force field (physics)-based, empirical-based, knowledge-based, and descriptor-based (Liu and Wang, 2015). Force field-based scoring functions attempt to account for the changes in energy due to van der Waals effects (effects of non-polar interactions), electrostatics (effects of charged interactions), hydrogen bonding, and sometimes solvation (Lionta *et al.*, 2014; Liu and Wang, 2015). Empirical-based scoring functions place weight on positive interactions regarding hydrogen bonding, lipophilicity, and metal ions, while placing penalties on steric clashes and the hindrance of rotatable bonds (Lionta *et al.*, 2014; Liu and Wang, 2015). Knowledge-based scoring functions are built using training sets of ligands bound to receptors to examine the average contacts between ligands and receptors to identify favorable and unfavorable interactions (Huang and Zou, 2008). The descriptor-based scoring functions incorporate machine learning techniques to build models based on certain descriptors such as number of hydrogen bonds, or by creating chemical fingerprints of the ligand interactions within the binding site (Liu and Wang, 2015). Currently, scoring functions are often able to identify the correct binding pose, but often struggle with accurately ranking predicted binding affinity (Lionta *et al.*, 2014). As a result, it is crucial to thoroughly evaluate the scoring functions for the target protein using training sets of both binding and non-binding compounds before completing the virtual screen (Lagarde *et al.*, 2015).

Computational Approach

With the stated goal of identifying novel inhibitors of SERT, a computational approach was taken to complete a structure-based virtual screen within the S1 binding pocket of the SERT

crystal structure. MOE software was chosen to complete the virtual screen based on initial benchmarking with a test set composed of SERT compounds with known affinity. The scoring functions within the docking module of MOE were analyzed to identify the appropriate parameters for the screen. The Maybridge Hit Discoverer, a compound structure collection distributed by ThermoFisher, was chosen as the library to be screened due to the affordability (compounds cost under \$80), commercial availability, and curation date. The top-ranking compounds were filtered utilizing the Lipinski Rule of 5 and estimated binding affinity by the docking protocol. The top 44 compounds were assessed for structural uniqueness using the Tanimoto coefficient with the top 10 compounds purchased for pharmacological testing.

Methodology

SERT Computational Model Preparation

A mutant human SERT crystal structure (Figure 2.1A; PDB id. 5I71, 3.15 Å resolution) was downloaded from the Protein Data Bank (Coleman *et al.*, 2016). Mutated residues within the structure were reverted to the wild type amino acid sequence from the UniProt sequence database using the Molecular Operating Environment (MOE) software (version 2018.01.01; Chemical Computing Group, 2017). Refinement of the SERT structure (Figure 2.1B) was completed through molecular dynamics simulations using the CHARMM36 forcefield with 1-palmitoyl-2-oleoylphosphatidylcholine (POPC) lipid membrane, solvated with TIP3P water at a 0.15M NaCl concentration with a temperature of 310K (Harvey *et al.*, 2009). The simulation was completed with ACEMD software for 40 ns until the backbone root-mean-square deviation (RMSD) converged, and the resulting structure was used as the starting point for the docking simulations (Figure 2.1C). The Structure Preparation module within MOE was utilized with side chains protonated using the Protonate 3D setting with the Amber 14:EHT forcefield, and structural issues

/ warnings were resolved. Since sodium atoms are often required for ligand binding, the 2 sodium atoms and 1 water molecule found within the crystal structure were reinserted into the binding pocket and the system was minimized using MOE (Aggarwal and Mortensen, 2017). The orthosteric binding pocket (S1 site) was identified using the Site Finder module using Alpha Spheres, and dummy atoms were placed within the binding pocket (Figure 2.1D). This site corresponded to the second binding pocket predicted by the software.

Virtual Screening (Docking) Protocol

The docking simulations were completed using MOE software 2018.01.01 using the Dock module. Initial protocol validation was completed using a test set of 24 compounds with experimentally determined binding affinity for SERT ranging from high micromolar to low nanomolar, which was converted into a free energy value (kcal). (Table 2.1) (Tatsumi *et al.*, 1997). The Pearson correlation coefficient was used to compare the predicted affinity to the experimental affinity using JASP software. The following settings used for the docking simulations included selecting the orthosteric binding pocket, use of a wall constraint around the pocket, and use of a structural pharmacophore on the oxygen atom of aspartic acid-98 (D98. DON2 with an R of 2). Ligands were selected out of preconstructed MOE database (MDB) files, and docking was carried out using the triangle matcher mode with the ASE scoring function retaining 10 poses. The poses were refined using induced fit (flexible side chains) with the London dG scoring function; one pose was selected for further work. The protocol for the VS study was validated using the 24-compound test set using the Pearson, Spearman, and Kendall correlation tests with JASP software.

Chemical Library

The Maybridge Hit Discoverer compound structure collection corresponding to 51,775 commercially available compounds was acquired from ThermoFisher. The collection was rebuilt

into 3-dimensional coordinates with the addition of hydrogen atoms and protonated at a pH of 7 using MOE software.

Analysis of Virtual Screen

The resulting output of the virtual screen was filtered by predicted affinity (S score below -17 (initial filter) and -18(final filter)), chemical properties (Lipinski Rule of 5), and chemical uniqueness using chemical fingerprinting (Tanimoto coefficient). The RDKit toolkit from the MayaChemTools software package was utilized to calculate the chemical fingerprinting and the similarity.

Results

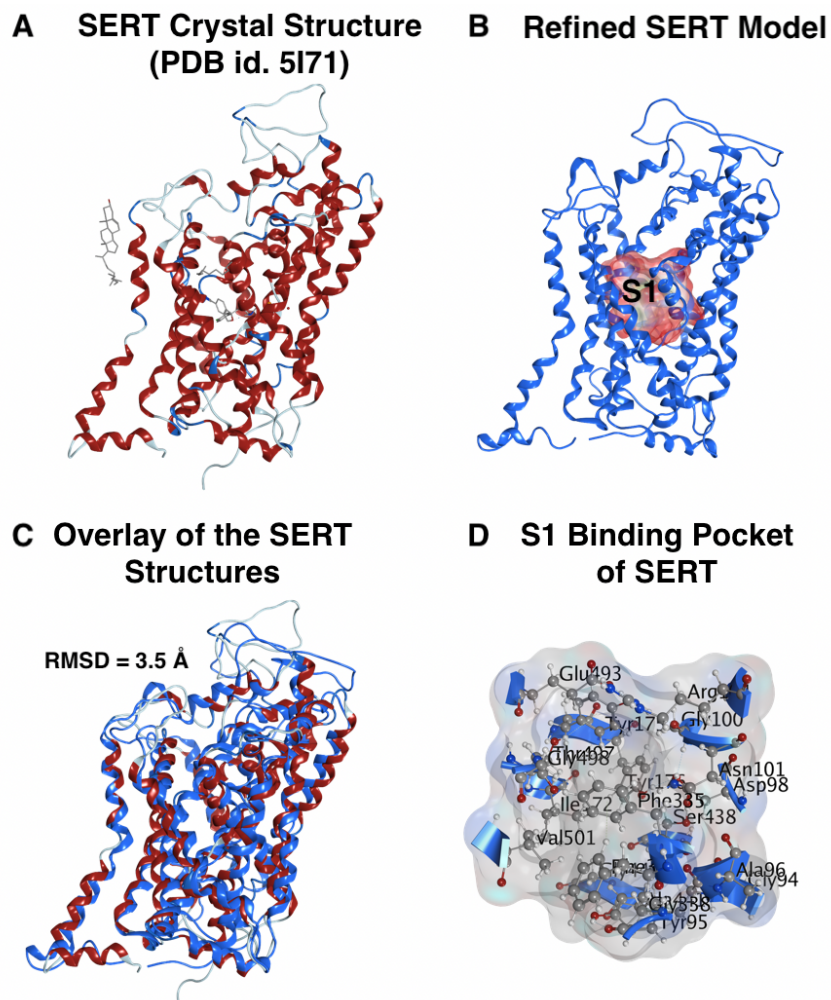


Figure 2.1: Serotonin Transporter Model. The backbone of the SERT crystal structure (red ribbons) co-crystallized with citalopram (PDB id. 5I71) within the S1 binding pocket and a cholesterol molecule in the kink of TM 12 (A). The refined SERT structure used for the virtual screen is shown in blue with the binding pocket highlighted with a surface map (B). An overlay of the SERT crystal structure (red) and the refined model (blue) revealed a backbone RMSD of 3.5 Å (C). The surface map of the binding pocket is highlighted with the amino acid residues shown in ball and stick form (D).

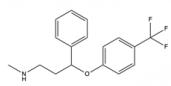
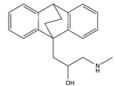
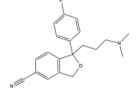
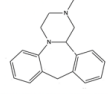
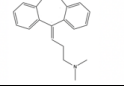
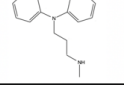
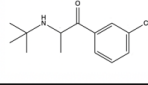
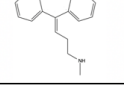
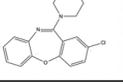
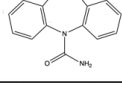
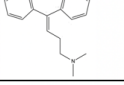
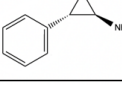
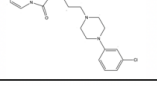
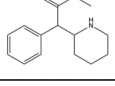
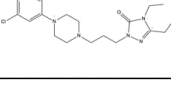
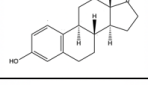
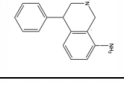
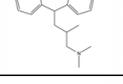
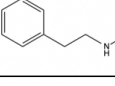
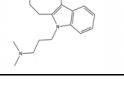
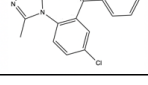
Compound	Structure	Experimental Binding Affinity (dG, kcal/s)	Compound	Structure	Experimental Binding Affinity (dG, kcal/s)
Fluoxetine		-12.9	Oxaprotiline		-7.67
Citalopram		-12.58	Mianserin		-7.66
Amitriptyline		-11.87	Maprotiline		-7.18
Desipramine		-11	Bupropion		-7.15
Nortriptyline		-10.99	Viloxazine		-6.75
Amoxapine		-10.26	Carbamazepine		-6.38
Doxepine		-10.17	Tranlycypromine		-6.26
Trazodone		-9.64	Methylphenidate		-6.18
Etoperidone		-8.58	Estrone		-6.1
Nomifensine		-8.5	Iproniazid		-5.67
Butriptyline		-8.26	Phenelzine		-5.67
Iprindole		-8.21	Alprazolam		-5.67

Table 2.1: Computational Testset for Docking Benchmarking. The name, structure, and experimental binding affinity of the 24 compound testset that was used to evaluate the performance of the docking software for the predictability against SERT.

Placement	Rescore	Pearson R	Pearson R2		Placement	Rescore	Pearson R	Pearson R2
ASE	ASE	0.473	0.223		Alpha HB	GBVI/WAS dG	0.54	0.292
ASE	Affinity dG	0.552	0.305		Alpha HB	London dG	0.674	0.455
ASE	Alpha HB	0.491	0.241		GBVI/WAS dG	ASE	0.572	0.327
ASE	GBVI/WAS dG	0.569	0.324		GBVI/WAS dG	Affinity dG	0.57	0.324
ASE	London dG	0.541	0.293		GBVI/WAS dG	Alpha HB	0.44	0.194
Affinity dG	ASE	0.59	0.348		GBVI/WAS dG	GBVI/WAS dG	-	-
Affinity dG	Affinity dG	0.491	0.241		GBVI/WAS dG	London dG	0.502	0.252
Affinity dG	Alpha HB	0.477	0.227		London dG	ASE	0.575	0.331
Affinity dG	GBVI/WAS dG	0.605	0.366		London dG	Affinity dG	0.508	0.259
Affinity dG	London dG	-	-		London dG	Alpha HB	0.451	0.203
Alpha HB	ASE	0.611	0.373		London dG	GBVI/WAS dG	0.559	0.313
Alpha HB	Affinity dG	0.592	0.351		London dG	London dG	0.554	0.306
Alpha HB	Alpha HB	0.477	0.227					

Table 2.2: SERT Correlation Testing without Ions. The performance of the scoring functions within the MOE software ability to predict binding affinity of the testset was evaluated using the Pearson correlation coefficient. Initial benchmarking was completed without the Na⁺ ions within the S1 binding pocket. The scoring function combinations are displayed in pairs with the first responsible for the placement and the second responsible for rescoring the identified pose. The correlation function comparing the output of the docking simulation to the experimental affinity is displayed as R along with R².

Placement	Rescore	Pearson R	Pearson R2		Placement	Rescore	Pearson R	Pearson R2
ASE	ASE	0.563	0.316		Alpha HB	GBVI/WAS dG	0.475	0.226
ASE	Affinity dG	0.623	0.388		Alpha HB	London dG	0.565	0.319
ASE	Alpha HB	0.519	0.269		GBVI/WAS dG	ASE	0.385	0.148
ASE	GBVI/WAS dG	0.532	0.283		GBVI/WAS dG	Affinity dG	0.302	0.091
ASE	London dG	0.738	0.544		GBVI/WAS dG	Alpha HB	0.517	0.267
Affinity dG	ASE	0.585	0.343		GBVI/WAS dG	GBVI/WAS dG	-	-
Affinity dG	Affinity dG	0.508	0.258		GBVI/WAS dG	London dG	0.553	0.305
Affinity dG	Alpha HB	0.574	0.33		London dG	ASE	0.543	0.296
Affinity dG	GBVI/WAS dG	0.559	0.312		London dG	Affinity dG	0.512	0.262
Affinity dG	London dG	0.64	0.409		London dG	Alpha HB	0.493	0.243
Alpha HB	ASE	0.588	0.346		London dG	GBVI/WAS dG	0.552	0.304
Alpha HB	Affinity dG	0.552	0.305		London dG	London dG	0.614	0.377
Alpha HB	Alpha HB	0.439	0.192					

Table 2.3: SERT Correlation Testing with Ions. The performance of the scoring functions within the MOE software ability to predict binding affinity of the testset was evaluated using the Pearson correlation coefficient. Initial benchmarking was completed with the Na⁺ ions within the S1 binding pocket. The scoring function combinations are displayed in pairs with the first responsible for the placement and the second responsible for rescoring the identified pose. The correlation function comparing the output of the docking simulation to the experimental affinity is displayed as R along with R².

Compound Name	Experimental Binding Affinity (kcal/s)	Predicted Binding Affinity (S score)
Fluoxetine	-12.9	-14.65
Citalopram	-12.58	-16.3
Amitriptyline	-11.87	-13.8
Desipramine	-11	-13.64
Nortriptyline	-10.99	-12.88
Amoxapine	-10.26	-14.6
Doxepin	-10.17	-14.25
Trazodone	-9.64	-15.03
Etoperidone	-8.58	-15.87
Nomidensine	-8.5	-11
Butriptyline	-8.26	-13.77
Iprindole	-8.21	-12.07
Oxaprotiline	-7.67	-13.09
Mianserin	-7.66	-12.31
Maprotiline	-7.18	-12.43
Bupropion	-7.15	-12.41
Viloxazine	-6.75	-11.12
Carbamazepine	-6.38	-11.59
Tranlycypromine	-6.26	Filtered
Methylphenidate	-6.18	-12.76
Estrone	-6.1	-11.77
Iproniazid	-5.67	-8.38
Phenelzine	-5.67	-9.9
Alprazolam	-5.67	Filtered
	Pearson	0.737
	Spearman	0.792
	Kendall	0.581

Table 2.4: Final Validation of the Docking Protocol with the Structural Pharmacophore. After the structural pharmacophore was placed on D98, the docking protocol was re-evaluated using the 24 compound test set using the Pearson, Spearman, and Kendall correlation tests. Each compound is sorted by its experimental affinity (kcal/s) and displayed is the predicted affinity of the docking simulation.

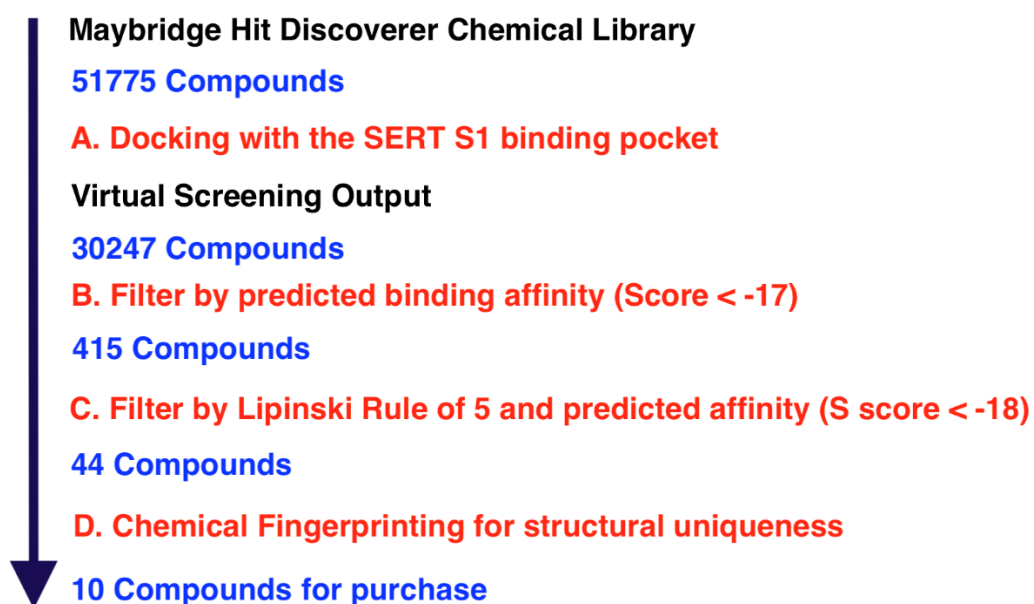


Figure 2.2: Virtual Screening Protocol. The Maybridge Hit Discoverer chemical library was chosen to be virtually screened within the S1 binding pocket of hSERT of which 30,247 compounds were scored and returned. In order to analytically choose the candidate compounds, a series of filters including predicted affinity, the Lipinski Rule of 5, and structural uniqueness were applied and 10 compounds were identified for purchase and pharmacological analysis.

Name	Structure	Maybridge Id.	S Score
Compound 1		SPB04886	-19.5
Compound 2		CD09803	-18.9
Compound 3		NRB03988	-19.7
Compound 4		AW00809	-20.2
Compound 5		KM03423	-18.9
Compound 6		JFD02691	-18.9
Compound 7		HTS10500	-18.8
Compound 8		PHG00899	-19.4
Compound 9		HTS11455	-19.2
Compound 10		HTS04068	-19.4

Table 2.5: Candidate Compounds Identified for Pharmacological Analysis. The completed virtual screen identified 10 compounds that were selected for pharmacological testing. The structure, catalogue identification number (Maybridge ID #.), and the predicted affinity (S score) are displayed within the table.

Results

Docking Software Benchmarking

Benchmarking studies were conducted to evaluate the performance of the scoring functions in the MOE to differentiate between binders and non-binders. Initial testing was completed without the two Na⁺ ions within the binding pocket. The Pearson correlation test was used to assess the relationship between the predicted affinity and the experimental affinity. Each scoring function combination for the flexible docking simulation (1st scoring function for placement and the 2nd for rescore) was evaluated (Table 2.2). The Pearson R coefficient values ranged from 0.44 – 0.67 ($R^2 = 0.19 - 0.45$) with the best correlation occurring with the scoring function combination Alpha Hb – London dG. The scoring function combinations Affinity dG – London dG and GBVI/WAS dG – GBVI/WAS dG failed midway through the simulation. The scoring functions were next evaluated with the 2 Na⁺ ions found in the crystal structure to see if the correlation improved (Table 2.3). The Pearson R coefficient values for the simulations with ions ranged from 0.30 – 0.73 ($R^2 = 0.09 - 0.54$). The scoring function combination ASE – London dG achieved the best correlation between predicted and experimental affinity. Further benchmarking was completed incorporating the ASE – London dG using a structural pharmacophore interaction with D98 (Table 2.4). Correlation testing was completed with the Pearson ($R = 0.737$), Spearman ($R = 0.792$), and Kendall coefficients ($R = 0.581$). In addition, the data were visually inspected, with nine of the top 12 compounds scoring under -13.5 and one compound of the bottom 12 ranking under -13.5. Six out of the top nine compounds with experimental affinity were ranked under -14.

Virtual Screen

The Maybride HitDiscoverer compound collection (51,775 compounds) was screened targeting the S1 binding pocket of SERT, which resulted in 30,247 compounds being returned and scored (Figure 2.2). A relatively small number (415) of the 30,247 were ranked by the docking software to have a predicted affinity S score under -17. The compounds were further filtered by predicted affinity (S score under -18) and the Lipinski Rule of 5, which brought the total to 44. The 44 compounds were examined for their chemical uniqueness assessed by the Tanimoto coefficient, which determined the chemical similarity between each compound. It was determined that the 10 compounds with the unique chemical structures would be purchased for pharmacological testing (Table 2.5).

Discussion

Structure-based virtual screens targeting the human SERT have been successfully completed using homology models based on the structural template LeuT (Manepalli *et al.*, 2011; Kortagere *et al.*, 2013; Gabrielsen, *et al.*, 2014; Nolan *et al.*, 2014). The OF conformation of SERT has been targeted in every virtual screen completed to date. The Surratt and Madura laboratories have completed two virtual screens that used 2A65 as the template structure and targeting the S2 (Manepalli *et al.*, 2011) or S1 (Nolan *et al.*, 2014) pocket. A homology model based on 2QJU targeted an allosteric site containing S2 but focused on extracellular loops 1 and 3 (Kortagere *et al.*, 2013). Since the OF structure is open to both the S1 and S2 sites, Gabrielsen *et al.* defined both as the targeted sites during the virtual screen with a homology model based on 3F3A (Gabrielsen, Rafal Kurczab, *et al.*, 2014).

The original intent of this project was to build and refine a SERT model based on the then recently published eukaryotic dDAT crystal structure due to its far greater sequence homology compared to the bacterial LeuT (Penmatsa *et al.*, 2013; Wasko *et al.*, 2015). This appeared to be the correct approach, as reported technical difficulties made the prospect of crystalizing the human SERT appeared unlikely (Green *et al.*, 2015). Homology models were constructed based on the dDAT structure (PDB id. 4M48), co-crystalized with the TCA nortriptyline within the S1 binding pocket, using MOE and MODELLER software (Eswar *et al.*, 2007; Chemical Computing Group, 2017). Before a virtual screen could be completed, the hSERT crystal structures were published and named by the number of thermostability mutations needed to improve stability during crystallization (Coleman *et al.*, 2016). The TS2 constructs were solved at a resolution of $\sim 4.5 \text{ \AA}$ while the construct containing the additional mutation (TS3) lowered the resolution to $\sim 3 \text{ \AA}$, but locked the protein into the OF conformation and lacked functional ability to transport [^3H]-

serotonin in cellular models (Coleman *et al.*, 2016). One mutation within the binding pocket (T439S) hindered the binding of the SSRI paroxetine, which subsequent crystal structures restored the T439 amino acid (Coleman and Gouaux, 2018). Since then, one virtual screen has been completed using the OF SERT structure (PDB ids. 5I73 and 5I6X) targeting the S1 and S2 sites, but no pharmacological analysis of the results was conducted (Erol *et al.*, 2017).

The SERT structure co-crystalized with the SSRI citalopram (PDB id. 5I71) was chosen as the starting point for this study due to its relatively high resolution (3.15 Å) and the ligand within the S1 binding pocket. Comparison between the human SERT amino acid sequence from the UniProt database and the 5I71 structure revealed 14 total mutations, which were corrected to the wild-type sequence using MOE software. Refinement was completed through molecular dynamics simulations occurring within a POPC membrane with TIP3P water and 0.15 mM NaCl to relax the protein backbone with the CHARMM36 force field. The simulation was run for 40 ns using ACEMD software, which was ended when the backbone RMSD converged at 3.5 Å compared to the initial structure and was used as the SERT model for this study.

Virtual screens utilize docking calculations to timely differentiate compounds with affinity and non-binders at the target protein. However, these simulations trade accuracy for speed. Docking has success with the correct placement of ligands within the binding pocket, but often struggles with accurately predicting relative affinity (Lionta *et al.*, 2014). Proper validation of the scoring functions within the docking software is crucial to determine the predictiveness of the simulations to identify novel compounds. At the basic level, a comparison between the crystalized ligand and the docked pose was used to evaluate Glide software (Erol *et al.*, 2017). A more thorough approach is to use a “seeded” library that contains compounds with known target affinity within a library of non-binding and uncharacterized compounds. By seeding 10 inhibitors (SSRIs

or SNRIs) within 1990 unknown compounds, the MOE docking protocol placed six compounds within the top 253 ranked compounds (Nolan *et al.*, 2014). Ideally, the scoring functions would rank the high affinity compounds as the top hits.

Pharmacophores have been applied to SERT screening, generated from either structural elements in the protein's ligand binding pocket or as a ligand-based filter based on SSRI structure. A hSERT 3D pharmacophore for the S2 binding pocket that included an ionic / hydrogen bonding feature between R104 (TM1) and E493 (TM10), a hydrogen bonding feature from K490, a hydrophobic feature from Y107, and a hydrophobic feature within a subpocket defined by L99, W103, and I179, previously termed the halogen binding pocket (Zhou *et al.*, 2009; Manepalli *et al.*, 2011) Similarly, Kortagere used a structural pharmacophore comprised of an hydrophobic feature at Y568, and hydrogen bonding features at D328, E494, and R564 (Kortagere *et al.*, 2013). Nolan *et al.* incorporated a minimalist structural pharmacophore with one hydrogen bonding feature on D98, while Gabrielsen *et al.* built a pharmacophore based on desmethyl-(R)-fluoxetine containing a positive ionizable feature, a hydrophobic feature, and an aromatic feature that was utilized to filter the screening library before the docking calculations were completed (Gabrielsen *et al.*, 2014; Nolan *et al.*, 2014).

An alternative approach is to quantitatively examine the relationship between the predicted affinity from the docking evaluation with the known experimental binding data, which is the approach taken by this study. A test set containing 24 compounds with known SERT affinity ranging from low nM affinity (< -12 kcal) to mM affinity (-5 kcal), which allowed for correlation testing to be completed to evaluate the performance of the software. MOE software was selected to complete the present virtual screen due to its ability to easily add side chain flexibility, the shorter computational time needed to complete the simulations, and general performance of the

available scoring functions against the human SERT compared to Schrödinger and Autodock software during initial benchmarking. The flexible docking protocol within MOE relies on the selection of two scoring functions; the first responsible for the ligand's initial placement within the binding pocket; the second is responsible for rescoring the pose. Therefore, combinations of the scoring functions in MOE (ASE, Affinity dG, Alpha HB, GBVI/WSA dG, and London dG) were used to evaluate the test set against the experimental affinity using the Pearson correlation test. The initial question examined if the two Na⁺ ions within the binding site impacted the scoring of the test set. The Pearson coefficient for the simulations without ions ranged from 0.44 – 0.67 ($R^2 = 0.19 - 0.45$) (Table 2.3). Completion of the simulations with the two Na⁺ ions revealed an improvement of the Pearson correlation coefficient with the ASE-London dG combination producing an R of 0.73 ($R^2 = 0.54$). The addition of sodium atoms within the binding pocket may stabilize the OF conformation of SERT and allows it to accept ligands from the extracellular side (Aggarwal and Mortensen, 2017).

With the desired scoring function combination identified for SERT, the next task was to optimize the performance of the simulations before completion of the virtual screen. The docking protocol was modified to include a structural pharmacophore applied to D98 similar to that used in the Nolan et al. study, which resulted in Pearson, Spearman, and Kendall correlation coefficients of 0.73, 0.79, and 0.58 respectively (Table 2.5). The Spearman coefficient is an additional correlation test that is rank-order in nature, which may pick up relationships missed by the Pearson coefficient. The ASE-London dG combination achieved a Spearman coefficient 0.79 in MOE compared to alternative Autodock and Schrödinger Glide software that ranged from 0.61 to 0.69 in initial benchmarking. The advantages of MOE software were apparent when allowing for side chain flexibility during the docking calculation. Autodock only allowed limited side chain

flexibility that could not encompass the entire S1 binding site, and Glide software required too much computational time to reasonably completed a virtual screen. The virtual screen targeting the S1 site by Erol et al. only allowed for flexibility of five amino acids within the pocket (D98, I172, Y176, F335, and S438) during the re-evaluation with GOLD docking software (Erol *et al.*, 2017). The structural pharmacophore was a filter used to eliminate compounds that lacked the crucial D98 interaction necessary for binding of high affinity ligands, which filtered two compounds of the test set (tranylcypromine and alprazolam) that display weak SERT binding experimentally (Table 2.5). The resulting predicted affinity (S score) of the test set ranged from -8.3 to -16.3 (Table 2.5). The benchmarking screen was completed in with 8 of the 9 top compounds scoring below -13.5 and 6 of the top 9 below -14. This gave assurances about the predictability of the software to target SERT, as poorly binding compounds ranked lower, with only one compound in the bottom 12 scoring below -13.5. One notable aspect was that citalopram constantly ranked as the top compound with an S score around -16. This may be due to the fact that the citalopram was originally co-crystallized within the binding pocket, although this should not be the case due to the refinement with molecular dynamics allowing the apo binding pocket to relax.

With the virtual screening protocol validated, focus shifted to its utilization to identify potential inhibitors (pharmacologically profiled in Chapter 3). The Maybridge HitDiscoverer chemical library was chosen explicitly due to its recent curation at the time of the screen, the commercial availability, and the relatively inexpensive cost. Commercial availability was a key consideration due to the associated cost and time savings compared to traditional synthesis. The Asinex, Chem-Bridge, ChemDiv, Enamine, Life Chemicals, Otavia, and ZINC chemical libraries have been previously screened using SERT models (Manepalli *et al.*, 2011; Gabrielsen *et al.*, 2014; Nolan *et al.*, 2014; Erol *et al.*, 2017). The structural coordinates of the HitDiscoverer library were

rebuilt in 3-dimensions following the same protocol as the docking test set and contained 51,775 compounds. The pharmacophore filtered 7,775 compounds while the remaining 44,000 compounds were scored and ranked. The first set of criteria to filter the compounds used the Lipinski Rule of 5 - a set of parameters initially utilized by Pfizer to define drug like molecules - in combination with predicted affinity (S score < - 17), yielding 415 compounds. The compounds highest-ranked by predicted affinity were next filtered with S score filter to < -18, which retained 44 compounds. Rather than pick compounds by visual inspection alone, an analytical route was chosen to identify the 10 compounds for purchase. Initially, compounds were sorted into groups by properties such as the number of hydrogen bond donors and acceptors, but the criteria used to filter the compounds displayed too much overlap to sufficiently separate the compounds. The 44 compounds were chemically fingerprinted using MayaChemTools scripts and ranked for their chemical uniqueness using the Tanimoto coefficient. Each of 44 compounds was structurally unique, and the 10 compounds with the lowest coefficient were selected for purchase. Unfortunately, Compound 3 was discontinued by the manufacturer after the initial purchase, preventing a thorough pharmacological analysis.

Chapter 3: Pharmacological Analysis of the Candidate Compounds

Background

Approximations within the scoring functions enable the computational software to complete virtual screens of large chemical libraries within feasible timeframes; unfortunately, these estimates also increase the likelihood of favorably scoring compounds later found to lack pharmacological activity (Huang *et al.*, 2010). Therefore, extensive validation of the computational protocol is crucial to provide the best opportunity to identify viable candidate compounds and filter out the unlikely ligands (Sliwoski *et al.*, 2014). Following acquisition of the candidate compounds either through synthesis or purchase, it is necessary to confirm the results of the screen through pharmacological analysis. The initial pharmacology of potential SERT ligands and inhibitors typically utilizes *in vitro* assays to determine if the candidate compounds bind to the protein, inhibit intracellular transport of serotonin, or promote efflux of stored substrate (Tatsumi *et al.*, 1997; Nolan *et al.*, 2014). Cell lines such as HEK-293 that are transfected to express SERT are combined with radiolabeled ligands and inhibitors to probe the pharmacological activity of the candidate compounds (Tatsumi *et al.*, 1997; Nolan *et al.*, 2014).

Determination of the candidate compound's SERT binding affinity is measured through their ability to displace radioligand inhibitors of SSRIs, or cocaine analogs such as RTI-55 that inhibit SERT, DAT, and NET (Little *et al.*, 1993; Tatsumi *et al.*, 1997). An initial total binding assay at a single concentration usually around 1-10 μM is typically used to establish candidates for full concentration response curves with competitive binding assays. Inhibitor binding alone does not indicate the ability to block transport of the endogenous substrate serotonin. Therefore, functional assays are necessary to determine inhibition potency and efficacy. Inhibition potential is established by preincubating the candidate compound with SERT-bearing cells before addition of

radiolabeled substrate, then measuring the ability of the compound to block transport of the radioligand into the cell. Certain compounds such as 3,4-methylenedioxy-N-methylamphetamine (MDMA; ecstasy) promote efflux, or reverse transport, of stored intracellular substrate (Sandtner *et al.*, 2016). The efflux assay is similar to the uptake assay except that the cells are preloaded with radiolabeled substrate, and the candidate compound's ability to block cellular release of the stored radioligand is measured (Wall *et al.*, 1995).

SERT Virtual Screens

Early SERT virtual screens focused on the allosteric binding pocket / S2 site, which was thought to be the antidepressant binding site on LeuT (Figure 3.1) (Singh *et al.*, 2007; Zhou *et al.*, 2009; Grouleff *et al.*, 2016). The Surratt and Madura laboratories were among the first by screening the ZINC chemical library through the S2 binding site of a SERT model (Manepalli *et al.*, 2011). The pharmacophore criteria returned 4097 compounds before using visual inspection and predicted affinity to rank the top 68 compounds (Manepalli *et al.*, 2011). Ten of the top

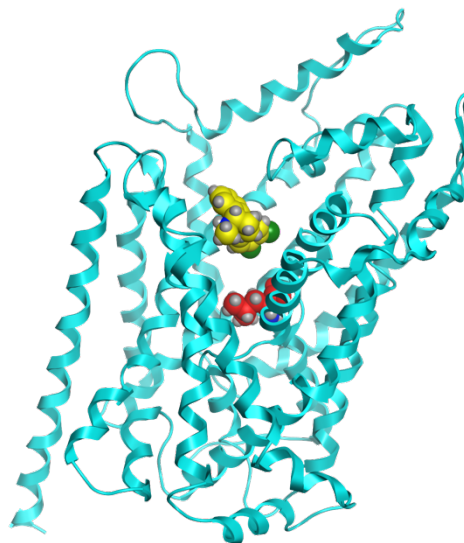


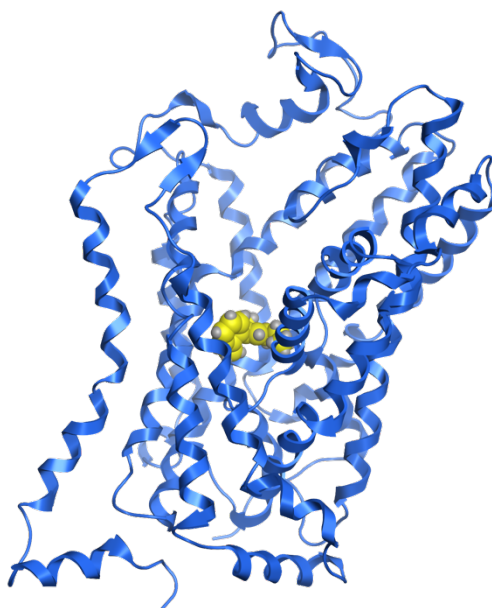
Figure 3.1: LeuT S1 and S2 Occupied. LeuT Crystal structure (teal; PDB id. 3GWU) with the antidepressant paroxetine (yellow) bound within the S2 site above the S1 site occupied by leucine (red).

15 compounds were purchased for pharmacological analysis. Initial binding was assessed at a 10 μM

concentration for the SERT, DAT, and NET proteins using a total binding assay against [^{125}I]-RTI-55, with compounds that significantly displace the radioligand further examined using competition binding assays (Manepalli *et al.*, 2011). Compounds SM-10 and SM-11 were determined to have micromolar binding affinity with K_i values of 38 and 17 μM (Manepalli *et al.*,

2011). Additionally, none of the compounds inhibited [³H]-5HT uptake at a 10 μM concentration (Manepalli *et al.*, 2011). The Kortagere study also screened the S2 site identifying 10 compounds for pharmacological evaluation using [³H]-5HT uptake and [³H]-5HT release assays (Kortagere *et al.*, 2013). One compound (ATM7) was characterized as an allosteric modulator that increased 5HT uptake and potentiated 5HT efflux by 3,4-methylenedioxy-N-methylamphetamine (MDMA; ecstasy) (Kortagere *et al.*, 2013). ATM7 was hypothesized to work through stabilizing the OF conformation of SERT (Kortagere *et al.*, 2013).

A fundamental shift in the understanding of binding occurred with the crystallization dDAT structures with inhibitors and substrates within the S1 or orthosteric binding pocket (Figure 3.2) (Penmatsa *et al.*, 2013). The first screen against the S1 pocket was completed by Gabrielson *et al.* using the Asinex, ChemBridge, ChemDiv, Enamine, and Life Chemical libraries (Gabrielsen *et al.*, 2014). Filtering by the Lipinski Rule of 5, Verber (oral bioavailability), basic property (pK_a between 3 and 11.5), ADMET properties, and a ligand-based pharmacophore



(positive ionic charge, aromatic feature, and hydrophobic portion) left 2293 compounds to be flexibly docked using a previously developed 4D

Figure 3.2: dDAT S1 Occupied. dDAT Crystal Structure (blue; PDB id. 4M48) with the tricyclic antidepressant amitriptyline (yellow) bound within the S1 binding pocket.

approach (Gabrielsen *et al.*, 2012; Gabrielsen *et al.*, 2014). Two-hundred and two compounds were purchased for pharmacological analysis at SERT. A total binding assay against [³H]-citalopram identified 23 compounds for competition binding curves with an additional 23

compound chosen to develop structure activity relationships. In all, 24 compounds were characterized with a K_i below 1000 nM with 13 additional compounds having a K_i between 1000 nM to 3100 nM (Gabrielsen *et al.*, 2014). Later screening of analogs identified an additional 22 compounds with a K_i under 1000 nM (Gabrielsen *et al.*, 2014).

The second SERT virtual screen published by the Surrat and Madura laboratories screened the PubChem database within the S1 binding pocket of the SERT model (Nolan *et al.*, 2014). The 13,378 compounds ranked compounds were visually inspected based on pharmacophore fit (D98), chemical complexity, and synthetic viability, which identified 49 compounds of interest (Nolan *et al.*, 2014). Nineteen compounds were commercially available and pharmacologically evaluated to determine binding affinity (K_i) for the MATs (SERT, DAT, and NET) and inhibition efficacy (IC_{50}) for SERT (Nolan *et al.*, 2014). Four compounds (TN-1, TN-5, TN-6, and TN-13) were selected for full competition binding curves for SERT with K_i values ranging from 668 to >20,000 nM and IC_{50} values ranging from 3845 to >20,000 nM from the [3H]-5HT uptake inhibition assay (Nolan *et al.*, 2014).

Following publication of the human SERT crystal structures, only one study virtual screen utilized the structures (PDB id. 5I6X and 5I73) and screened the Otava Chemicals Drug Like Green chemical library through both the S1 and S2 pockets (Erol *et al.*, 2017). Glide software was initially used and compounds scored within -2 kcal of the top ranked compound were kept leaving 9163 for the S1 and 999 for S2 (Erol *et al.*, 2017). Consensus scoring by docking algorithms within the Schrödinger software suite identified 3 compounds for S1 (compounds 160234, 159166, 69419) and 1 compound for S2 (compound 93507) (Erol *et al.*, 2017). Molecular dynamics simulations and free energy calculations using MM/GBSA within Schrödinger software were used to computationally validate these compounds as SERT inhibitors (Erol *et al.*, 2017). Although this

is technically the first virtual screen utilizing the human SERT crystal structures, the lack of pharmacological validation hinders the final conclusions made by the study. The prior 4 SERT virtual screens pharmacologically profiled 241 compounds with only 44 compounds displaying moderate binding affinity or modulated serotonin transport (Manepalli *et al.*, 2011; Kortagere *et al.*, 2013; Gabrielsen *et al.*, 2014; Nolan *et al.*, 2014). This hit rate of 18% highlights the necessity of pharmacological evaluation to validate the computational approach.

Pharmacological Approach

Chapter 2 of this thesis detailed the computational approach taken to identify 10 candidate compounds for pharmacological profiling. While all 10 compounds were purchased from ThermoFisher, only 9 were able to be fulfilled by the manufacturer and evaluated. A HEK-293 cell line that stably expressed SERT was acquired to determine binding, inhibition efficacy, and release potential of the candidate compounds. A total binding assay using 10 μM of candidate compound against [^3H]-citalopram was completed to identify compounds that bound to SERT. One compound displaced the radioligand comparable to the positive control paroxetine and was chosen for full concentration response curves. Additionally, each compound was tested at 10 μM for inhibition potential and release potential using [^3H]-serotonin. Two compounds blocked serotonin below 50% of vehicle and concentration response curves were completed. No compound promoted the release of stored substrate in the release assays.

Methodology

Candidate Compound Preparation. The nine candidate compounds identified from the virtual screen were purchased from Thermo Fisher as part of the Maybridge chemical collection. To prepare the compounds for pharmacological testing, the 5 mg of candidate compounds were suspended in DMSO under sterile conditions to achieve 10 mM concentration stocks.

Cell Culture. To pharmacologically classify the candidate compounds against SERT using *in vitro* experiments, a Human Embryonic Kidney – 293 (HEK293) stably transfected to express the human SERT (HEK293-SERT) was acquired as a generous gift from Dr. Randy D. Blakely (Florida Atlantic University, Boca Raton, FL). The initial culturing of the HEK293-SERT cells was completed by thawing the cryovial by hand and resuspending the cells with 10 ml of media in a 15 ml tube, which was centrifuged at 10,000 rpm for 10 minutes to separate the freezing media (10% DMEM:F-12, 10% DMSO, 80% FBS) from the cells. Following the aspiration of the liquid within the 15 ml tube, the pellet of cells was resuspended with 12 ml of media (DMEM:F-12, 10% FBS, 1% Pen/Strep) and cultured in a medium sized flask (T75) at 37° C and 5% CO₂. The HEK293-hSERT cell line was cultured under the conditions as described (Tatsumi *et al.*, 1997) until confluence. Cells were then scraped into 15 ml screw tubes and lightly pelleted by centrifugation (500 rpm) for 10 minutes. The media was aspirated, and the remaining pellet was layered with medium before freezing at -20C.

Total Binding Assay. To assess whether the candidate compounds bound to SERT, radioligand binding assays were performed using [³H]-citalopram. To assess for specific binding, saturating (10µM) concentrations of sertraline was added to parallel sets of tubes. To calculate the total,

specific and non-specific binding of the 9 candidate compounds, the positive control (sertraline) and the vehicle (DMSO), 4 vials per compound were collected (2 vials for total binding and 2 vials for specific) in 24 well racks. 20 μ l of buffer (50 mM TRIS) was added to each vial (40 μ l for the total binding), followed by the addition of 20 μ l of the cold compound to achieve a final concentration of 10 μ M. 20 μ l of the hot radioligand [3 H]-citalopram (Perkin Elmer, citalopram, [N-METHYL- 3 H], product # NET1039250UC) was added using a 1/42 dilution to achieve a final concentration of 16 nM. Two hundred μ l of the membrane preparations were then added to each vial, which was calculated to contain 1.6 mg of protein per ml or 320 μ g of protein per vial. Each vial was washed three times utilizing a 0.5% PEI soaked filter with a Brandel Harvester. The filter for each sample was collected in a scintillation vial with 5 ml of fluid and counted with a scintillation counter. The total, specific and non-specific binding was then normalized to the amount of protein present in the membrane preparation.

Competition Binding Assay. The candidate compounds determined from the total [3 H]-citalopram binding assays that demonstrated any specific binding were subjected to further analysis using competition binding assays using [3 H]-citalopram. Increasing concentration of the candidate compounds were run in the presence of a constant concentration of [3 H]-citalopram (16 nM). This was to calculate affinity of the candidate compounds to SERT (K_i). For each candidate compound tested and the positive control (sertraline), a rack consisting of 24 vials was used that contained 6 vials for total binding and duplicate vials for the drug concentrations ranging from 1 pM to 100 nM. Once the rack setup was complete, 20 μ l of buffer (50 mM TRIS) was added to each vial with 40 μ l added to the total binding vials. This was followed by the addition of the cold drug in 20 μ l amounts to achieve the desired final concentration. The hot radioligand [3 H]-citalopram was

added in 20 μ l amounts to each vial using a 1/42 dilution to get to a final concentration of 16 nM. The cell lysates were next added in 200 μ l amounts followed by vortexing and incubated at room temperature for 1 hour. A Brandel harvester with 0.5% PEI soaked filters was used to filter the 24 vials, which were washed 3 times. The filter for each sample was then collected within a scintillation vial with 5 ml of fluid and counted with a scintillation counter. Data points were fit by non-linear regression analysis and the best fit was determined through least squares fit.

Total [3 H]-Serotonin Uptake Inhibition. To assess whether or not the candidate compounds inhibited at all 3H-serotonin uptake, initial screens were performed using 10 μ M candidate compounds. This was conducted to identify any candidate compounds that demonstrated 50% or greater inhibition. The HEK293-SERT cells were cultured on 24 well plates precoated with poly-d lysine (PDL) over night at 37° C at 5% CO₂. The media within each well was aspirated with a vacuum pump and washed twice with 1 ml of KRH buffer. KRH buffer (0.5 ml) was added to each well followed by the addition of 0.5 μ l of the 10 mM candidate compound stock completed in duplicate. The vehicle (DMSO; wells 1 and 2), positive control (citalopram; wells 3 and 4), and the basal response (no treatment; wells 23 and 24) were measured in duplicate. After the addition of the candidate compound or control, each well was incubated at room temperature for ten minutes. The [3 H]-serotonin stock was prepared by addition of KRH buffer in a 1:1 ration (13 μ l serotonin to 13 μ l KRH buffer). Following the ten-minute drug incubation, 1 μ l of [3 H]-serotonin mixture was added to each well for 5 minutes before aspiration and subsequently washed twice with KRH buffer to end the uptake. To assess the concentration of the [3 H]-serotonin within the cells, 1 ml of SDS was added to each well and shaken at room temperature for 1 hour to break

open the cells, which were further scraped and transferred to scintillation vials with 5 ml of scintillation fluid and counted with scintillation counter.

Concentration Response [³H]-Serotonin Uptake Inhibition. Candidates that were found to inhibit [³H]-5HT uptake by 50% or greater were subjected to further analysis by constructing concentration response curves using concentrations of compounds between 100 pM to 1 μM. This was completed to calculate potency and efficacy of compounds which were then compared to the vehicle (DMSO) and the positive control Citalopram. Data points were fit by non-linear regression analysis using variable slopes. Potency, IC₅₀, or efficacy were calculated.

[³H]-Serotonin Release Assay. To assess if any of the candidate compounds promoted the release of [³H]-5HT (Perkin Elmer, 5-hydroxy tryptamine, [³H], product # NET1167250UC) from within the cell, a serotonin release assay was completed using [³H]-5HT. The candidate compounds, vehicle (DMSO), positive control (citalopram), and basal response (no treatment) were measured in triplicate for this assay. The HEK293-SERT cells were cultured in PDL coated 24 well plates overnight at 37°C with 5% CO₂ and 100% humidity, which was aspirated and washed twice with KRH buffer. The [³H]-5HT stock mixture for this experiment was created using a 1:1 ratio of radioligand to KRH buffer (15 μl [³H]-5HT with 15 μl KRH buffer). Each well received 0.5 ml of KRH buffer followed by the addition of 1 μl of [³H]-5HT and incubated at room temperature for 30 minutes. Each well was aspirated of its media and washed with 0.5 ml of KRH buffer both of which were collected in a scintillation vial (count 1; load). The plates were reloaded with 0.5 ml of KRH buffer and 0.5 μl of the 10 mM candidate compound stocks were added to each well and incubated at room temperature for 30 minutes. The media was then aspirated, and each well

was washed with 0.5 ml of KRH buffer, which was collected in scintillation vials and counted (count 2; release). To count the contents of the cells, 1 ml of SDS buffer was added to each well and the plates were shaken at room temperature for 1 hour. The cells were scrapped and collected in scintillation vials (count 3; load). The uptake efficiency of the experiment was calculated by dividing the total (count 1) by the load (count 3). To examine the release of [³H]-5HT, the release (count 2) normalized by the load (count 3) as release / load. The released [³H]-5HT was also examined with its relationship to the initial amount of [³H]-5HT added by dividing the release (count 2) by the total (count 1).

GPCR Screen from the PDSP. To determine the potential selectivity of the candidate compounds, the Mark Roth lab at the University of North Carolina completed a functional screen against a panel of GPCRs containing over 300 receptors including the serotonin, dopamine, and norepinephrine receptors (full list of receptors found in Appendix Tables A.2-A.11). The PDSP used a PRESTO-TANGO assay, which is a modified arrestin assay designed to promote luminescence upon activation of the GPCR (Kroeze *et al.*, 2015). The candidate compounds were tested at a 3 μM final concentration completed with quadruplicate with the dopamine d2 agonist quinpirole at 400 nM concentration serving as the positive control. The complete results can be found in Appendix Tables A.2 – A.11.

Results

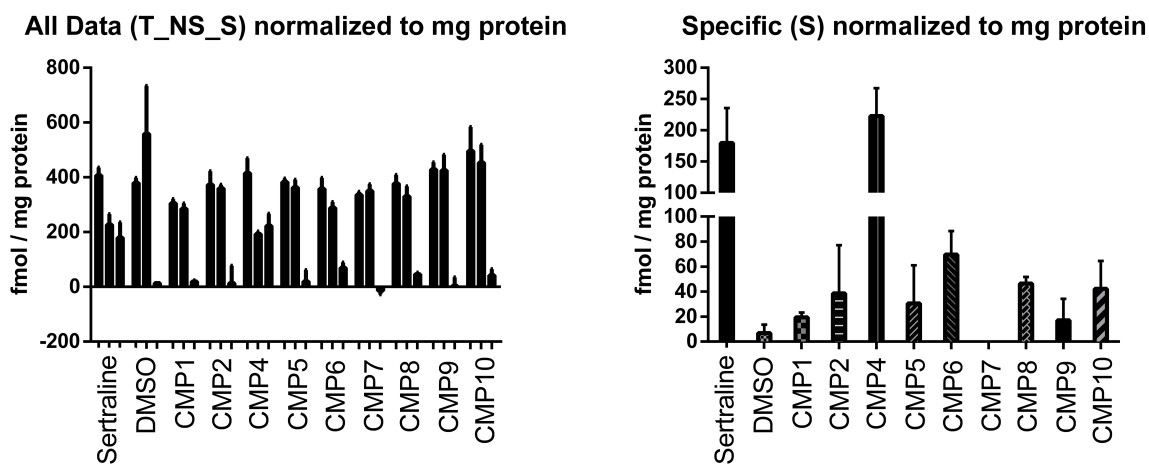
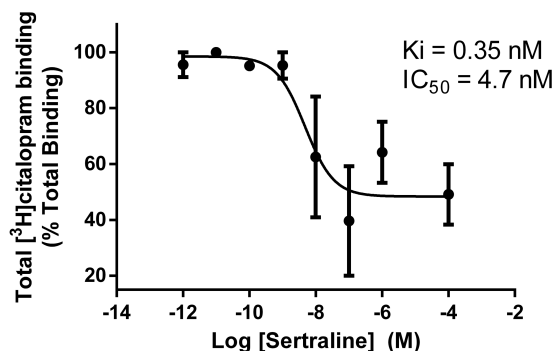
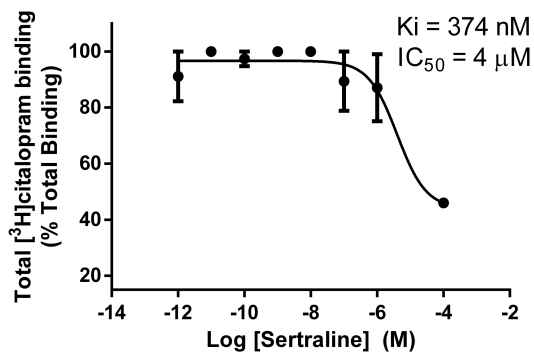


Figure 3.3: Total Binding Analyses of Candidate Compounds to SERT. Candidate compounds (1, 2, 4, 5, 6, 7, 8, 9, 10) were screened for their ability to bind to SERT using [³H]-citalopram [16 nM]. Data in (A) depict total, non-specific and specific binding of [³H]-citalopram to SERT normalized by total protein while those depicted in (B) represent specific binding only. Parallel sets of experiments using the positive SSRI control, sertraline (10 μ M) and the vehicle, DMSO were run. Each bar graph represents the mean \pm (SD) of preformed in duplicate.

A. Composite Binding Curve



B. Assay 1



C. Assay 2

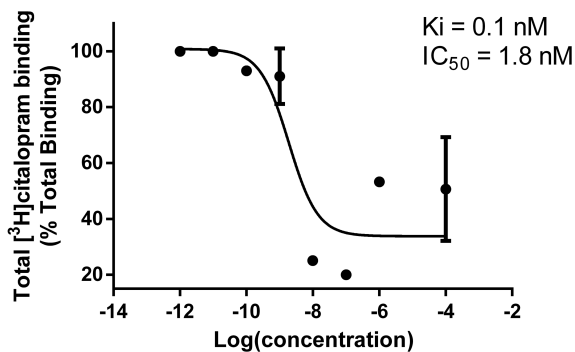
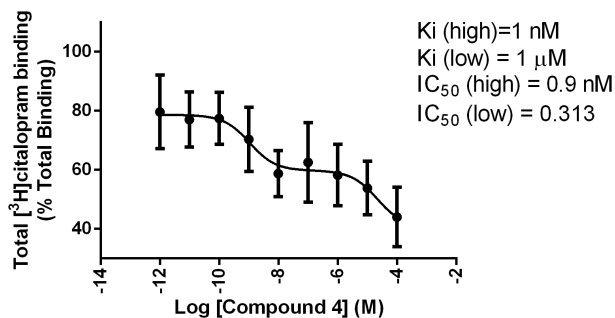
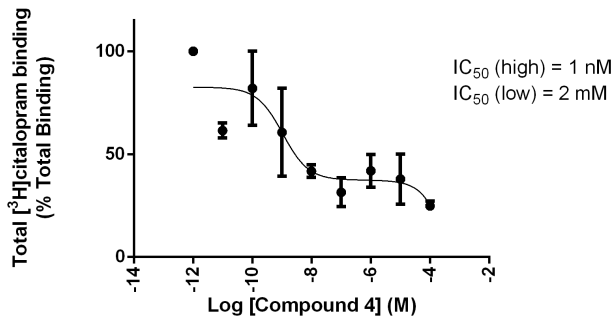


Figure 3.4: Competition of Sertraline for [³H]-Citalopram Binding to SERT. The affinity of sertraline (1pM-100mM) for SERT was assessed by competition binding using the radioligand [³H]-citalopram. A composite binding curve (A) was constructed from individual curves shown in (B) and (C). Individual (B, C) or composite (A) affinity (IC_{50} , K_i) values were derived by GraphPad Prism non-linear regression analyses least squares fit. Each data point represents the mean \pm (SD) of two independent experiments performed in duplicate for (A) or one experiment performed in duplicate (B, C).

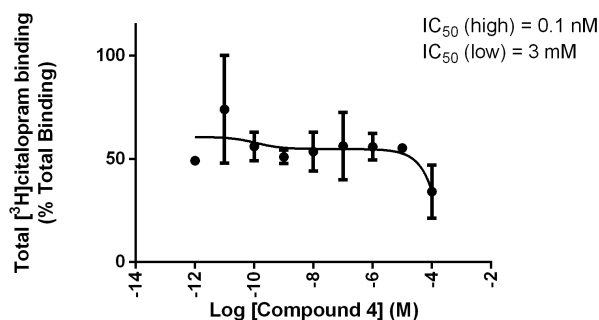
A. Composite



B. Assay 1



C. Assay 2



D. Assay 3

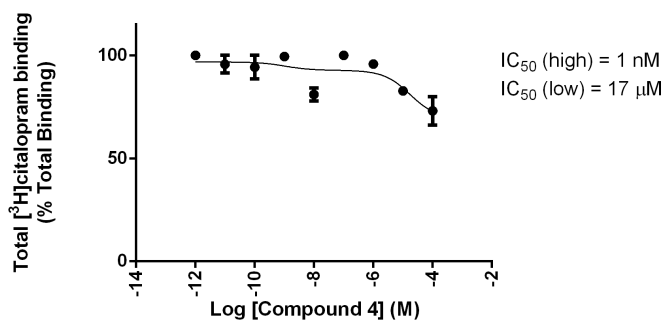


Figure 3.5: Competition of Compound 4 for $[^3H]$ -Citalopram Binding to SERT. The affinity of compound 4 (1pM-100mM) for SERT was assessed by competition binding using the radioligand $[^3H]$ -citalopram. A composite binding curve (A) was constructed from individual curves shown in (B), (C), and (D). Individual (B, C, D) or composite (A) affinity (IC_{50}) values were derived by GraphPad Prism non-linear regression analyses least squares fit. Each data point represents the mean of three independent experiments performed in duplicate for (A) or one experiment performed in duplicate (B, C, D).

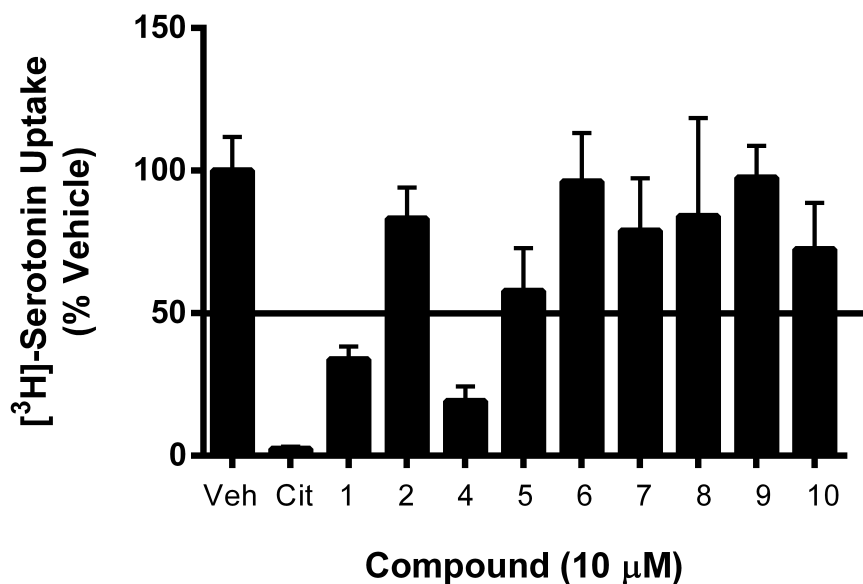
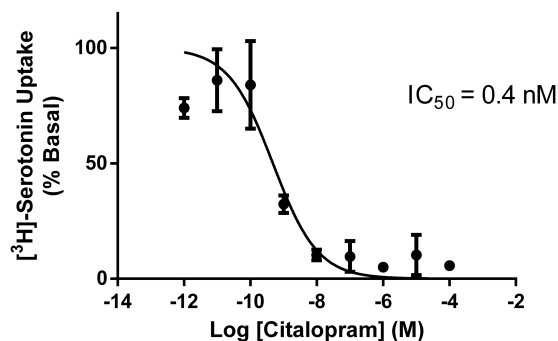
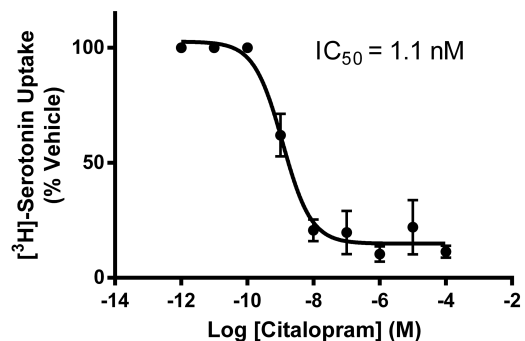
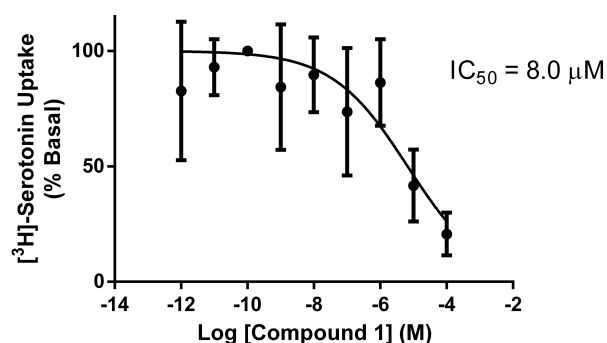
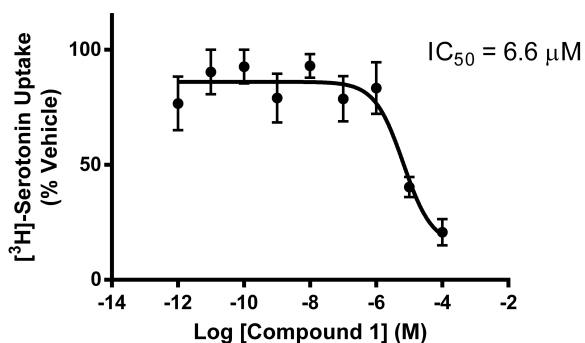


Figure 3.6 Single Point Substrate Uptake Inhibition of Candidate Compounds to SERT. Initial screen of hit compounds to inhibit [³H]-serotonin transport with HEK-293 cells stably expressing the SERT protein. The cells were preincubated with 10 μM concentration of each compound, citalopram, vehicle (DMSO), and basal. Data represents the mean +/- (SD) of 6 independent assays performed in duplicate. Active compounds were defined as inhibiting greater than 50% uptake of the vehicle.

Citalopram (Positive Control)



Compound 1



Compound 4

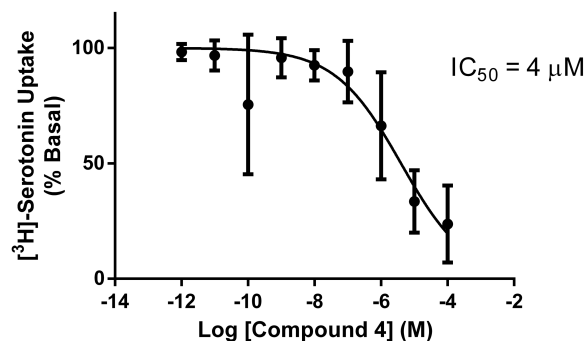
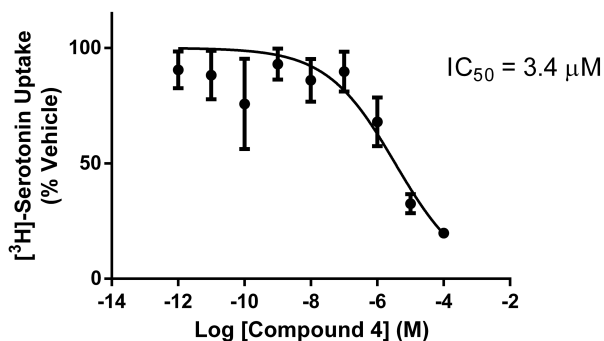


Figure 3.7: Concentration Response Substrate Uptake Inhibition with Citalopram, Compound 1, and Compound 4 for SERT. Compounds 1 and 4 were determined to be active inhibitors of the SERT protein (Figure 3.6). Full dose response curves (100 μM to 1 pM) were completed with compounds 1, 4, and citalopram (positive control). Data is presented as the mean expressed as percent vehicle (DMSO treatment) or percent basal (no treatment) +/- (SD) of 3-4 independent assays performed in duplicate.

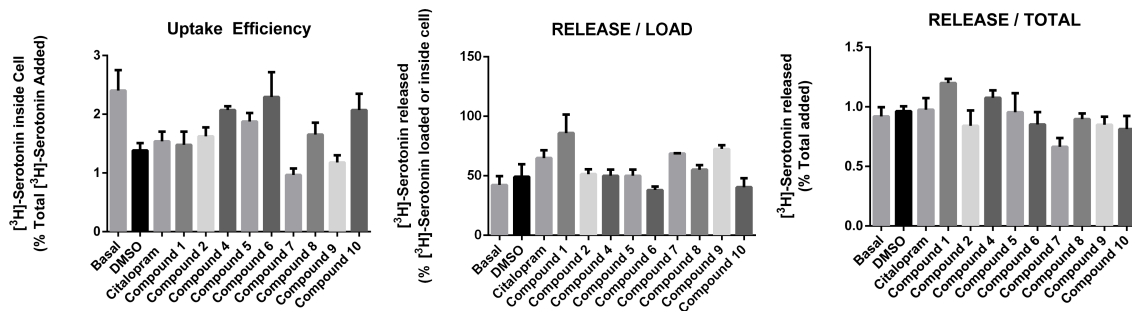


Figure 3.8: Release Assay with the 9 Compounds. To assess the ability to of the hit compounds to export $[^3\text{H}]$ -serotonin from HEK-293 cells stably expressing the SERT protein. Cells were preloaded with $[^3\text{H}]$ -serotonin for 30 minutes before incubation with hit compounds, citalopram, vehicle (DMSO), and basal response (no treatment). Experimental compounds and citalopram were assessed at 10 μM concentration. Media was collected and counted after 30-minute addition of $[^3\text{H}]$ -serotonin (total), after drug treatment (release), and within the cell (load). Assay represents the mean \pm (SD) performed in triplicate.

Compound	Predicted Affinity (S Score)	Specific Binding (fmol/mg protein)	[3H]-5HT Uptake Assay % Vehicle
Compound 4	-20.2	222.8	19.2
Compound 3	-19.7	-	-
Compound 1	-19.5	19.4	33.8
Compound 8	-19.4	46.4	84.1
Compound 10	-19.4	42.1	72.4
Compound 9	-19.2	3.5	97.5
Compound 2	-18.9	13.9	83.2
Compound 5	-18.9	19.6	57.8
Compound 6	-18.9	69.5	96.1
Compound 7	-18.8	0	78.9
Citalopram	-	-	2
Sertraline	-	179.2	-

Table 3.1 Comparison Between Virtual Screening Analysis and Pharmacology. Compounds are sorted by predicted binding affinity to compare the results of the Total Binding assay and the [³H]-5HT uptake assay. Compounds identified as inhibitors of SERT are highlighted in yellow. The SSRI controls are listed at the bottom for each assay.

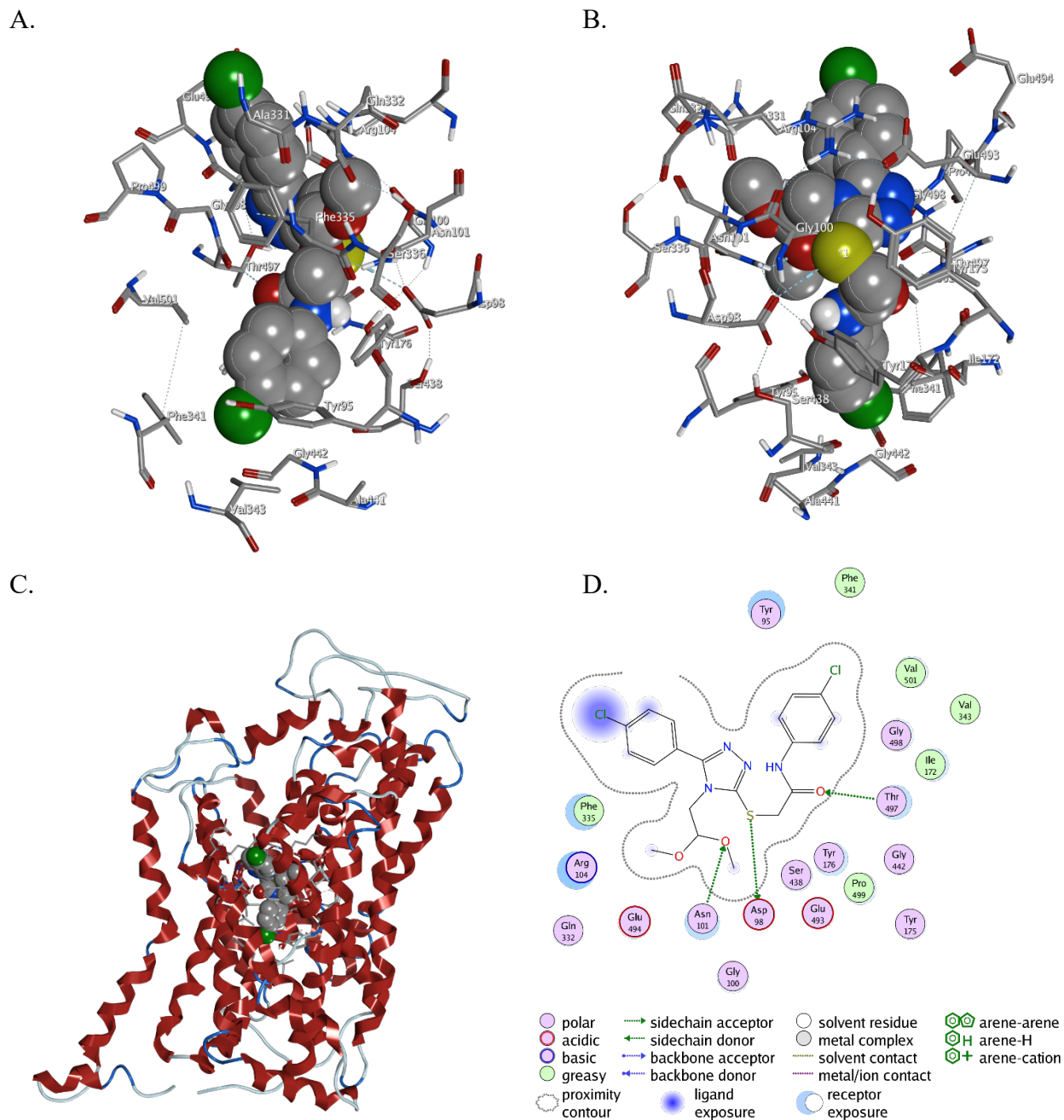


Figure 3.9: Binding Interactions Between Compound 1 and the S1 Binding Pocket of SERT. Two vantage points of compound 1 in the space filling model is shown in panels A and B, which the overall position of the compound within SERT is shown in panel C. To clarify the binding interactions shown in A and B, a 2D representation is shown in panel D.

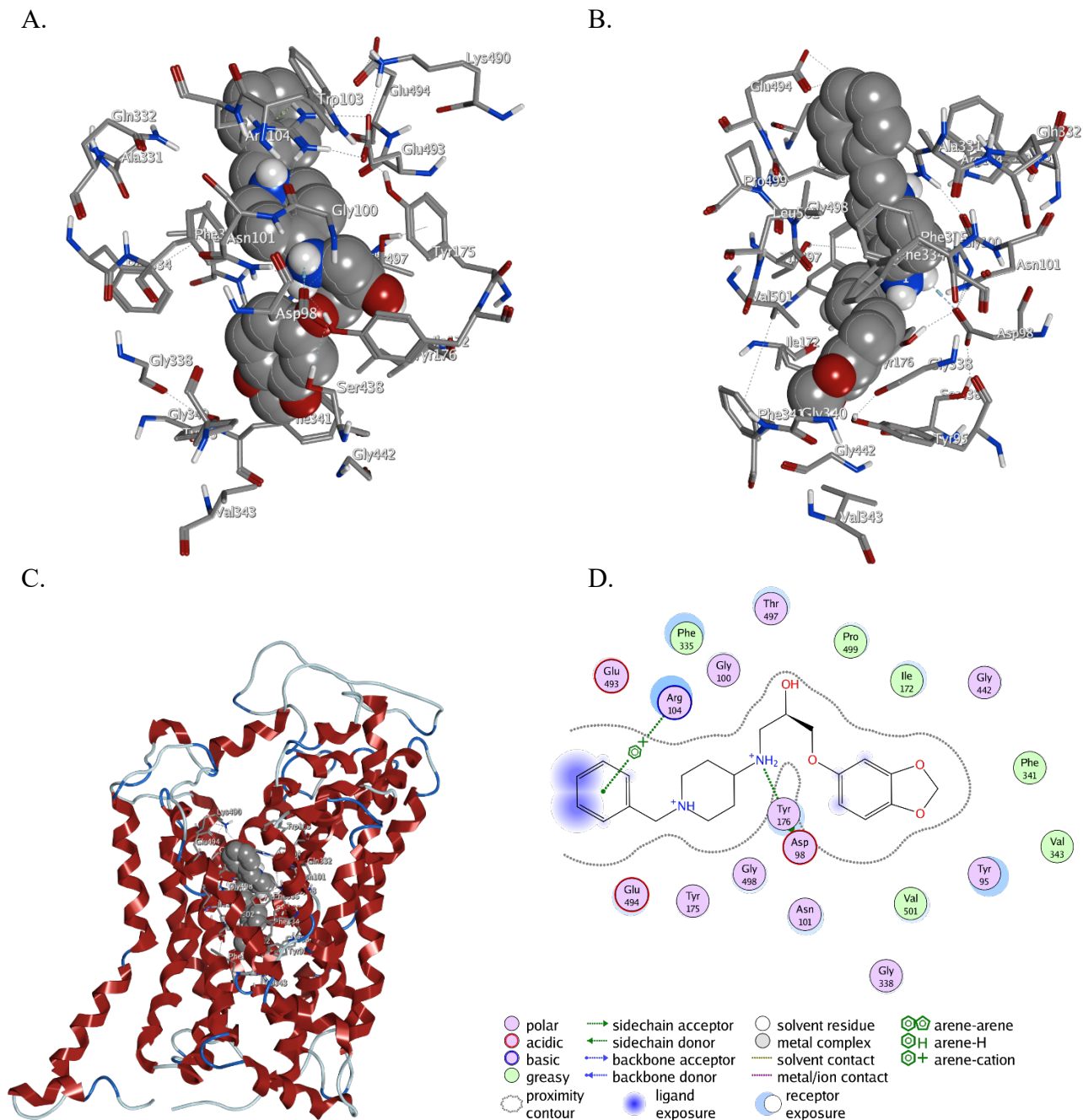


Figure 3.10: Binding Interactions Between Compound 4 and the S1 Binding Pocket of SERT. Two vantage points of compound 4 in the space filling model is shown in panels A and B, which the overall position of the compound within SERT is shown in panel C. To clarify the binding interactions shown in A and B, a 2D representation is shown in panel D.

Results

Total Binding Assay

To establish if any of the 9 experimental compounds bound to the SERT protein, a total binding assay was completed utilizing [³H]-citalopram. The total binding (T), non-specific binding (NS) and specific binding (S) values for each experimental compound were recorded along with the positive control sertraline and the vehicle DMSO, which were normalized to mg of protein used in the assay (Figure 3.3A) and plotted with the isolated specific binding (Figure 3.3B). Compound 4 (222.8 fmol / mg protein) showed comparable binding to sertraline (179.2 fmol / mg protein). Compounds 1 (19.4 fmol / mg protein), 6 (69.5 fmol / mg protein), 8 (46.4 fmol / mg protein), and 10 (42.1 fmol / mg protein) showed limited specific binding while compounds 2, 5, 7, and 9 had negligible specific binding.

Competition Binding Assays

To further define the binding profile of the experimental compounds that displayed specific binding in the total binding assay (Compounds 1, 4, 6, 8, and 10), competitive binding assays were completed using concentrations of the candidate compounds ranging from 1 pM to 100 mM against 16 nM of [³H]-citalopram. Assays for compounds 1, 6, 8, and 10 were completed but displayed no convergence. IC₅₀ values (high and low) for calculated as a composite graph (IC₅₀ high of 0.9 nM and an IC₅₀ low of 313 mM) and as calculated from averaged individual experiments for compound 4 (0.5 nM (range 250 pm to 1.07 nM) and IC₅₀ low of 0.4 mM (range 90 μM to 2.6 mM) (Figure 3.5). The positive control sertraline was reported to have a K_i value of 0.35 nM (Figure 3.4).

Total [³H]-Serotonin Uptake Inhibition

To determine if the novel compounds are SERT inhibitors, a single concentration (10 μM) of compounds 1 through 10 was administered to stably transfected SERT cell line before addition of [³H]-5HT to examine if the novel compounds blocked the transport of the serotonin. Inhibitors are defined as compounds blocking at least 50% of [³H]-5HT compared to vehicle. Citalopram was used as a positive control and resulted in 2% of vehicle (98% inhibition of uptake). Compounds 1 (33% of vehicle) and compound 4 (19% of vehicle) were classified as inhibitors, while compound 5 was a borderline candidate (57% of vehicle) due to the standard error falling below the 50% threshold (Figure 3.6).

Concentration Response [³H]-Serotonin Uptake Inhibition

To establish the potency of compounds 1 and 4 as inhibitors of SERT, concentration response curves were conducted using 1pM to 10 mM concentrations (Figure 3.7). The positive control citalopram was chosen in an IC₅₀ of 1.1 nM compared to vehicle and 0.4 nM compared to basal. Compound 1 resulted in an IC₅₀ of 6.6 μM compared to vehicle (8.0 μM compared to basal response), while compound 4 had an IC₅₀ of 3.4 μM compared to vehicle (4 μM compared to basal response).

[³H]-Serotonin Release Assay

To assess the novel compounds ability to release (export) [³H]-5HT from within the HEK-293 cells, the cells were preloaded with [³H]-5HT for thirty minutes before incubation with compounds 1 through 10. The media was collected for counting after the 30-minute addition of [³H]-5HT (total), after drug treatment (release), and stored within the cell (load). To assess the uptake efficiency (load (5HT within the cell) divided by total 5HT added), which was under 3% for the 9

experimental compounds, positive control (citalopram), basal (no treatment) and vehicle (DMSO) groups. To assess the release of [³H]-5HT, the release measurement was divided by the load and showed no statistical difference between the 9 experimental compounds and citalopram compared to the vehicle DMSO group. To assess if the total [³H]-5HT initially added affected the released amount, the release measurement was divided by the total measurement. In all groups, the release / total was under 1.5% with no statistical differences compared to vehicle (Figure 3.8).

Discussion

The work within this doctoral thesis was completed with the goal of using computational modeling to rationally discover novel inhibitors of hSERT. The computational approach, detailed in Chapter 2, targeted the orthosteric binding pocket (S1) of hSERT using MOE software. The virtual screen analytically identified 10 candidate compounds with 9 compounds commercially available for purchase from Thermo-Fisher. The initial pharmacological analysis was completed using human embryonic kidney cells – 293 (HEK-293) that stably expressed hSERT, which was generously donated by Dr. Randy D. Blakely of the Florida Atlantic University, and examined binding, efficacy as inhibitors, and release potential. In addition, the agonist functional data was generously provided by the National Institute of Mental Health's Psychoactive Drug Screening Program, Contract # HHSN-271-2018-00023-C (NIMH PDSP). The NIMH PDSP is Directed by Bryan L. Roth at the University of North Carolina at Chapel Hill and Project Officer Jamie Driscoll at NIMH, Bethesda MD, USA. The PDSP screened 8 of the 9 candidate compounds against a wide panel of GPCRs including the serotonin, dopamine and adrenergic receptors (see Appendix Tables A2-A11).

In order to determine if the candidate compounds bind to hSERT, a total binding assay was completed at an initial concentration of 10 μ M of compounds 1 through 10 and the positive control sertraline against [³H]-citalopram (Figure 3.3). This assay identified that 5 of the 9 compounds had specific binding to hSERT although only compound 4 (222.8 fmol / mg protein) had comparable specific binding compared to sertraline (179.2 fmol / mg protein). Compounds 1 (19.4 fmol / mg protein), compound 6 (69.5 fmol / mg protein), compound 8 (46.4 fmol / mg protein), and 10 (42.1 fmol / mg protein) were chosen for further evaluation with competitive binding assays along with compound 4, while compounds 2, 5, 7, and 9 were disregarded due to negligible specific

binding. Competition binding assays were completed using a range of concentrations from 1pM-100mM with sertraline as the positive control. The competition for compound 4 was analyzed as a composite graph (Figure 3.5A) comprised of three individual experiments (Figure 3.5 B, C, and D), and as an averaged value derived from the individual experiments with both situations having a 2-site fit. Data for the composite was recorded as K_i values (1 nM high and 1 μ M) and IC_{50} values (0.9 nM high and 313 mM low), while IC_{50} values were reported for the averaged values (0.5 nM high and 0.4 mM low). Compounds 1, 6, 8, and 10 were characterized with competition binding assays but the graphs were determined to be non-convergent. The positive control sertraline was also analyzed as a composite graph (Figure 3.4A) with a K_i of 0.35 nM and individual graphs (Figure 3.4B and C). Both the total binding and competitive binding assays were hindered by issues with high non-specific binding, which could be due to low receptor expression and the potential of the radioligand being “sticky”. In addition, the competitive binding assays were impacted by the concentration of [3 H]-citalopram used in the experiments. A concentration of 16 nM was chosen due to being roughly 80% of the B_{Max} value on recommendation by advisors but it was much higher concentration than reported in the literature. Compounds 1, 6, 8, and 10 were unable to displace the radioligand at that concentration, which combined with the high non-specific bindings led to no convergence when examining their competition binding curves.

The primary goal of this study was to identify inhibitors of hSERT through computational modeling. Therefore, the efficacy the candidate compounds were determined using a substrate uptake inhibition assay that measured each compound’s ability to inhibit the transport of [3 H]-5HT into the cell. The 9 compounds along with the positive control citalopram were initially tested at a 10 μ M concentration with inhibition being defined as a greater than 50% reduction of internal [3 H]-5HT compared to the vehicle DMSO (Figure 3.6). This criterion established compounds 1

(33% of vehicle) and 4 (19% of vehicle) as hSERT inhibitors and candidates for full concentration response curves. The efficacy of the SSRI citalopram was evident with the almost complete blockage of [³H]-5HT at 3% of uptake compared to vehicle. Compound 5 (56% of vehicle) was a borderline candidate for further examination due to its proximity to the 50% mark. When full concentration response curves were completed, compound 4 (IC₅₀ = 3.4 μM compared to vehicle) was found to be more potent than compound 1 (IC₅₀ = 6.6 μM compared to vehicle) (Figure 3.7) matching the results of the single point assay. The positive control citalopram was found to have an IC₅₀ of 1.1 nM compared to vehicle. A concentration response curve for compound 5 was initially examined but quickly abandoned when the 10 μM concentrations were found to above the 50% of vehicle mark to conserve limited [³H]-5HT supplies.

A [³H]-5HT release assay was the last pharmacological assay completed, which was used to determine if the candidate compounds act as “releasers” through efflux or reverse transport. Examples of releasers at the MATs include the amphetamine family of compounds most notably working through DAT. The [³H]-5HT release assay is essentially the reverse of the [³H]-5HT uptake inhibition assay with the radioligand being preloaded into the cells before the addition of the candidate compounds. The inhibitor citalopram was used as a positive control due to the lack of a releaser to use with this assay. To determine if the candidate compounds caused efflux, the amount of [³H]-5HT released was normalized to the amount of [³H]-5HT loaded into the cell (release / load; Figure 3.8B), which showed no statistical difference between the candidate compounds compared to vehicle. The release / load was comparable to the amount of baseline efflux seen in other studies. To determine if the initial concentration of [³H]-5HT added affected release, uptake efficiency (load / total) was assessed at under 3% for all candidate compounds and controls with no statistical difference compared to vehicle. Additionally, the release / total for

each compound was at under 1.5% for all compounds with no statistical difference compared to vehicle. Therefore, none of the 9 candidate compounds were determined to be releasers through SERT.

In total, this study targeted the S1 binding pocket of SERT and identified 10 candidate compounds for pharmacological analysis. Of the 9 compounds acquired, compound 1 and compound 4 were characterized as inhibitors of SERT with 6.6 μM and 3.4 μM IC_{50} values determined by the [^3H]-5HT uptake inhibition assay (Figure 3.7). To the authors knowledge, there have been 5 virtual screens targeting SERT reported in the literature with 4 studies that utilized LeuT based homology models and completed pharmacological analysis of the identified compounds. The lone study that utilized the hSERT crystal structure did not complete any pharmacology associated with the study. The results of the 5 studies along with the data from this study is summarized in Table 3.2. In comparison, the first virtual screen (Manepalli *et al.*, 2011) targeted the S2 site and identified two SERT ligands with 17 μM (compound SM-11) and 38 μM (compound SM-10) K_i values but were unable to block [^3H]-serotonin transport in uptake inhibition assay at 10 μM concentration (Manepalli *et al.*, 2011). A sister study from the same lab screening the DAT S2 binding pocket identified one compound (MI-17) that was selective towards SERT with a 284 nM K_i value over DAT and NET (Nolan *et al.*, 2011). MI-17 was developed into DJLDU-3-79 through molecular hybridization improving its binding affinity (K_i value) to 37 nM and its [^3H]-5HT uptake inhibition potency to 441 nM from 1167 nM (MI-17) (Nolan *et al.*, 2011). One compound (ATM7) from the Kortagere *et al.* was established as an allosteric modulator of SERT that increased [^3H]-5HT uptake and potentiated [^3H]-5HT efflux elicited by 3,4-methylenedioxy-N-methylamphetamine (MDMA; ecstasy) through stabilizing an OF conformation of SERT (Kortagere *et al.*, 2013).

SERT Virtual Screen	Computational Model	Site Targeted	Compounds Tested	Pharmacological Analysis	Major Findings
Manepalli et al., 2011	Human SERT Homology Model LeuT based (PDB. id 2A65)	S2	10	Competition Binding Assay [3H]-5HT Uptake assay	Identified 2 SERT ligands (SM-10 with 38 μ M and SM-11 17 μ M) Neither compound inhibited [3H]-5HT uptake
Kortagere et al., 2013	Human SERT Homology Model LeuT based (PDB. id)	Allosteric site / S2	10	Binding Assay [3H]-5HT Uptake assay [3H]-5HT Release Assay	1 Allosteric Modulator (ATM7) with Kd of 8.3 nM Increased [3H]-5HT uptake at low concentrations Potentiated [3H]-5HT efflux by MDMA
Gabrielson et al., 2014	Human SERT Homology Model LeuT based (PDB. id)	S1	202	Competition Binding Assay	Identified 24 compounds with Ki < 1 μ M
Nolan et al., 2014	Human SERT Homology Model LeuT based (PDB. id 2A65)	S1	19	Competition Binding Assay [3H]-5HT Uptake Assay	Identified 4 compounds with Ki values from 668 to > 20,000 nM IC50 values ranged from 3845 to > 20,000 nM
Erol et al., 2017	Human SERT Crystal Structure PDB id.	S1 and S2	Did Not Complete Pharmacological Analysis	NA	NA
Wasko	Human SERT Crystal Structure PDB id. 5I73	S1	9	Competition Binding Assay [3H]-5HT uptake assay [3H]-5HT Release Assay	Compound 4 had Ki of 1nM (high) and 1 μ M (low) Compound 4 had IC50 of 3.4 μ M and compound 1 had 6.6 μ M No Compound caused efflux of [3H]-5HT

Table 3.2: Comparison of Pharmacology from SERT Virtual Screens. Each study is summarized by model used, site targeted, number of compounds tested, pharmacological assays used, and by major findings.

The publication of the LeuBAT and dDAT structures altered the focus of antidepressant binding from S2 to S1 (Gabrielsen *et al.*, 2014; Nolan *et al.*, 2014). Gabrielson *et al.* examined 202 identified compounds for SERT binding and characterized 37 compounds with having a $K_i < 3100$ nM (Gabrielsen *et al.*, 2014). The second S1 screen focused on 19 compounds for pharmacological analysis, which characterized 4 compounds with K_i values ranging 668 to >20,000 nM and IC_{50} values ranging from 3845 to >20,000 nM (Nolan *et al.*, 2014). This is comparable to the 2 compounds identified within this virtual screen that have IC_{50} values of 3400 nM (compound 4) and 6600 nM (compound 1) (Figure 3.7).

After the internal pharmacological analysis was completed, the 9 candidate compounds were evaluated using the NIMH's PDSP service through the Bryon Roth lab at the University of North Carolina. A functional screen was chosen against a wide panel of over 300 GPCRs including the serotonin, dopamine, norepinephrine, adrenergic, and opiate receptors (see Appendix Table A3 for a complete list of screened receptors). This was completed using a parallel receptor-ome expression and screening via transcriptional output – transcriptional activation following arrestin

translocation (PRESTO-TANGO) assay, which is a modified β -arrestin recruitment assay that links receptor activation to the promotion of a transcription factor for luminescence (Kroeze *et al.*, 2015). The PDSP examined 8 of the 9 submitted compounds at a concentration of 3 μ M (Appendix Tables A3-11) while the dopamine d2 receptor agonist quinpirole (400 nM concentration) served as the positive control. Compound 8 was displayed 47% activation of the atypical chemokine receptor 3 (CXCR7), which is structurally similar to the chemokine receptors but lack G-protein recruitment upon activation (Ulvmar *et al.*, 2011). Originally an orphan receptor, CXCL11 and CXCL12 were identified as ligands with the receptor proposed to promote their sequestration (Ulvmar *et al.*, 2011). Recent studies have suggested that the atypical chemokine receptor 3 is an atypical opiate receptor that binds many of the endogenous opiate peptides and prevents their activation of the classical opiate receptors (Meyrath *et al.*, 2020). No other receptor within in panel displayed greater than 7% activation with any of the 8 experimental compounds screened by the PDSP although this does not preclude any of the compounds from acting in an antagonistic function. The PDSP Ki database, which catalogs the results of binding experiments, determined that the SSRIs bind to other receptors than the MATs. Receptors with a $K_i < 5 \mu$ M include the 5HT_{2A} (fluoxetine, sertraline), the 5HT_{2B} (fluoxetine), 5HT_{2C} (citalopram, fluoxetine, sertraline), alpha₁ adrenergic (citalopram, fluoxetine, paroxetine, sertraline), alpha₂ adrenergic (paroxetine, sertraline), muscarinic acetylcholine M1 (citalopram, fluoxetine, paroxetine, sertraline), M2 (fluoxetine), M3 (fluoxetine), M4 (fluoxetine), M5(citalopram), histamine H1 (citalopram, fluoxetine), and sigma 1 receptors (sertraline) (Ki Database; (Roth *et al.*, 2000)). Activation of 5HT₂ receptors within the brain are thought to contribute to many of the adverse effects of the SSRIs including anxiety, insomnia, irritability, while receptors within the spinal cord contribute to sexual dysfunction (Clayton *et al.*, 2014). Gastro intestinal issues are thought to be due to

activation of 5HT₃ receptors (Browning, 2015). The SSRI fluoxetine is a 5HT_{2C} antagonist (Ni and Miledi, 1997). The results of the PDSP screen suggest that the two identified SERT inhibitors (compound 1 and 4) may display an alternative side effect profile due to their lack of activation of any GPCR within the panel. Although the serotonin receptors could still be activated by the inhibition of SERT by these compounds. The results of the 9 candidate compounds against the DAT and NET proteins are still awaiting analysis from the PDSP.

With the initial pharmacology completed, comparisons between the molecular modeling completed in chapter 2 can begin to be compared to the total binding assay and the substrate uptake inhibition assay that tested each of the candidate compounds at 10 μ M concentration (Table 3.1). Each candidate compound was sorted by the predicted affinity (S score), which ranked 1 compound scored in the -20s, 5 compounds in the -19s, and 4 compounds in the -18s. The first interesting observation is that compound 4 was ranked the highest in predicted affinity (S score = -20.2), total binding assay (specific binding = 222.8 fmol / mg protein), and [³H]-5HT uptake inhibition (19.2 % of vehicle). The second highest ranked compound by the modeling is compound 3, which was discontinued by Thermo-Fisher after the purchasing for this study was completed. Compound 1 was the third highest ranked compound by modeling (S score = -19.5) and was ranked second in the [³H]-5HT uptake inhibition (33.8 % of vehicle). While the results of compound 1 and 4 were favorably ranked in comparison, it should be reminded that each of the ten compounds were chosen in part due to their high predicted affinity ranking while weak binders in the benchmarking study were ranked with an S score under -13. Nonetheless, the data demonstrates that the virtual screen successfully identified 2 inhibitors of SERT in an analytically driven process.

Computational modeling can be used to provide insight into the differences between compound 1 and 4. Examination of the molecular interactions of compound 1 revealed that the chlorobenzene sits near the opening of the binding pocket forming an aromatic / hydrophobic interaction with F335, which is considered one of the external gating residues for SERT, with the

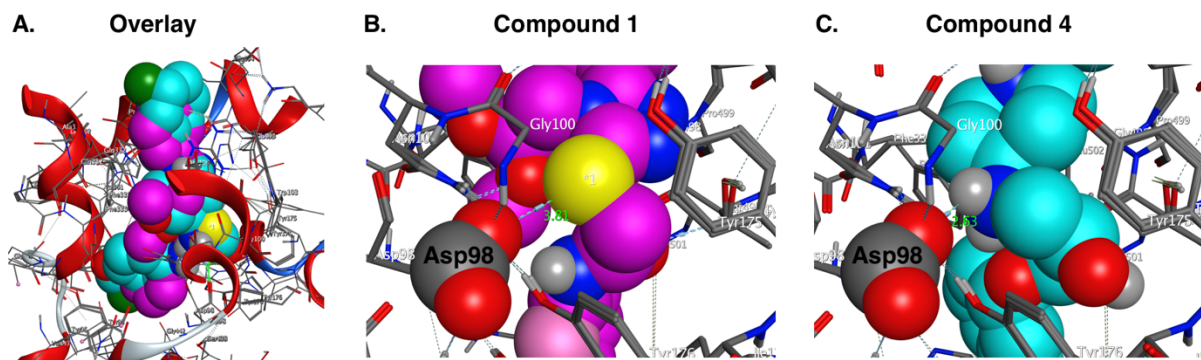


Figure 3.11: Overlay of Compound 1 and Compound 4 within the S1 Binding Pocket. (Panel A). The sulfur atom on compound 1 (magenta) forms a hydrogen bond with D98 separated by 3.81Å (Panel B). In comparison, the amine group on compound 4 (teal) forms an ionic interaction between D98 at 2.53Å (Panel C), which is most likely responsible for compound 4's greater potency.

chlorine atom exposed to the vestibule (Figure 3.9). Compound 1 forms hydrogen bonds with D98, N101, and T497. The second chlorobenzene group sits within a hydrophobic pocket near Y95, Y176, F341, G498, and V501. Compound 4 adopts a strikingly similar pose within the binding site compared to compound 1 (Figure 3.10). The benzene ring is partly exposed to the vestibule and forms a non-polar interaction with R104 (Figure 3.10). An important difference between the compounds is that compound 4 contains a protonated amine that forms an ionic interaction with D98. This can be more clearly seen in the distance between D98 with compound 1 (3.81 Å; Figure 3.11B) and compound 4 (2.53 Å; Figure 3.11C). This is most likely why compound 4 is a more potent inhibitor of SERT over compound 1. In comparison, the amine groups on the SSRIs citalopram and paroxetine are 4.1 Å and 3.1 Å away from D98 respectively, which was suggested as the reason why paroxetine has greater binding affinity over citalopram

(Coleman *et al.*, 2016). The benzodioxol group sits within a hydrophobic pocket surrounded by Y95, I172, F341, V343, and V501 similarly to the chlorobenzene group seen in compound 1 (Figure 3.10). It should be noted that both compound 1 and 4 sit higher up within the binding pocket compared to the crystalized SSRIs. Figure 3.12 shows an overlap of compound 4 (teal) with citalopram (yellow) from the PDB id. 5I73. The fluorophenol group on citalopram sits deeper within the S1 binding pocket surrounded by A169, I172, A173, Y175, and L443. The

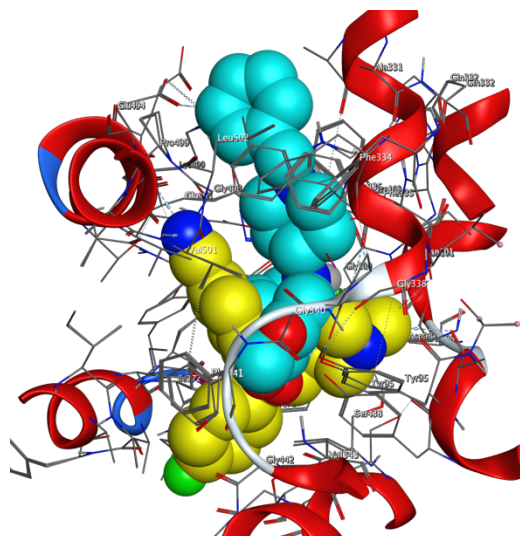


Figure 3.12: Comparison Between Compound 4 with Citalopram. Compound 4 (teal) sits higher within the binding pocket compared to citalopram (yellow).

computational modeling provides some insight into the two inhibitors identified by the virtual screen.

Chapter 4: Strengths and Limitations

Strengths

The computational approach utilized for this study thoroughly examined the performance of the docking software against SERT with benchmarking using a test set of known ligands. This provided the best opportunity to identify potential inhibitors and establish confidence that the software would filter / rank unfavorably unlikely compounds. Additionally, this study utilized the the S1 binding pocket of the hSERT crystal structure rather than a LeuT based model, which was utilized in the four virtual screens that were validated with pharmacological analysis. Nine compounds were purchased and evaluated for binding, inhibition, and release potential with 2 compounds (compounds 1 and 4) established as SERT inhibitors with low μM IC_{50} values while the PDSP results concluded that the compounds displayed selectivity by not activating any of the serotonin, dopamine or norepinephrine receptors during their GPCR functional screen. In total, this study had a 22% hit rate (2 / 9) compared to the accumulated 18% (44 / 251) of the prior 4 virtual screens. The last consideration is the cost benefit of the study with the overall cost of each compound purchased averaging \$80, which made the entire study a reasonable endeavor for an academic research lab.

Weaknesses

Many of the limitations of the study involve technical limitations of the pharmacological assays. The first being a high incidence of non-specific binding within the total binding and competition binding assays against [^3H]-citalopram. This could be due to a variety of factors including low transporter expression within the cell line and the radioligand being “sticky” through binding to the membrane preps rather than the transporter. In addition, the concentration of the radioligand used within the binding assays was chosen based on the recommendation of near the K_d value,

which was a concentration higher than reported in the literature and potentially led to the issues with the binding assays due to the candidate compounds not able to displace the radioligand. In addition, the limited supply of the radioligands ($[^3\text{H}]$ -serotonin and $[^3\text{H}]$ -citalopram) led to compromises in number of assays that could be with the focus taken on the substrate inhibition assays and the competition binding assays rather than the total binding and release assay. In addition, the positive control, the SSRI sertraline, used with the binding assays was old stock found within the laboratory, which the age of the compound may have contributed to some of the erratic results of the compound. Also, the release assay was completed using the inhibitor citalopram as a control due to the lack of a releaser such as amphetamine.

Chapter 5: Conclusions

This doctoral thesis is the accumulation of many years of work between the Surratt and Madura laboratories, which were among the first groups merging computational chemistry with classical pharmacology to target the MATs. One of the primary goals was to showcase how an academic research environment can be used to efficiently identify candidate compounds through computational methods, which is traditionally a costly endeavor of preclinical development. The publication of the LeuBAT and dDAT crystal structures in 2013 provided structural templates more closely aligned to the human SERT than the LeuT based SERT model used in the prior two virtual screens by the laboratories. Thus, construction of SERT homology models based on these templates began before shifting focus when the SERT crystal structures were eventually published by the Gouaux lab in 2016. The virtual screen completed within this study targeted the S1 binding site, which is now firmly believed to be the antidepressant binding site rather than the S2 site on the LeuT proteins. The computational approach utilized the MOE software and set out to thoroughly examine the scoring functions using a test set of known binders to identify the parameters that will provide the best opportunity to identify novel inhibitors within a reasonable amount of computational time to screen chemical libraries. The Maybridge chemical library as part of ThermoFisher was a logical library to screen due to its recent curation of the HitDiscoverer collection and the affordability of the compounds itself at under \$100 per compound. An analytical route was chosen to rank and filter the results of the virtual screen leading to a focus on the 10 compounds purchased from ThermoFisher. In all, only 9 compounds were able to be fulfilled for this study. With a HEK-293 cell line stably expressing SERT that was generously donated by Dr. Randy Blakely, assays were completed to assess binding, inhibition, and release potential of the candidate compounds to SERT. While only compound 4 had comparable specific binding

compared to the positive control sertraline in the total binding assay, compounds 1 and 4 were determined to inhibit SERT with IC₅₀s in the single μ M range. None of the compounds were shown to cause the release of serotonin. Computational modeling of compounds 1 and 4 revealed that both adopted similar orientations within the S1 site, but also revealed that compound 4 forming an ionic interaction with Asp98, which might be responsible for the increased potency. This study successfully demonstrated that the computational approach is a valid direction to identify inhibitors in a cost-effective manner and suitable for academic research laboratories.

Chapter 6: References

- (National Institute of Mental Health) (n.d.) Major Depression.
- Adams S V., and DeFelice LJ (2002) Flux coupling in the human serotonin transporter. *Biophys J* **83**:3268–3282.
- Aggarwal S, and Mortensen O V (2017) Overview of Monoamine Transporters. *Curr Protoc Pharmacol* **79**:12.16.1-12.16.17.
- Akil H, Gordon J, Hen R, Javitch J, Mayberg H, McEwen B, Meaney MJ, and Nestler EJ (2018) Treatment resistant depression: A multi-scale, systems biology approach. *Neurosci Biobehav Rev* **84**:272–288, Elsevier.
- Anderluh A, Klotzsch E, Reismann A WAF, Brameshuber M, Kudlacek O, Newman AH, Sitte HH, and Schutz GJ (2014) Single molecule analysis reveals coexistence of stable serotonin transporter monomers and oligomers in the live cell plasma membrane. *J Biol Chem* **289**:4387–4394.
- Andersen J, Ladefoged LK, Wang D, Bjerre Kristensen TN, Bang-Andersen B, Kristensen AS, Schiøtt B, and Strømgaard K (2015) Binding of the Multimodal Antidepressant Drug Vortioxetine to the Human Serotonin Transporter. *ACS Chem Neurosci* **6**:1892–1900.
- Andrusier N, Mashiah E, Nussinov R, and Wolfson HJ (2008) Principles of flexible protein-protein docking. *Proteins* **73**:271–89.
- Badalà F, Nouri-mahdavi K, and Raof DA (2008) Recent Advances in Ligand-Based Drug Design: Relevance and Utility. *Computer (Long Beach Calif)* **144**:724–732.
- Berman HM, Westbrook J, Feng Z, Gilliland G, Bhat TN, Weissig H, Shindyalov IN, and Bourne PE (2000) The Protein Data Bank. *Nucleic Acids Res* **28**:235–42.
- Best J, Nijhout HF, and Reed M (2010) Serotonin synthesis, release and reuptake in terminals: A mathematical model. *Theor Biol Med Model* **7**:1–26.
- Bourne HR, Bunney WE, Colburn RW, Davis JM, Davis JN, Shaw DM, and Coppen AJ (1968) Noradrenaline, 5-hydroxytryptamine, and 5-hydroxyindoleacetic acid in hindbrains of suicidal patients. *Lancet (London, England)* **2**:805–8.
- Browning KN (2015) Role of central vagal 5-HT₃ receptors in gastrointestinal physiology and pathophysiology. *Front Neurosci* **9**:1–10.
- Cartwright C, Gibson K, Read J, Cowan O, and Dehar T (2016) Long-term antidepressant use: patient perspectives of benefits and adverse effects. *Patient Prefer Adherence* **10**:1401–7.
- Chemical Computing Group (2017) Molecular Operating Environment (MOE), Chemical Computing Group ULC, Montreal, QC, Canada.
- Chen GL, and Miller GM (2013) Tryptophan hydroxylase-2: An emerging therapeutic target for stress disorders. *Biochem Pharmacol* **85**:1227–1233.
- Cheng MH, and Bahar I (2015) Molecular Mechanism of Dopamine Transport by Human Dopamine Transporter. *Structure* **23**:2171–2181, Elsevier Ltd.
- Cheng MH, and Bahar I (2019) Monoamine transporters: structure, intrinsic dynamics and allosteric regulation. *Nat Struct Mol Biol* **26**:545–556.
- Chessin M, Kramer ER, and Scott CC (1957) Modifications of the pharmacology of reserpine and serotonin by iproniazid. *J Pharmacol Exp Ther* **119**:453–60.
- Chilmonczyk Z, Bojarski A, Pilc A, and Sylte I (2015) Functional Selectivity and Antidepressant Activity of Serotonin 1A Receptor Ligands. *Int J Mol Sci* **16**:18474–18506.
- Chockalingam R, Gott BM, and Conway CR (2019) Tricyclic Antidepressants and Monoamine Oxidase Inhibitors: Are They Too Old for a New Look?, in *Antidepressants* pp 37–48.

- Clarke M, Razmjou S, Prowse N, Dwyer Z, Litteljohn D, Pentz R, Anisman H, and Hayley S (2017) Ketamine modulates hippocampal neurogenesis and pro-inflammatory cytokines but not stressor induced neurochemical changes. *Neuropharmacology* **112**:210–220.
- Clayton AH, Croft HA, and Handiwala L (2014) Antidepressants and sexual dysfunction: mechanisms and clinical implications. *Postgrad Med* **126**:91–9.
- Coleman JA, and Gouaux E (2018) Structural basis for recognition of diverse antidepressants by the human serotonin transporter. *Nat Struct Mol Biol*, doi: 10.1038/s41594-018-0026-8, Springer US.
- Coleman JA, Green EM, and Gouaux E (2016) X-ray structures and mechanism of the human serotonin transporter. *Nature* **532**:334–339, Nature Publishing Group.
- Coleman JA, Yang D, Zhao Z, Wen P-C, Yoshioka C, Tajkhorshid E, and Gouaux E (2019) Serotonin transporter–ibogaine complexes illuminate mechanisms of inhibition and transport. *Nature*, doi: 10.1038/s41586-019-1135-1, Springer US.
- Dahlin JL, Inglese J, and Walters MA (2015) Mitigating risk in academic preclinical drug discovery. *Nat Rev Drug Discov* **14**:279–294, Nature Publishing Group.
- Doerr A (2017) Cryo-electron tomography. *Nat Methods* **14**:34–34, Nature Publishing Group.
- Erol I, Aksoydan B, Kantarcioglu I, Salmas RE, and Durdagi S (2017) Identification of novel serotonin reuptake inhibitors targeting central and allosteric binding sites: A virtual screening and molecular dynamics simulations study. *J Mol Graph Model* **74**:193–202, Elsevier Inc.
- Eswar N, Webb B, Marti-Renom M a, Madhusudhan MS, Eramian D, Shen M-Y, Pieper U, and Sali A (2007) Comparative protein structure modeling using MODELLER. *Curr Protoc Protein Sci* **Chapter 2**:Unit 2.9.
- Fava M, and Davidson KG (1996) Definition and epidemiology of treatment-resistant depression. *Psychiatr Clin North Am* **19**:179–200.
- Ferguson JM (2001) SSRI Antidepressant Medications: Adverse Effects and Tolerability. *Prim Care Companion J Clin Psychiatry* **3**:22–27.
- Ferreira LG, Dos Santos RN, Oliva G, and Andricopulo AD (2015) Molecular docking and structure-based drug design strategies. *Molecules* **20**:13384–421.
- Fiser A, and Šali A (2003) MODELLER: Generation and Refinement of Homology-Based Protein Structure Models. *Methods Enzymol* **374**:461–491.
- Food and Drug Administration / United States of America (n.d.) Depression Medicines.
- Forrest LR, Zhang Y-W, Jacobs MT, Gesmonde J, Xie L, Honig BH, and Rudnick G (2008) Mechanism for alternating access in neurotransmitter transporters. *Proc Natl Acad Sci* **105**:10338–10343.
- Gabrielsen M, Kurczab R, Ravna AW, Kufareva I, Abagyan R, Chilmonczyk Z, Bojarski AJ, and Sylte I (2012) Molecular mechanism of serotonin transporter inhibition elucidated by a new flexible docking protocol. *Eur J Med Chem* **47**:24–37.
- Gabrielsen M, Kurczab Rafa, Siwek A, Ravna AW, Kristiansen K, Kufareva I, Abagyan R, Nowak G, Sylte I, and Bojarski AJ (2014) Identification of Novel Serotonin Transporter Compounds by Virtual Screening. *J Chem Inf Model* **9**:933–943.
- Gabrielsen M, Kurczab Rafal, Siwek A, Wolak M, Ravna AW, Kristiansen K, Kufareva I, Abagyan R, Nowak G, Chilmonczyk Z, Sylte I, and Bojarski AJ (2014) Identification of novel serotonin transporter compounds by virtual Screening. *J Chem Inf Model* **54**:933–943.
- Gillman PK (2007) Tricyclic antidepressant pharmacology and therapeutic drug interactions updated. *Br J Pharmacol* **151**:737–748.

- Green EM, Coleman JA, and Gouaux E (2015) Thermostabilization of the Human Serotonin Transporter in an Antidepressant-Bound Conformation. *PLoS One* **10**:e0145688.
- Grouleff J, Koldsø H, Miao Y, and Schiøtt B (2016) Ligand Binding in the Extracellular Vestibule of the Neurotransmitter Transporter Homologue LeuT. *ACS Chem Neurosci* **7**:600359.
- Haase J, and Brown E (2015) Integrating the monoamine, neurotrophin and cytokine hypotheses of depression — A central role for the serotonin transporter? *Pharmacol Ther* **147**:1–11, Elsevier Inc.
- Harvey MJ, Giupponi G, and De Fabritiis G (2009) ACEMD: Accelerating biomolecular dynamics in the microsecond time scale. *J Chem Theory Comput* **5**:1632–1639.
- Hillhouse TM, and Porter JH (2015) A brief history of the development of antidepressant drugs: from monoamines to glutamate. *Exp Clin Psychopharmacol* **23**:1–21.
- Hillisch A, Pineda LF, and Hilgenfeld R (2004) Utility of homology models in the drug discovery process. *Drug Discov Today* **9**:659–69.
- Hong WC, and Amara SG (2010) Membrane cholesterol modulates the outward facing conformation of the dopamine transporter and alters cocaine binding. *J Biol Chem* **285**:32616–32626.
- Huang S-Y, Grinter SZ, and Zou X (2010) Scoring functions and their evaluation methods for protein-ligand docking: recent advances and future directions. *Phys Chem Chem Phys* **12**:12899–12908.
- Huang S-Y, and Zou X (2008) An iterative knowledge-based scoring function for protein-protein recognition. *Proteins Struct Funct Bioinforma* **72**:557–579.
- ImmadiSETTY K, Geffert LM, Surratt CK, and Madura JD (2013) New design strategies for antidepressant drugs. *Expert Opin Drug Discov* **8**:1399–414, Informa UK, Ltd.
- Inglese J, Johnson RL, Simeonov A, Xia M, Zheng W, Austin CP, and Auld DS (2007) High-throughput screening assays for the identification of chemical probes. *Nat Chem Biol* **3**:466–79.
- Insel TR, and Wang PS (2009) The STAR*D trial: revealing the need for better treatments. *Psychiatr Serv* **60**:1466–7.
- Iurescia S, Seripa D, and Rinaldi M (2017) Looking Beyond the 5-HTTLPR Polymorphism: Genetic and Epigenetic Layers of Regulation Affecting the Serotonin Transporter Gene Expression. *Mol Neurobiol* **54**:8386–8403, Molecular Neurobiology.
- Jacobs BL (2002) Adult brain neurogenesis and depression. *Brain Behav Immun* **16**:602–609.
- Jørgensen TN, Christensen PM, and Gether U (2014) Serotonin-induced down-regulation of cell surface serotonin transporter. *Neurochem Int* **73**:107–112.
- Kessler RC, Petukhova M, Sampson NA, Zaslavsky AM, and Wittchen H-U (2012) Twelve-month and lifetime prevalence and lifetime morbid risk of anxiety and mood disorders in the United States. *Int J Methods Psychiatr Res* **21**:169–84.
- Kilic F, and Rudnick G (2000) Oligomerization of serotonin transporter and its functional consequences. *Proc Natl Acad Sci U S A* **97**:3106–3111.
- Kortagere S, Fontana ACK, Renée Rose D, and Mortensen OV (2013) Identification of an allosteric modulator of the serotonin transporter with novel mechanism of action. *Neuropharmacology* **72**:282–290, Elsevier Ltd.
- Krishnamurthy H, and Gouaux E (2012) X-ray structures of LeuT in substrate-free outward-open and apo inward-open states. *Nature* **481**:469–74, Nature Publishing Group.
- Krishnan V, and Nestler EJ (2008) The molecular neurobiology of depression. *Nature* **455**:894–

902.

- Kristensen AS, Andersen J, Jorgensen TN, Sorensen L, Eriksen J, Loland CJ, Stromgaard K, and Gether U (2011) SLC6 Neurotransmitter Transporters: Structure, Function, and Regulation. *Pharmacol Rev* **63**:585–640.
- Kroeze WK, Sassano MF, Huang X-P, Lansu K, McCorvy JD, Giguère PM, Sciaky N, and Roth BL (2015) PRESTO-Tango as an open-source resource for interrogation of the druggable human GPCRome. *Nat Struct Mol Biol* **22**:362–9.
- Kroeze Y, Zhou H, and Homberg JR (2012) The genetics of selective serotonin reuptake inhibitors. *Pharmacol Ther* **136**:375–400, Elsevier Inc.
- Kuhn R (1958) The treatment of depressive states with G 22355 (imipramine hydrochloride). *Am J Psychiatry* **115**:459–64.
- Lagarde N, Zagury JF, and Montes M (2015) Benchmarking Data Sets for the Evaluation of Virtual Ligand Screening Methods: Review and Perspectives. *J Chem Inf Model* **55**:1297–1307.
- Lang PT, Holton JM, Fraser JS, and Alber T (2014) Protein structural ensembles are revealed by redefining X-ray electron density noise. *Proc Natl Acad Sci U S A* **111**:237–242.
- Lin Z, Canales JJ, Björgvinsson T, Thomsen M, Qu H, Liu Q-R, Torres GE, and Caine SB (2011) Monoamine transporters: vulnerable and vital doorkeepers. *Prog Mol Biol Transl Sci* **98**:1–46.
- Lionta E, Spyrou G, Vassilatis D, and Cournia Z (2014) Structure-Based Virtual Screening for Drug Discovery: Principles, Applications and Recent Advances. *Curr Top Med Chem* **14**:1923–1938.
- Little KY, Kirkman JA, Carroll FI, Breese GR, and Duncan GE (1993) [125I]RTI-55 binding to cocaine-sensitive dopaminergic and serotonergic uptake sites in the human brain. *J Neurochem* **61**:1996–2006.
- Liu J, and Wang R (2015) Classification of current scoring functions. *J Chem Inf Model* **55**:475–482.
- López-Muñoz F, and Alamo C (2009) Monoaminergic neurotransmission: the history of the discovery of antidepressants from 1950s until today. *Curr Pharm Des* **15**:1563–86.
- López-Muñoz F, Alamo C, Rubio G, and Cuenca E (2004) Half a century since the clinical introduction of chlorpromazine and the birth of modern psychopharmacology. *Prog Neuropsychopharmacol Biol Psychiatry* **28**:205–8.
- Lovenberg W, Weissbach H, and Udenfriend S (1962) Aromatic L-amino acid decarboxylase. *J Biol Chem* **237**:89–93.
- Madura JD (2016) *Molecular Modeling*, 1st ed., Self.
- Manepalli S, Geffert LM, Surratt CK, and Madura JD (2011) Discovery of novel selective serotonin reuptake inhibitors through development of a protein-based pharmacophore. *J Chem Inf Model* **51**:2417–2426.
- Mendez-David I, David DJ, Darcet F, Wu M V., Kerdine-Römer S, Gardier AM, and Hen R (2014) Rapid anxiolytic effects of a 5-HT₄ receptor agonist are mediated by a neurogenesis-independent mechanism. *Neuropsychopharmacology* **39**:1366–1378.
- Meyrath M, Szpakowska M, Zeiner J, Massotte L, Merz MP, Benkel T, Simon K, Ohnmacht J, Turner JD, Krüger R, Seutin V, Ollert M, Kostenis E, and Chevigné A (2020) The atypical chemokine receptor ACKR3/CXCR7 is a broad-spectrum scavenger for opioid peptides. *Nat Commun* **11**, Springer US.
- Mohs RC, and Greig NH (2017) Drug discovery and development: Role of basic biological

- research. *Alzheimer's Dement Transl Res Clin Interv* **3**:651–657, Elsevier Inc.
- Nestler EJ, Barrot M, DiLeone RJ, Eisch AJ, Gold SJ, and Monteggia LM (2002) Neurobiology of depression. *Neuron* **34**:13–25.
- Ni YG, and Miledi R (1997) Blockage of 5HT_{2C} serotonin receptors by fluoxetine (Prozac). *Proc Natl Acad Sci U S A* **94**:2036–2040.
- Nichols DE, and Nichols CD (2008) Serotonin receptors. *Chem Rev* **108**:1614–41.
- Nicolaou KC (2014) Advancing the Drug Discovery and Development Process. *Angew Chemie* **126**:9280–9292.
- Nolan Tammy L, Geffert LM, Kolber BJ, Madura JD, and Surratt CK (2014) Discovery of Novel-Scaffold Monoamine Transporter Ligands via in Silico Screening with the S1 Pocket of the Serotonin Transporter. *ACS Chem Neurosci*, doi: 10.1021/cn500133b.
- Nolan Tammy L., Geffert LM, Kolber BJ, Madura JD, and Surratt CK (2014) Discovery of Novel-scaffold monoamine transporter ligands via in silico screening with the S1 pocket of the serotonin transporter. *ACS Chem Neurosci* **5**:784–792.
- Nolan TL, Lapinsky DJ, Talbot JN, Indarte M, Liu Y, Manepalli S, Geffert LM, Amos ME, Taylor PN, Madura JD, and Surratt CK (2011) Identification of a novel selective serotonin reuptake inhibitor by coupling monoamine transporter-based virtual screening and rational molecular hybridization. *ACS Chem Neurosci* **2**:544–552.
- Pagadala NS, Syed K, and Tuszynski J (2017) Software for molecular docking: a review. *Biophys Rev* **9**:91–102, Biophysical Reviews.
- Penmatsa A, Wang KH, and Gouaux E (2013) X-ray structure of dopamine transporter elucidates antidepressant mechanism. *Nature* **503**:85–90, Nature Publishing Group.
- Periole X, Zeppelin T, and Schiøtt B (2018) Dimer Interface of the Human Serotonin Transporter and Effect of the Membrane Composition. *Sci Rep* **8**:1–15.
- Piscitelli CL, Kean J, de Graaf C, and Deupi X (2015) A Molecular Pharmacologist's Guide to G Protein-Coupled Receptor Crystallography. *Mol Pharmacol* **88**:536–51.
- Piscitelli CL, Krishnamurthy H, and Gouaux E (2010) Neurotransmitter/sodium symporter orthologue LeuT has a single high-affinity substrate site. *Nature* **468**:1129–1132, Nature Publishing Group.
- Pletscher A, Shore PA, and Brodie BB (1955) Serotonin release as a possible mechanism of reserpine action. *Science* **122**:374–5.
- Pratt LA, Brody DJ, and Gu Q (2017) Antidepressant use among persons aged 12 and over: United States, 2011–2014 key findings data from the national health and nutrition examination survey. *Natl Cent Heal Stat* 2011–2014.
- Roth BL, Lopez E, Patel S, and Kroeze WK (2000) The Multiplicity of Serotonin Receptors: Uselessly Diverse Molecules or an Embarrassment of Riches? *Neurosci* **6**:252–262.
- Rudnick G (2007) What is an antidepressant binding site doing in a bacterial transporter? *ACS Chem Biol* **2**:606–9.
- Saha A, Varghese T, Liu A, Allen SJ, Mirzadegan T, and Hack MD (2018) An Analysis of Different Components of a High-Throughput Screening Library. *J Chem Inf Model* **58**:2057–2068, American Chemical Society.
- Samuels BA, Anacker C, Hu A, Levinstein MR, Pickenhagen A, Tsetsenis T, Madroñal N, Donaldson ZR, Drew LJ, Dranovsky A, Gross CT, Tanaka KF, and Hen R (2015) 5-HT_{1A} receptors on mature dentate gyrus granule cells are critical for the antidepressant response. *Nat Neurosci* **18**:1606–1616.
- Sandtner W, Stockner T, Hasenhuetl PS, Partilla JS, Seddik A, Zhang Y-W, Cao J, Holy M,

- Steinkellner T, Rudnick G, Baumann MH, Ecker GF, Newman AH, and Sitte HH (2016) Binding Mode Selection Determines the Action of Ecstasy Homologs at Monoamine Transporters. *Mol Pharmacol* **89**:165–75.
- Sansone RA, and Sansone LA (2012) Antidepressant adherence: Are patients taking their medications? *Innov Clin Neurosci* **9**:41–46.
- Santarsieri D, and Schwartz TL (2015) Antidepressant efficacy and side-effect burden: A quick guide for clinicians. *Drugs Context* **4**:1–12.
- Scheuing L, Chiu C-T, Liao H-M, and Chuang D-M (2015) Antidepressant mechanism of ketamine: perspective from preclinical studies. *Front Neurosci* **9**:1–7.
- Schmid JA, Scholze P, Kudlacek O, Freissmuth M, Singer EA, and Sitte HH (2001) Oligomerization of the Human Serotonin Transporter and of the Rat GABA Transporter 1 Visualized by Fluorescence Resonance Energy Transfer Microscopy in Living Cells. *J Biol Chem* **276**:3805–3810.
- Shaw DM, Camps FE, and Eccleston EG (1967) 5-Hydroxytryptamine in the hind-brain of depressive suicides. *Br J Psychiatry* **113**:1407–11.
- Shi L, Quick M, Zhao Y, Weinstein H, and Javitch J a. (2008) The Mechanism of a Neurotransmitter:Sodium Symporter—Inward Release of Na⁺ and Substrate Is Triggered by Substrate in a Second Binding Site. *Mol Cell* **30**:667–677.
- Shulman KI, Herrmann N, and Walker SE (2013) Current place of monoamine oxidase inhibitors in the treatment of depression. *CNS Drugs* **27**:789–797.
- Singh SK, Yamashita A, and Gouaux E (2007) Antidepressant binding site in a bacterial homologue of neurotransmitter transporters. *Nature* **448**:952–956.
- Sitte HH, Farhan H, and Javitch JA (2004) Sodium-dependent neurotransmitter transporters: oligomerization as a determinant of transporter function and trafficking. *Mol Interv* **4**:38–47.
- Sliwoski G, Kothiwale S, Meiler J, and Lowe EW (2014) Computational methods in drug discovery. *Pharmacol Rev* **66**:334–95.
- Smith K (2014) Mental health: a world of depression. *Nature* **515**:181.
- Tatsumi M, Groshan K, Blakely RD, and Richelson E (1997) Pharmacological profile of antidepressants and related compounds at human monoamine transporters. *Eur J Pharmacol* **340**:249–258.
- Tiger M, Varnäs K, Okubo Y, and Lundberg J (2018) The 5-HT 1B receptor - a potential target for antidepressant treatment. *Psychopharmacology (Berl)* **235**:1317–1334, Psychopharmacology.
- Ulvmar MH, Hub E, and Rot A (2011) Atypical chemokine receptors. *Exp Cell Res* **317**:556–68, Elsevier Inc.
- Wall SC, Gu H, and Rudnick G (1995) Biogenic amine flux mediated by cloned transporters stably expressed in cultured cell lines: amphetamine specificity for inhibition and efflux. *Mol Pharmacol* **47**:544–550.
- Wang H, Goehring A, Wang KH, Penmatsa A, Ressler R, and Gouaux E (2013) Structural basis for action by diverse antidepressants on biogenic amine transporters. *Nature* **503**:141–5, Nature Publishing Group.
- Wang KH, Penmatsa A, and Gouaux E (2015) Neurotransmitter and psychostimulant recognition by the dopamine transporter. *Nature* **521**:322–327.
- Wang S-M, Han C, Lee S-J, Patkar AA, Masand PS, and Pae C-U (2016) Vilazodone for the Treatment of Depression: An Update. *Chonnam Med J* **52**:91–100.

- Wasko M, Witt-Enderby PA, and Surratt CK (2018) DARK Classics in Chemical Neuroscience: Ibogaine. *ACS Chem Neurosci* acschemneuro.8b00294.
- Wasko MJ, Pellegrine K a., Madura JD, and Surratt CK (2015) A Role for Fragment-Based Drug Design in Developing Novel Lead Compounds for Central Nervous System Targets. *Front Neurol* **6**:1–11.
- Wawer MJ, Li K, Gustafsdottir SM, Ljosa V, Bodycombe NE, Marton MA, Sokolnicki KL, Bray MA, Kemp MM, Winchester E, Taylor B, Grant GB, Hon CSY, Duvall JR, Wilson JA, Bittker JA, Dančík V, Narayan R, Subramanian A, Winckler W, Golub TR, Carpenter AE, Shamji AF, Schreiber SL, and Clemons PA (2014) Toward performance-diverse small-molecule libraries for cell-based phenotypic screening using multiplexed high-dimensional profiling. *Proc Natl Acad Sci U S A* **111**:10911–10916.
- Wong DT, Perry KW, and Bymaster FP (2005) Case history: the discovery of fluoxetine hydrochloride (Prozac). *Nat Rev Drug Discov* **4**:764–74.
- Wong M, and Licinio J (2001) Research and treatment approaches to depression. *Nat Rev Neurosci* **2**:343–351.
- Yamashita A, Singh SK, Kawate T, Jin Y, and Gouaux E (2005) Crystal structure of a bacterial homologue of Na⁺/Cl⁻-dependent neurotransmitter transporters. *Nature* **437**:215–23.
- Yee AA, Savchenko A, Ignachenko A, Lukin J, Xu X, Skarina T, Evdokimova E, Liu CS, Semesi A, Guido V, Edwards AM, and Arrowsmith CH (2005) NMR and X-ray crystallography, complementary tools in structural proteomics of small proteins. *J Am Chem Soc* **127**:16512–7.
- Yohn CN, Gergues MM, and Samuels BA (2017) The role of 5-HT receptors in depression. *Mol Brain* **10**:28, Molecular Brain.
- Youdim MBH, Edmondson D, and Tipton KF (2006) The therapeutic potential of monoamine oxidase inhibitors. *Nat Rev Neurosci* **7**:295–309.
- Zeller, E.A., Barsky, J., Fouts, J.R, Kirchheimer, W.F., Van Orden LS (1952) Influence of isonicotinic acid hydrazide (INH) and 1-isonicotinyl-2-isopropyl hydrazide (IIH) on bacterial and mammalian enzymes. *Experientia* **8**:349–350.
- Zeppelin T, Ladefoged LK, Sinning S, and Schiøtt B (2019) Substrate and inhibitor binding to the serotonin transporter: Insights from computational, crystallographic, and functional studies. *Neuropharmacology*, doi: 10.1016/j.neuropharm.2019.02.030.
- Zhang D, Zhao Q, and Wu B (2015) Structural Studies of G Protein-Coupled Receptors. *Mol Cells* **38**:836–42.
- Zhou Z, Zhen J, Karpowich NK, Law CJ, Reith MEA, and Wang D-N (2009) Antidepressant specificity of serotonin transporter suggested by three LeuT-SSRI structures. *Nat Struct Mol Biol* **16**:652–7.

Appendix

Compound Name	Experimental Binding Affinity (kcal)	Predicted Binding Affinity (S score)
Fluoxetine	-12.9	-15.2
Citalopram	-12.58	-16.51
Amitriptyline	-11.87	-13.61
Desipramine	-11	-12.85
Nortriptyline	-10.99	-13.19
Amoxapine	-10.26	-14.7
Doxepin	-10.17	-14.27
Trazodone	-9.64	-15.4
Etoperidone	-8.58	-15.8
Nomidensine	-8.5	-11.06
Butriptyline	-8.26	-13.8
Iprindole	-8.21	-13.18
Oxaprotiline	-7.67	-13.35
Mianserin	-7.66	-12.33
Maprotiline	-7.18	-13.76
Bupropion	-7.15	-12.98
Viloxazine	-6.75	-12.26
Carbamazepine	-6.38	-10.18
Tranlycypromine	-6.26	Filtered
Methylphenidate	-6.18	-12.26
Estrone	-6.1	-11.75
Iproniazid	-5.67	-10.4
Phenelzine	-5.67	-9.66
Alprazolam	-5.67	Filtered
	Pearson	0.719
	Spearman	0.75
	Kendall	0.581

Table A1. Second Validation of the Docking Protocol with the Structural Pharmacophore. After the structural pharmacophore was placed on D98, the docking protocol was re-evaluated using the 24 compound test set using the Pearson, Spearman, and Kendall correlation tests. Each compound is sorted by its experimental affinity (kcal) and displayed is the predicted affinity of the docking simulation.

DNA	Protein	DNA	Protein	DNA	Protein
ADCYAP1R1	Adenylate Cyclase Activating Polypeptide 1	GPR27	G Protein Coupled Receptor 27	LHCGR	Luteinizing Hormone/Choriogonadotropin Receptor
ADORA1	Adenosine A1 Receptor	GPR31	G Protein Coupled Receptor 31	LPAA	Lysophosphatidic Acid Receptor 4
ADORA2A	Adenosine A2A Receptor	GPR32	G Protein Coupled Receptor 32	LPAR2	Lysophosphatidic Acid Receptor 2
ADORA2B	Adenosine A2B Receptor	GPR34	G Protein Coupled Receptor 34	LPAR5	Lysophosphatidic Acid Receptor 5
ADORA3	Adenosine A3 Receptor	GPR35	G Protein Coupled Receptor 35	LPAR6	Lysophosphatidic Acid Receptor 6
ADRA1A	Adrenocortical Receptor Alpha 1A	GPR37	G Protein Coupled Receptor 37	LT4R	Leukotriene B4 Receptor
ADRA1B	Adrenocortical Receptor Alpha 1B	GPR37L1	G Protein Coupled Receptor 37 Like 1	LTB4R2B	Leukotriene B4 Receptor 2B
ADRA1D	Adrenocortical Receptor Alpha 1D	GPR39	G Protein Coupled Receptor 39	MAS1	MAS1 Proto-Oncogene, G Protein-Coupled Receptor
ADRA2A	Adrenocortical Receptor Alpha 2A	GPR44	G Protein Coupled Receptor 44	MAS1L	MAS1 Proto-Oncogene Like, G Protein-Coupled Receptor
ADRA2B	Adrenocortical Receptor Alpha 2B	GPR45	G Protein Coupled Receptor 45	MC1R	Melanocortin 1 Receptor
ADRA2C	Adrenocortical Receptor Alpha 2C	GPR50	G Protein Coupled Receptor 50	MC2R	Melanocortin 2 Receptor
ADRB1	Adrenocortical Receptor Beta 1	GPR52	G Protein Coupled Receptor 52	MC3Rb	Melanocortin 3 Receptor B
ADRB2	Adrenocortical Receptor Beta 2	GPR55	G Protein Coupled Receptor 55	MC4R	Melanocortin 4 Receptor
ADRB3	Adrenocortical Receptor Beta 3	GPR56	G Protein Coupled Receptor 56	MC5R	Melanocortin 5 Receptor
AGTR1	Angiotensin II Receptor Type 1	GPR61	G Protein Coupled Receptor 61	MCHR1R	Melanin Concentrating Hormone Receptor 1
AGTR2	Angiotensin II Receptor Type 2	GPR62	G Protein Coupled Receptor 62	MCHR2R	Melanin Concentrating Hormone Receptor 2
APJ	Apelin Receptor	GPR63	G Protein Coupled Receptor 63	MLNR	Motilin Receptor
AVPR1A	Arginine Vasopressin Receptor 1A	GPR64	G Protein Coupled Receptor 64	MRGPRD	MAS Related GPR Family Member D
AVPR1B	Arginine Vasopressin Receptor 1B	GPR65	G Protein Coupled Receptor 65	MRGPRE	MAS Related GPR Family Member E
AVPR2	Arginine Vasopressin Receptor 2	GPR68	G Protein Coupled Receptor 68	MRGPRF	MAS Related GPR Family Member F
BB2	Bombesin Receptor Subtype 3	GPR75	G Protein Coupled Receptor 75	MRGPRG	MAS Related GPR Family Member G
BDKBR1	Bradykinin Receptor B1	GPR77	G Protein Coupled Receptor 77	MRGPRX1	MAS Related GPR Family Member X1
BDKBR2	Bradykinin Receptor B2	GPR78	G Protein Coupled Receptor 78	MRGPRX2	MAS Related GPR Family Member X2
C3AR1	Complement C3a Receptor 1	GPR82	G Protein Coupled Receptor 82	MRGPRX3	MAS Related GPR Family Member X3
CSA	Complement C5a Receptor	GPR83	G Protein Coupled Receptor 83	MRGPRX4	MAS Related GPR Family Member X4
CALCRb	Calcitonin Receptor	GPR84	G Protein Coupled Receptor 84	MTNR1A	Melatonin Receptor 1A
CALCRl	Calcitonin Receptor Like Receptor	GPR85	G Protein Coupled Receptor 85	MTNR1B	Melatonin Receptor 1B
CASR	Calcium Sensing Receptor	GPR87	G Protein Coupled Receptor 87	NMBR	Neurotensin Receptor
CKKAR	Cholecystokinin A Receptor	GPR88	G Protein Coupled Receptor 88	NMUR1	Neurotensin Receptor 1
CKKBR	Cholecystokinin B Receptor	GPR97	G Protein Coupled Receptor 97	NMUR2	Neurotensin Receptor 2
CCR2	C-C Motif Chemokine Receptor 2	GPR101	G Protein Coupled Receptor 101	NPPF1	Neuropeptide FF Receptor 1
CCR3	C-C Motif Chemokine Receptor 3	GPR110	G Protein Coupled Receptor 110	NPPF2	Neuropeptide FF Receptor 2
CCR4	C-C Motif Chemokine Receptor 4	GPR111	G Protein Coupled Receptor 111	NPBW1	Neuropeptides B And W Receptor 1
CCR5	C-C Motif Chemokine Receptor 5	GPR113	G Protein Coupled Receptor 113	NPBW2	Neuropeptides B And W Receptor 2
CCR6	C-C Motif Chemokine Receptor 6	GPR114	G Protein Coupled Receptor 114	NPY1R	Neuropeptide Y Receptor Y1
CCR7	C-C Motif Chemokine Receptor 7	GPR115	G Protein Coupled Receptor 115	NPY2R	Neuropeptide Y Receptor Y2
CCR8	C-C Motif Chemokine Receptor 8	GPR116	G Protein Coupled Receptor 116	NPY4R	Neuropeptide Y Receptor Y4
CCR10	C-C Motif Chemokine Receptor 10	GPR119	G Protein Coupled Receptor 119	NPY5R	Neuropeptide Y Receptor Y5
CCR12	C-C Motif Chemokine Receptor Like 2	GPR120	G Protein Coupled Receptor 120	NPS	LIM Homeobox Transcription Factor 1, Beta
CHRM1	Cholinergic Receptor Muscarinic 1	GPR123	G Protein Coupled Receptor 123	NTR1	Neurotensin Receptor 1
CHRM2	Cholinergic Receptor Muscarinic 2	GPR124	G Protein Coupled Receptor 124	NTR2	Neurotensin Receptor 2
CHRM3	Cholinergic Receptor Muscarinic 3	GPR125	G Protein Coupled Receptor 125	OPN3	Opioid Receptor 3
CHRM4	Cholinergic Receptor Muscarinic 4	GPR126	G Protein Coupled Receptor 126	OPN5	Opioid Receptor 5
CHRM5	Cholinergic Receptor Muscarinic 5	GPR132	G Protein Coupled Receptor 132	OPRD1	Opioid Receptor Delta 1
CMKR1	Chemerin Chemokine-Like Receptor 1	GPR133	G Protein Coupled Receptor 133	OPRL1	Opioid Related Nociceptin Receptor 1
CNR1	Cannabinoid Receptor 1	GPR135	G Protein Coupled Receptor 135	OPRK1	Opioid Receptor Kappa 1
CNR2	Cannabinoid Receptor 2	GPR141	G Protein Coupled Receptor 141	OPRM1	Opioid Receptor Mu 1
CRHR1	Corticotropin Releasing Hormone Receptor 1	GPR142	G Protein Coupled Receptor 142	OXER1	Oxoeicosanoid Receptor 1
CRHR2	Corticotropin Releasing Hormone Receptor 2	GPR143	G Protein Coupled Receptor 143	OXGR1	Oxoglutarate Receptor 1
CX3CR1	C-X3-C Motif Chemokine Receptor 1	GPR144	G Protein Coupled Receptor 144	OXYTR	Oxytocin Receptor
CXCR1	C-X-C Motif Chemokine Receptor 1	GPR146	G Protein Coupled Receptor 146	P2RY1	Pyrimidinergic Receptor P2Y1
CXCR2	C-X-C Motif Chemokine Receptor 2	GPR148	G Protein Coupled Receptor 148	P2RY2	Pyrimidinergic Receptor P2Y2
CXCR3	C-X-C Motif Chemokine Receptor 3	GPR149	G Protein Coupled Receptor 149	P2RY4	Pyrimidinergic Receptor P2Y4
CXCR4	C-X-C Motif Chemokine Receptor 4	GPR150	G Protein Coupled Receptor 150	P2RY6	Pyrimidinergic Receptor P2Y6
CXCR5	C-X-C Motif Chemokine Receptor 5	GPR151	G Protein Coupled Receptor 151	P2RY8	Pyrimidinergic Receptor P2Y8
CXCR6	C-X-C Motif Chemokine Receptor 6	GPR152	G Protein Coupled Receptor 152	P2RY10	Pyrimidinergic Receptor P2Y10
CXCR7	C-X-C Motif Chemokine Receptor 7	GPR153	G Protein Coupled Receptor 153	P2RY11	Pyrimidinergic Receptor P2Y11
CYSLTR1	Cysteinyl Leukotriene Receptor 1	GPR156	G Protein Coupled Receptor 156	P2RY12	Pyrimidinergic Receptor P2Y12
CYSLTR2	Cysteinyl Leukotriene Receptor 2	GPR157	G Protein Coupled Receptor 157	P2RY13	Pyrimidinergic Receptor P2Y13
DRD1	Dopamine Receptor D1	GPR158	G Protein Coupled Receptor 158	P2RY14	Pyrimidinergic Receptor P2Y14
DRD2	Dopamine Receptor D2	GPR160	G Protein Coupled Receptor 160	PK1	Prokineticin 1
DRD3	Dopamine Receptor D3	GPR161	G Protein Coupled Receptor 161	PK2	Prokineticin 2
DRD4	Dopamine Receptor D4	GPR162	G Protein Coupled Receptor 162	PRRP	Prolactin Releasing Hormone Receptor
DRD5	Dopamine Receptor D5	GPR171	G Protein Coupled Receptor 171	PTAFR	Platelet Activating Factor Receptor
EDNRA	Endothelin Receptor Type A	GPR173	G Protein Coupled Receptor 173	PTGDR	Prostaglandin D2 Receptor
EDNRB	Endothelin Receptor Type B	GPR174	G Protein Coupled Receptor 174	PTGER1	Prostaglandin E Receptor 1
ELTD1	Adhesion G Protein-Coupled Receptor L4	GPR176	G Protein Coupled Receptor 176	PTGER2	Prostaglandin E Receptor 2
F2R	Coagulation Factor II Thrombin Receptor	GPR182	G Protein Coupled Receptor 182	PTGER3	Prostaglandin E Receptor 3
F2R-L1	Coagulation Factor II Thrombin Like Receptor 1	GPR183	G Protein Coupled Receptor 183	PTGER4	Prostaglandin E Receptor 4
F2R-L2	Coagulation Factor II Thrombin Like Receptor 2	GPRCSA	G Protein-Coupled Receptor Class C Group 5, Member A	PTGFR	Prostaglandin F Receptor
F2R-L3	Coagulation Factor II Thrombin Like Receptor 3	GPRCSB	G Protein-Coupled Receptor Class C Group 5, Member B	PTGIR	Prostaglandin I2 Receptor
FFA1	Free Fatty Acid Receptor 1	GPRCS5	G Protein-Coupled Receptor Class C Group 5, Member C	PTH1R	Parathyroid Hormone 1 Receptor
FFA2	Free Fatty Acid Receptor 2	GPRCSD	G Protein-Coupled Receptor Class C Group 5, Member D	PTH2R	Parathyroid Hormone 2 Receptor
FFA3	Free Fatty Acid Receptor 3	GPRCSA	G Protein-Coupled Receptor Class C Group 5, Member A	QRPP	Pyroglutamylated Rfamide Peptide
FFR1	Formyl Peptide Receptor 1	GRM1	Glutamate Metabotropic Receptor 1	RXFP1	Relaxin Family Peptide Receptor 1
FFR2	Formyl Peptide Receptor 2	GRM4	Glutamate Metabotropic Receptor 4	RXFP2	Relaxin Family Peptide Receptor 2
FFR3	Formyl Peptide Receptor 3	GRM5	Glutamate Metabotropic Receptor 5	RXFP3	Relaxin Family Peptide Receptor 3
FSHR	Follicle Stimulating Hormone Receptor	GRM6	Glutamate Metabotropic Receptor 6	RXFP4	Relaxin Family Peptide Receptor 4
GABBR1	Gamma-Aminobutyric Acid Type B Receptor Subunit 1	GRM7	Glutamate Metabotropic Receptor 7	SLPR1	Sphingosine-1-Phosphate Receptor 1
GAL1	Galanin And GMAP Prepropeptide	GRM8	Glutamate Metabotropic Receptor 8	SLPR2	Sphingosine-1-Phosphate Receptor 2
GAL2	Galanin And GMAP Prepropeptide 2	GRPR	Gastrin Releasing Peptide Receptor	SLPR3	Sphingosine-1-Phosphate Receptor 3
GAL3	Galanin And GMAP Prepropeptide 3	HCA1	Hypertaluria, Absorptive, 1	SLPR4	Sphingosine-1-Phosphate Receptor 4
SGR	Glucagon Receptor	HCA2	Hypertaluria, Absorptive, 2	SLPR5	Sphingosine-1-Phosphate Receptor 5
GHRHR	Growth Hormone Releasing Hormone Receptor	HCA3	Hypertaluria, Absorptive, 3	SCTR	Secretin Receptor
GHSR	Growth Hormone Secretagogue Receptor	HCTR1	Solute Carrier Family 31 Member 1	SSTR1	Somatostatin Receptor 1
GIPR	Gastric Inhibitory Polypeptide Receptor	HCTR2	Solute Carrier Family 31 Member 2	SSTR2	Somatostatin Receptor 2
GLP1R	Glucagon Like Peptide 1 Receptor	HRH2	Histamine Receptor H2	SSTR3	Somatostatin Receptor 3
GLP2R	Glucagon Like Peptide 2 Receptor	HRH4	Histamine Receptor H4	SSTR4	Somatostatin Receptor 4
GM2R	Cyclic di-GMP phosphodiesterase Gm2	HTR1A	5-Hydroxytryptamine Receptor 1A	SSTR5	Somatostatin Receptor 5
GNHRH	Gonadotropin Releasing Hormone Receptor	HTR1B	5-Hydroxytryptamine Receptor 1B	SUCNR1	Succinate Receptor 1
GPBA	G Protein-Coupled Bile Acid Receptor 1	HTR1D	5-Hydroxytryptamine Receptor 1D	TA1	Trace Amine Associated Receptor 1
GPBR	G Protein-Coupled Estrogen Receptor 1	HTR1E	5-Hydroxytryptamine Receptor 1E	TAAR2	Trace Amine Associated Receptor 2
GPR1	G Protein Coupled Receptor 1	HTR1F	5-Hydroxytryptamine Receptor 1F	TAAR5	Trace Amine Associated Receptor 5
GPR3	G Protein Coupled Receptor 3	HTR2A	5-Hydroxytryptamine Receptor 2A	TAAR6	Trace Amine Associated Receptor 6
GPR4	G Protein Coupled Receptor 4	HTR2B	5-Hydroxytryptamine Receptor 2B	TAAR8	Trace Amine Associated Receptor 8
GPR6	G Protein Coupled Receptor 6	HTR2CINI	5-Hydroxytryptamine Receptor 2C INI	TAAR9	Trace Amine Associated Receptor 9
GPR12	G Protein Coupled Receptor 12	HTR2CVNV	5-Hydroxytryptamine Receptor 2C VNV	TACR1	Tachykinin Receptor 1
GPR15	G Protein Coupled Receptor 15	HTR2CVGV	5-Hydroxytryptamine Receptor 2C VGV	TACR2	Tachykinin Receptor 2
GPR17	G Protein Coupled Receptor 17	HTR2CVSV	5-Hydroxytryptamine Receptor 2C VSV	TACR3	Tachykinin Receptor 3
GPR18	G Protein Coupled Receptor 18	HTR4	5-Hydroxytryptamine Receptor 4	TBKX2R	Thrombospondin A2 Receptor
GPR19	G Protein Coupled Receptor 19	HTR5	5-Hydroxytryptamine Receptor 5	TSHR	Thyroid Stimulating Hormone Receptor
GPR20	G Protein Coupled Receptor 20	HTR6	5-Hydroxytryptamine Receptor 6	UTSR2	Urotenstin 2 Receptor
GPR21	G Protein Coupled Receptor 21	HTR7	5-Hydroxytryptamine Receptor 7	VIPR1	Vasoactive Intestinal Peptide Receptor 1
GPR22	G Protein Coupled Receptor 22	HRH1	Histamine Receptor H1	VIPR2	Vasoactive Intestinal Peptide Receptor 2
GPR25	G Protein Coupled Receptor 25	HRH3	Histamine Receptor H3		
GPR26	G Protein Coupled Receptor 26	KISSPEPTIN	KISS1 Receptor		

Table A.2: Table of the DNA genes and the decoded proteins utilized by the PDSP during the GPCR screen.

PDSP GPCR Results for Compound 1

DNA	% Activation	DNA	% Activation	DNA	% Activation	DNA	% Activation
BB3	6.3	GPR78	1.1	RXFP4	0.8	C3AR1	0.3
FPR1	3.9	MCHR1R	1.1	HTR2CINI	0.8	F2RL2	0.3
ADRB1	2.4	GPR45	1.1	NMUR1	0.7	GPR125	0.3
GPR52	2.4	P2RY1	1.1	GPR148	0.7	GPRC5A	0.3
P2RY6	2.3	CCR6	1.1	NTSR2	0.7	PK1	0.3
CALCR6	2.3	SSTR2	1.1	PTGFR	0.7	CHRM5	0.3
SSTR4	2.3	HTR4	1.1	KISSPEPTIN	0.7	GPR113	0.3
GPR34	2.3	MC2R	1.0	OPN3	0.7	GPR62	0.3
FPR2	2.3	AVPR2	1.0	OXGR1	0.7	GPR65	0.3
GPR150	2.2	GPR116	1.0	NPY5R	0.7	P2RY12	0.3
GPR6	2.2	MC4R	1.0	LPA4	0.7	CRHR2	0.3
ADORA1	2.1	GPR110	1.0	CXCR7	0.7	GRM1	0.3
GPR88	2.0	HTR2CVGV	1.0	GPR21	0.7	NPY1R	0.3
S1PR4	2.0	GPR44	1.0	CD97	0.7	LTBR2B	0.3
FPR3	1.9	OXER1	1.0	TAAR2	0.7	ADRA1A	0.3
PTAFR	1.9	TACR1	1.0	GRM5	0.7	NPFF2	0.3
FFA1	1.8	CXCR2	1.0	GPR1	0.7	AVPR1A	0.3
GPR174	1.7	CCR7	1.0	CXCR4	0.7	HCA1	0.3
GPR119	1.7	PTH2R	1.0	TACR3	0.7	ADRB2	0.3
CCR3	1.7	HRH4	1.0	P2RY4	0.7	GRM4	0.2
P2RY14	1.7	GPR85	1.0	CHRM2	0.6	GPR115	0.2
GPRC5C	1.7	MARGPRX3	1.0	CXCR6	0.6	PTH1R	0.2
GPR3	1.7	APJ	1.0	GPR31	0.6	GPR161	0.2
TAAR5	1.7	HTR1B	1.0	GPR97	0.6	GPR142	0.2
AGTR2	1.6	SCTR	1.0	GPR22	0.6	GPR132	0.2
MARGPRX1	1.6	GPR61	1.0	LHCGR	0.6	GPRC6A	0.2
CCR10	1.6	GPBA	1.0	HTR2C VNV	0.6	GPR64	0.2
CCKBR	1.6	S1PR1	1.0	MCHR2R	0.6	F2R-L1	0.2
CALCRL	1.6	VIPR1	1.0	NPBW1	0.6	NPS	0.2
HRH3	1.6	HTR6	1.0	NPY4R	0.6	ADORA3	0.2
HTR5	1.6	GMR2	1.0	GPFR	0.6	GPR37L1	0.2
MARGPRE	1.5	OPRD1	1.0	HRH2	0.6	NMUR2	0.2
LPAR1	1.5	HTR1D	1.0	HTR1F	0.6	CNR2	0.2
ADRA2B	1.5	GPR146	1.0	GPR4	0.6	CSA	0.2
GAL1	1.5	GPR84	0.9	PK2	0.6	CMKLR1	0.2
OPN5	1.5	CCR8	0.9	GRM6	0.6	ADRA1D	0.2
GPR87	1.5	S1PR5	0.9	GAL3	0.6	GRM7	0.2
FSHR	1.4	GPR144	0.9	OPRK1	0.6	ADORA2A	0.2
HRH1	1.4	BDKBR1	0.9	FFA2	0.6	GPR143	0.2
NMBR	1.4	NTSR1	0.9	P2RY2	0.6	GPR83	0.2
S1PR2	1.4	GPR114	0.9	RXFP3	0.6	GPR19	0.2
MARGPRX4	1.4	GPR55	0.9	DRD5	0.6	TAAR6	0.2
CHRM3	1.4	GPR135	0.9	HTR2C VSV	0.6	CYSLTR1	0.2
GPR156	1.4	PTGER3	0.9	CHRM4	0.6	LPAR6	0.2
GPR173	1.3	GPR12	0.9	GPR149	0.6	MARGPRG	0.2
VIPR2	1.3	MC1R	0.9	GPR111	0.5	GPR37	0.2
MCSR	1.3	GPR101	0.9	SSTR3	0.5	F2R	0.2
ADRB3	1.3	CX3CR1	0.9	HCA3	0.5	GPR68	0.2
ELTD1	1.3	PRRP	0.9	TBXA2R	0.5	GPR160	0.2
GPR20	1.3	HCTR2	0.9	GPR15	0.5	PTGER2	0.2
GPR151	1.3	MAS1L	0.9	GPR25	0.5	CCKAR	0.2
MTNR1A	1.3	CRHR1	0.9	GNRHR	0.5	GLP2R	0.1
ADRA2A	1.3	GPR56	0.9	GPR162	0.5	CCR5	0.1
MTNR1B	1.3	GPR32	0.9	GCCR	0.5	GPR123	0.1
GPR141	1.3	OPRL1	0.9	GABBR1	0.5	GLP1R	0.1
CXCR5	1.3	LTBR	0.8	MARGPRX2	0.5	CCR4	0.1
GPRC5B	1.3	TSHR	0.8	GPR63	0.5	GPR124	0.1
UTS2R	1.3	GIPR	0.8	LPAR5	0.5	DRD1	0.1
GPR27	1.3	GPR157	0.8	ADORA2B	0.5	GRPR	0.1
GPR17	1.3	CXCR3	0.8	MARGPRF	0.5	CNR1	0.1
CYSLTR2	1.3	P2RY13	0.8	P2RY10	0.4	FFA3	0.1
OPRM1	1.3	DRD4	0.8	GPR18	0.4	TAAR9	0.1
MAS1	1.2	ADCYAP1R1	0.8	TACR2	0.4	BDKBR2	0.1
HTR1E	1.2	S1PR3	0.8	SUCNR1	0.4	GPR158	0.1
GAL2	1.2	CCR2	0.8	GPR176	0.4	ADRA1B	0.1
ADRA2C	1.2	CHRM1	0.8	PTGDR	0.4	HTR2A	0.1
DRD2	1.2	GPR77	0.8	GRM8	0.4	F2RL3	0.1
MARGPRD	1.2	GPR50	0.8	HTR2B	0.4	P2RY8	0.1
NPFF1	1.2	HCTR1	0.8	GPR133	0.4	HTR1A	0.1
SSTR5	1.2	OXTR	0.8	AVPR1B	0.4	RXFP2	0.1
PTGIR	1.2	GPR26	0.8	TA1	0.4	NPY2R	0.1
GPR182	1.2	GPR75	0.8	HTR7	0.4	TAAR8	0.1
RXFP1	1.2	DRD3	0.8	LPAR2	0.4	PTGER4	0.1
GHSR	1.1	PTGER1	0.8	CXCR1	0.4	EDNRA	0.1
CCRL2	1.1	P2RY11	0.8	MC3Rb	0.4	GPR39	0.1
SSTR1	1.1	EDNRB	0.8	HCA2	0.4	GPRC5D	0.1
GPR120	1.1	AGTR1	0.8	GPR183	0.3	GPR153	0.1
NPBW2	1.1	CASR	0.8	GPR35	0.3	GPR152	0.1
GPR82	1.1	QRFP	0.8	GHRHR	0.3		
GPR126	1.1	MLNR	0.8	GPR171	0.3		

Table A.3: Results of the PDSP GPCR functional screen for candidate compound 1. Each receptor listed while the average percent of activation is list.

PDSP GPCR Results for Compound 2

DNA	% Activation	DNA	% Activation	DNA	% Activation	DNA	% Activation
HTR2CVGV	1.9	GPR21	1.2	PTGIR	1.0	DRD1	0.9
ADRA2B	1.8	CHRM3	1.1	PTGER2	1.0	GPR156	0.9
PTAFR	1.8	GAL1	1.1	CCR10	1.0	GPR78	0.9
GPR61	1.8	ADORA2A	1.1	TA1	1.0	HTR2CVSV	0.9
NMUR1	1.7	GPR142	1.1	F2RL2	1.0	GPR161	0.9
CCR6	1.7	GPR55	1.1	C3AR1	1.0	ADRA1B	0.9
GPR6	1.7	GPR152	1.1	HTR1B	1.0	MTNR1B	0.9
ADRB1	1.6	P2RY14	1.1	GPR37	1.0	GPRC6A	0.9
GPR150	1.6	HTR5	1.1	GPR65	1.0	ADRB3	0.9
SSTR1	1.6	FFA3	1.1	CCRL2	1.0	TACR1	0.9
MRGPRE	1.6	HTR1E	1.1	CCKBR	1.0	OXER1	0.9
S1PR3	1.6	GAL2	1.1	ADRA1A	1.0	RXF2	0.9
GPR31	1.6	EDNRA	1.1	CXCR2	1.0	NMUR2	0.9
ELTD1	1.6	AVPR2	1.1	F2R	1.0	CNR1	0.9
HRH4	1.6	P2RY10	1.1	GAL3	1.0	PRRP	0.9
GPR62	1.6	HCA2	1.1	CSA	1.0	P2RY4	0.9
NPBW2	1.6	P2RY2	1.1	GPR26	1.0	CHRM4	0.9
GPR151	1.6	GPR1	1.1	GPR113	1.0	PTGER1	0.9
SSTR3	1.6	BB3	1.1	GPRC5C	1.0	OPRM1	0.9
CASR	1.5	LPAR6	1.1	OPN5	1.0	P2RY11	0.9
CHRM2	1.5	GPR87	1.1	F2R-L1	1.0	GPR120	0.9
GPR84	1.5	GPR77	1.1	HTR6	1.0	HTR2CINI	0.9
LPA4	1.5	NTSR2	1.1	HTR1A	1.0	GPR174	0.9
NPY5R	1.4	GPR32	1.1	GPR132	1.0	PTH1R	0.9
CALCR1	1.4	MRGPRX1	1.1	CHRM5	1.0	GABBR1	0.9
CHRM1	1.4	GPR4	1.1	GRPR	1.0	GPR146	0.9
CYSLTR2	1.4	GPR82	1.1	GPR37L1	1.0	NPS	0.9
FFA1	1.4	GHSR	1.1	GPR19	1.0	P2RY13	0.9
LTB4R	1.3	MC4R	1.1	GPR158	1.0	PTGFR	0.9
ADORA2B	1.3	HTR2A	1.1	MC3Rb	1.0	PK2	0.8
DRD2	1.3	GPR25	1.1	P2RY12	1.0	ADCYAP1R1	0.8
HTR2C VNV	1.3	GPR35	1.1	CX3CR1	1.0	HTR4	0.8
TAA9	1.3	HCA1	1.1	GPR22	1.0	GPR148	0.8
TACR3	1.3	GPR124	1.1	MLNR	1.0	GPR119	0.8
KISSPEPTIN	1.3	NPBW1	1.1	GPR101	1.0	CXCR3	0.8
GPR44	1.3	RXF3	1.1	EDNRB	1.0	P2RY1	0.8
GPR141	1.3	GRM7	1.1	GLP2R	1.0	GPR88	0.8
GRM1	1.3	GPR18	1.1	CXCR1	1.0	GPR143	0.8
GPR144	1.3	GPR63	1.1	HTR7	1.0	GPR114	0.8
VIPR2	1.3	GCCR	1.1	AVPR1A	1.0	GPR135	0.8
CNR2	1.3	GPR34	1.1	HTR1D	1.0	CRHR1	0.8
CCR3	1.3	DRD3	1.1	GPER	1.0	GPRC5A	0.8
NPFF1	1.3	DRD4	1.1	OPRK1	1.0	GPR149	0.8
HRH3	1.3	GPR153	1.1	GPR27	1.0	GPR50	0.8
HRH1	1.3	GPR116	1.1	ADRA1D	1.0	UTS2R	0.8
MCSR	1.2	F2RL3	1.1	MRGPRF	1.0	GM2	0.8
TAA5	1.2	AVPR1B	1.1	GPR52	1.0	AGTR1	0.8
S1PR5	1.2	GPRC5D	1.1	NPY1R	1.0	GPR45	0.8
CXCR6	1.2	GPR123	1.1	GPR15	1.0	GRM5	0.8
OPN3	1.2	GPR173	1.1	CCR7	1.0	QRFP	0.8
LPAR1	1.2	TAAR6	1.1	SUCNR1	1.0	GPR12	0.8
OPRD1	1.2	MCHR2R	1.1	GPBA	1.0	ADRA2C	0.8
ADORA2A	1.2	ADORA3	1.1	SSTR5	1.0	GPR176	0.8
CRHR2	1.2	MAS1	1.1	NPY2R	1.0	GPR75	0.8
OXGR1	1.2	PTGDR	1.1	PK1	1.0	TACR2	0.7
PTGER3	1.2	GRM8	1.1	RXF1P1	1.0	SCTR	0.7
LPAR2	1.2	S1PR4	1.1	CYSLTR1	1.0	CCR2	0.7
GPR20	1.2	OXTR	1.1	LTB4R2B	1.0	MAS1L	0.7
LPAR5	1.2	GPR133	1.1	GPR110	1.0	NMBR	0.7
MRGPRX4	1.2	GPR97	1.1	GPR171	1.0	GPR183	0.7
APJ	1.2	MRGPRX2	1.1	TSHR	1.0	GPR162	0.7
GPR85	1.2	HTR2B	1.1	CMKLR1	1.0	FSHR	0.7
GPR182	1.2	CCKAR	1.1	GPR115	1.0	GNRHR	0.7
HCTR1	1.2	P2RY6	1.1	SSTR2	0.9	CCR8	0.7
GPR17	1.2	VIPR1	1.1	S1PR2	0.9	FPR1	0.7
PTH2R	1.2	FFA2	1.1	NTSR1	0.9	HTR1F	0.7
CCRS	1.2	P2RY8	1.1	PTGER4	0.9	HCA3	0.7
MCHR1R	1.2	GPRC5B	1.1	GPR68	0.9	MRGPRX3	0.7
GIPR	1.2	NPFF2	1.0	MRGPRD	0.9	LHCGR	0.7
DRD5	1.2	CXCR7	1.0	MTNR1A	0.9	HRH2	0.6
FPR2	1.2	CXCR4	1.0	RXF4P	0.9	GPR126	0.6
NPY4R	1.2	GPR56	1.0	BDKBR2	0.9	OPRL1	0.6
MRGPRG	1.2	BDKBR1	1.0	CXCR5	0.9	FPR3	0.6
MC1R	1.2	ADORA1	1.0	CALCRb	0.9	GRM4	0.6
GPR3	1.2	TBXA2R	1.0	S1PR1	0.9	GRM6	0.5
ADRB2	1.2	GPR125	1.0	GPR64	0.9	TAAR2	0.5
GPR83	1.2	CD97	1.0	HCTR2	0.9	GPR111	0.5
SSTR4	1.2	TAAR8	1.0	GPR39	0.9	GPR157	0.3
AGTR2	1.2	GPR160	1.0	GLP1R	0.9		
GHRHR	1.2	CCR4	1.0	MC2R	0.9		

Table A.4: Results of the PDSP GPCR functional screen for candidate compound 2. Each receptor listed while the average percent of activation is list.

PDSP GPCR Results for Compound 4

DNA	% Activation	DNA	% Activation	DNA	% Activation	DNA	% Activation
CXCR7	5.3	HTR1D	1.1	GPR25	1.0	ADRA1D	0.9
GPR150	2.6	GPR111	1.1	GPR149	1.0	HTR2A	0.9
LHCGR	2.3	GPR124	1.1	GPR22	1.0	GPR133	0.8
GPR62	2.0	LPA6	1.1	MAS1	1.0	HCA1	0.8
HRH1	1.9	GNRHR	1.1	GPRC5B	1.0	GPR83	0.8
S1PR2	1.9	MTNR1B	1.1	GPR132	1.0	GPR27	0.8
GPR6	1.9	MRGPRX1	1.1	CXCR5	1.0	NMUR2	0.8
BB3	1.8	GPR115	1.1	GRM1	1.0	GPR97	0.8
P2RY14	1.8	CCR10	1.1	EDNRB	1.0	ADORA2B	0.8
GPR151	1.7	DRD1	1.1	ADORA3	1.0	CCR2	0.8
MRGPRE	1.7	MCHR1R	1.1	ADRA1A	1.0	NPBW1	0.8
CCR3	1.7	MRGPRF	1.1	GPR173	0.9	GPR144	0.8
GPR20	1.7	CXCR2	1.1	ADRA2A	0.9	OXGR1	0.8
GPR3	1.7	CHRM1	1.1	PTGIR	0.9	CCR7	0.8
BDKBR1	1.6	OPRK1	1.1	DRD5	0.9	KISSPEPTIN	0.8
SSTR1	1.6	NTSR1	1.1	CNR2	0.9	NPY2R	0.8
GPR61	1.6	GPR141	1.1	EDNRA	0.9	GPR143	0.8
FPR3	1.5	GRM5	1.1	HTR2B	0.9	CSA	0.8
GPR34	1.5	GPR171	1.1	S1PR1	0.9	CD97	0.8
HCA3	1.5	OXTR	1.1	GPRC6A	0.9	GRM4	0.8
HRH2	1.5	ADRA2B	1.1	AGTR1	0.9	HRH3	0.8
CHRM3	1.5	GPR119	1.1	GPR156	0.9	NTSR2	0.8
GHRHR	1.4	GPR125	1.1	P2RY12	0.9	GPR161	0.8
GPR50	1.4	CALCRl	1.1	F2R	0.9	GABBR1	0.8
GPR85	1.4	F2R-L1	1.1	OXER1	0.9	GPR126	0.8
GPRC5C	1.4	LPA4	1.1	CALCRb	0.9	PK1	0.8
TAAR5	1.4	GPR17	1.1	HCA2	0.9	GMR2	0.8
ADRA2C	1.4	PTGER1	1.1	GPR152	0.9	NPY4R	0.8
HTR2CVGV	1.4	ADRB3	1.1	GPR19	0.9	OPRM1	0.8
GPR120	1.4	SUCNR1	1.1	GIPIR	0.9	GPFR	0.8
MC1R	1.4	CX3CR1	1.1	GLP2R	0.9	GPR162	0.8
MRGPRX3	1.4	PRRP	1.1	CXCR3	0.9	GPR39	0.8
FFA1	1.4	CHRM5	1.0	GPR146	0.9	GPR37	0.8
GPR26	1.4	GPR45	1.0	F2RL2	0.9	AVPR1A	0.8
ADRB1	1.3	MCSR	1.0	GPRC5A	0.9	SSTR3	0.8
GPR110	1.3	GRM7	1.0	CCRL2	0.9	DRD2	0.8
S1PR4	1.3	GPR87	1.0	FPR2	0.9	PTGER2	0.8
MC4R	1.3	HTR2CINI	1.0	GPR75	0.9	NPS	0.8
CRHR1	1.3	GPR52	1.0	SSTR4	0.9	NPY1R	0.8
NPBW2	1.3	CYSLTR2	1.0	HCTR2	0.9	GPR37L1	0.8
VIPR1	1.3	HTR5	1.0	GPR82	0.9	AVPR1B	0.8
GRM8	1.3	GPR123	1.0	F2RL3	0.9	NMBR	0.8
MRGPRD	1.3	SSTR2	1.0	GLP1R	0.9	GPR176	0.8
PTH2R	1.3	TAAR9	1.0	GPR64	0.9	TAAR8	0.8
CHRM2	1.3	TACR1	1.0	GPR18	0.9	PK2	0.8
SCTR	1.3	HRH4	1.0	GPR1	0.9	GPRC5D	0.8
P2RY6	1.3	MLNR	1.0	ADRA1B	0.9	LPA5	0.8
GPR4	1.3	GPR158	1.0	PTGER4	0.9	GAL1	0.8
GHSR	1.3	CCR8	1.0	GPR101	0.9	HTR2CVNV	0.8
ELTD1	1.2	P2RY1	1.0	CXCR1	0.9	HTR1A	0.8
GPR44	1.2	RXFP1	1.0	P2RY8	0.9	GPR77	0.8
NPFF1	1.2	TBKA2R	1.0	TA1	0.9	P2RY11	0.7
FSHR	1.2	GPR56	1.0	MTNR1A	0.9	GPR15	0.7
GAL2	1.2	LPA2	1.0	GPR63	0.9	GPR148	0.7
HCTR1	1.2	HTR1E	1.0	FFA3	0.9	ADORA2A	0.7
CXCR6	1.2	MRGPRG	1.0	OPRL1	0.9	MC2R	0.7
GPR116	1.2	GPBA	1.0	CHRM4	0.9	MC3Rb	0.7
P2RY4	1.2	GPR31	1.0	CNR1	0.9	HTR4	0.7
UTS2R	1.2	GPR35	1.0	LTB4R	0.9	PTGDR	0.7
C3AR1	1.2	CMKLR1	1.0	NMUR1	0.9	S1PR5	0.7
FPR1	1.2	GPR153	1.0	GPR55	0.9	CCR4	0.7
GPR182	1.2	OPN5	1.0	P2RY2	0.9	P2RY10	0.7
MAS1L	1.2	NPY5R	1.0	BDKBR2	0.9	PTH1R	0.7
GPR21	1.2	CCKBR	1.0	GCGR	0.9	CRHR2	0.7
RXFP3	1.2	CCKAR	1.0	GPR113	0.9	DRD3	0.7
GPR78	1.2	LTB4R2B	1.0	GPR114	0.9	GPR12	0.7
GPR135	1.2	TACR3	1.0	CXCR4	0.9	MRGPRX4	0.7
OPRD1	1.2	RXFP2	1.0	LPAR1	0.9	NPFF2	0.7
ADORA1	1.2	OPN3	1.0	ADRB2	0.9	VIPR2	0.7
MCHR2R	1.2	TAAR6	1.0	P2RY13	0.9	DRD4	0.6
FFA2	1.2	CCRS	1.0	S1PR3	0.9	ADCYAP1R1	0.6
GPR84	1.1	TACR2	1.0	GPR183	0.9	CASR	0.6
QRFP	1.1	TSHR	1.0	CCR6	0.9	SSTR5	0.6
HTR1B	1.1	HTR6	1.0	HTR1F	0.9	PTGFR	0.6
PTGER3	1.1	HTR7	1.0	MRGPRX2	0.9	GPR88	0.6
AGTR2	1.1	PTAFR	1.0	CYSLTR1	0.9	GRM6	0.6
GPR32	1.1	GPR68	1.0	AVPR2	0.9	TAAR2	0.5
GAL3	1.1	HTR2C VSV	1.0	GPR142	0.9	GPR157	0.3
GPR160	1.1	GPR65	1.0	RXFP4	0.9		
APJ	1.1	GPR174	1.0	GRPR	0.9		

Table A.5: Results of the PDSP GPCR functional screen for candidate compound 4. Each receptor listed while the average percent of activation is list.

PDSP GPCR Results for Compound 5

DNA	% Activation	DNA	% Activation	DNA	% Activation	DNA	% Activation
GPR62	3.1	GPGR	1.0	CMKLR1	0.9	MTNR1A	0.8
GPR150	2.4	GPR173	1.0	MRGPRX1	0.9	HTR2CINI	0.8
F2R-L1	2.0	GPR82	1.0	HTR2CVGV	0.9	P2RY2	0.8
HTR6	1.6	PTGER4	1.0	P2RY8	0.9	P2RY11	0.8
ADRA2A	1.5	GPR21	1.0	AVPR1B	0.9	DRD4	0.8
GPR149	1.5	C3AR1	1.0	AGTR1	0.9	MRGPRF	0.8
NPY4R	1.4	TACR3	1.0	S1PR1	0.9	HRH3	0.8
SSTR4	1.4	MAS1L	1.0	ADRA1B	0.9	NMUR1	0.8
CXCR3	1.4	MRGPRG	1.0	MAS1	0.9	ADORA2B	0.8
PRRP	1.4	PTGDR	1.0	ADR81	0.9	HTR1F	0.8
SSTR5	1.4	OXER1	1.0	MRGPRX2	0.9	HTR4	0.8
MC1R	1.4	GPR162	1.0	OPN5	0.9	GRM4	0.8
CCR10	1.4	GPR158	1.0	GPR20	0.9	GPR113	0.8
CHRM3	1.4	P2RY6	1.0	GPR50	0.9	GPR111	0.8
GPR110	1.3	LTBR2B	1.0	HTR2B	0.9	GPR142	0.8
GPR114	1.3	GRM8	1.0	GPR124	0.9	CXCR2	0.8
ADRB3	1.3	GPR132	1.0	MCSR	0.9	GRM5	0.8
QRFP	1.3	ADORA2A	1.0	ADRA1D	0.9	CSA	0.8
CD97	1.3	UTS2R	1.0	GPR68	0.9	BDKBR2	0.8
GPR6	1.3	LTBR4	1.0	GPR152	0.9	GPR44	0.8
P2RY14	1.3	F2R	1.0	F2RL3	0.9	GPR144	0.8
GPR45	1.3	CCR4	1.0	GPR3	0.9	GPR126	0.8
GPR34	1.3	GPR156	1.0	MC3Rb	0.9	CRHR2	0.8
RXFP2	1.3	CNR1	1.0	RXFP1	0.9	CNR2	0.8
PTGIR	1.2	ADRA1A	1.0	CHRM5	0.9	LPAR2	0.8
CXCR6	1.2	S1PR4	1.0	P2RY13	0.9	HTR1D	0.8
ADCYAP1R1	1.2	NTSR1	1.0	GAL3	0.9	GPR97	0.8
GPR15	1.2	PTGER2	1.0	CCR2	0.9	HCTR1	0.8
GPR56	1.2	GPR4	1.0	GLP2R	0.9	MRGPRX4	0.8
GAL1	1.2	GPR125	1.0	CHRM4	0.9	NMUR2	0.8
NPF2	1.2	CCR6	1.0	TA1	0.9	S1PR2	0.8
PTH2R	1.2	GPR120	1.0	HRH2	0.9	NPY1R	0.7
GPR171	1.2	GPR83	1.0	CCKAR	0.9	PTGER1	0.7
TACR1	1.2	OPRL1	1.0	NPBW1	0.9	P2RY4	0.7
MC4R	1.2	GPR115	1.0	GPR55	0.9	CXCR1	0.7
GPRC5A	1.2	HTR1E	1.0	CXCR4	0.9	GPR148	0.7
GPR27	1.2	GPR133	1.0	RXFP3	0.9	GPRC5C	0.7
GPR32	1.2	TAAAR8	1.0	DRD2	0.9	PTGFR	0.7
FPR3	1.2	PK1	1.0	CCR3	0.9	GPR78	0.7
GPR116	1.2	MRGPRX3	1.0	GPR77	0.9	GPR12	0.7
FPR2	1.2	LPAR5	1.0	AGTR2	0.9	OXTR	0.7
ADORA1	1.1	OPRD1	1.0	PTH1R	0.9	SSTR2	0.7
RXFP4	1.1	GPR141	1.0	P2RY12	0.9	GPR143	0.7
GHSR	1.1	P2RY10	1.0	GRPR	0.9	GPBA	0.7
OPN3	1.1	GAL2	1.0	TSHR	0.9	MCHR2R	0.7
VIPR1	1.1	BB3	1.0	GPR182	0.9	MLNR	0.7
SSTR1	1.1	FFA1	1.0	GPR37	0.9	GPR37L1	0.7
GPR151	1.1	GPR1	1.0	GPR63	0.9	ADRB2	0.7
GPR26	1.1	MRGPRE	1.0	LPAR6	0.9	NPS	0.7
ELTD1	1.1	GLP1R	1.0	GPRC5D	0.9	GPR174	0.7
BDKBR1	1.1	PTAFR	1.0	GHRHR	0.9	LHCGR	0.7
FFA2	1.1	GPR84	1.0	HTR2A	0.9	HTR2C VNV	0.7
CXCR5	1.1	SUCNR1	1.0	HCA1	0.9	GRM1	0.7
FFA3	1.1	MRGPRD	1.0	GPR22	0.9	CALCRb	0.7
GPR52	1.1	GPR35	1.0	LPAR1	0.9	HRH4	0.7
ADRA2C	1.1	GPR65	1.0	GPR123	0.9	GPR183	0.7
HTR5	1.1	OPRK1	1.0	GPR61	0.9	MTNR1B	0.7
MC2R	1.1	GPR64	1.0	GPR160	0.9	HTR1A	0.7
GIPR	1.1	DRD5	1.0	GRM7	0.9	SSTR3	0.7
FPR1	1.1	TAAAR6	1.0	GPR161	0.9	HCA3	0.7
CYSLTR1	1.1	CX3CR1	1.0	GPR39	0.9	FSHR	0.6
GPR31	1.1	GPR25	1.0	OXGR1	0.9	TBXA2R	0.6
GABBR1	1.1	CASR	1.0	KISSPEPTIN	0.9	MCHR1R	0.6
NPBW2	1.1	HCA2	1.0	CRHR1	0.9	NTSR2	0.6
NPF1	1.1	DRD3	1.0	HTR2C VSV	0.8	GPR176	0.6
TAAAR5	1.1	S1PR5	0.9	NPY5R	0.8	CCR7	0.6
CHRM1	1.1	GPR153	0.9	GMR2	0.8	TACR2	0.6
CHRM2	1.1	ADORA3	0.9	GPR87	0.8	EDNRA	0.6
HRH1	1.1	F2RL2	0.9	GPR119	0.8	GPR75	0.6
GPR135	1.1	CALCLR	0.9	NPY2R	0.8	TAAAR2	0.6
GPR146	1.1	GPR85	0.9	AVPR2	0.8	GPR88	0.6
P2RY1	1.1	GPRC6A	0.9	GCCR	0.8	GPRC5B	0.6
GNRHR	1.1	AVPR1A	0.9	ADRA2B	0.8	S1PR3	0.5
CCRL2	1.0	CCKBR	0.9	HTR1B	0.8	HCTR2	0.5
TAAAR9	1.0	APJ	0.9	HTR7	0.8	CCR8	0.5
DRD1	1.0	GPR18	0.9	CXCR7	0.8	CYSLTR2	0.5
SCTR	1.0	GPR19	0.9	OPRM1	0.8	GRM6	0.5
EDNRB	1.0	VIPR2	0.9	LPA4	0.8	GPR157	0.2
NIMBR	1.0	GPR17	0.9	PTGER3	0.8		
PK2	1.0	GPR101	0.9	CCRS	0.8		

Table A.6: Results of the PDSP GPCR functional screen for candidate compound 5. Each receptor listed while the average percent of activation is list.

PDSP GPCR Results for Compound 6

DNA	% Activation	DNA	% Activation	DNA	% Activation	DNA	% Activation
GPR61	2.2	S1PR2	1.1	GPR63	1.0	NPS	0.9
GPR27	2.1	LPA5	1.1	OPRM1	1.0	ADRA1D	0.9
ADRA2B	2.1	VIPR2	1.1	HTR2B	1.0	AGTR1	0.9
GPR151	1.8	GPR174	1.1	S1PR1	1.0	GPR176	0.9
GPR150	1.8	GPR123	1.1	TSHR	1.0	GMR2	0.9
NMUR1	1.8	NPBW2	1.1	RXFP4	1.0	HCA1	0.9
MC2R	1.7	CASR	1.1	TAAAR8	1.0	GPR22	0.9
GPRC5B	1.7	TACR2	1.1	GPR34	1.0	OPRL1	0.9
GPR6	1.7	GABBR1	1.1	CCR3	1.0	MRGPRD	0.9
GPR156	1.7	ADRA2A	1.1	GPR65	1.0	PTH2R	0.9
CHRM3	1.6	GPR20	1.1	GPR125	1.0	ADRA1B	0.9
CX3CR1	1.5	CXCR7	1.1	CHRM5	1.0	ELTD1	0.9
HRH3	1.5	CCKBR	1.1	GPR124	1.0	GPR25	0.9
DRD3	1.5	ADRA1A	1.1	BDKBR2	1.0	SUCNR1	0.9
ADORA1	1.5	GIPR	1.1	GPR39	1.0	GPR64	0.9
GAL2	1.5	ADRA2C	1.1	GPR50	1.0	SCTR	0.9
OPRD1	1.5	TACR1	1.1	NTSR1	1.0	GPR119	0.9
GPR26	1.4	GPR120	1.1	GPR3	1.0	NTSR2	0.9
GPR110	1.4	HTR1B	1.1	FFA1	1.0	DRD5	0.9
KISSPEPTIN	1.4	DRD1	1.1	GPR115	1.0	P2RY12	0.9
BB3	1.3	OPRK1	1.0	MRGPRF	1.0	CCR2	0.9
GPR78	1.3	GPR52	1.0	CSA	1.0	NPFF2	0.8
CXCR4	1.3	TAAAR6	1.0	SSTR3	1.0	GPR149	0.8
MLNR	1.3	AGTR2	1.0	GPR132	1.0	PRRP	0.8
P2RY6	1.3	GPR15	1.0	F2R	1.0	C3AR1	0.8
ADRB3	1.3	CYSLTR1	1.0	HCTR1	1.0	GPR146	0.8
LPAR1	1.3	CCR5	1.0	EDNRA	1.0	S1PR3	0.8
LHCGR	1.3	PTGER4	1.0	PTGDR	1.0	GPR143	0.8
PTAFR	1.3	GPR68	1.0	MRGPRX2	1.0	GPR142	0.8
TAAAR5	1.3	OPN5	1.0	GPR1	1.0	HTR2CINI	0.8
FPR1	1.3	FPR3	1.0	GPRC5D	1.0	GPR113	0.8
ADRB2	1.3	GCCR	1.0	GLP2R	0.9	GPR114	0.8
CHRM2	1.3	MCHR2R	1.0	GPR111	0.9	F2R-L1	0.8
SSTR2	1.2	GPR19	1.0	P2RY8	0.9	MRGPRX4	0.8
GPR133	1.2	CRHR2	1.0	CCR8	0.9	MC1R	0.8
NPFF1	1.2	HTR1E	1.0	MC4R	0.9	PTH1R	0.8
HTR5	1.2	P2RY10	1.0	GPR88	0.9	GPR135	0.8
HCTR2	1.2	GRM5	1.0	SSTR5	0.9	GPR144	0.8
GPR32	1.2	FFA3	1.0	GRM1	0.9	ADCYAP1R1	0.8
FFA2	1.2	GRM7	1.0	CCR7	0.9	HTR2A	0.8
GPR183	1.2	CYSLTR2	1.0	HTR4	0.9	S1PR5	0.8
CD97	1.2	TACR3	1.0	MAS1	0.9	GPBA	0.8
GPR160	1.2	MRGPRE	1.0	GPR4	0.9	GPR44	0.8
CCR4	1.2	HTR2C VSV	1.0	HTR1D	0.9	AVPR1B	0.8
P2RY4	1.2	AVPR1A	1.0	CRHR1	0.9	ADORA2B	0.8
NPY4R	1.2	PTGER3	1.0	HTR7	0.9	MCHR1R	0.8
RXFP1	1.2	GPR17	1.0	RXFP2	0.9	GPR12	0.8
TAAAR9	1.2	LTB4R2B	1.0	GHRHR	0.9	OXER1	0.8
HCA2	1.2	GPR77	1.0	GPR161	0.9	HTR6	0.8
SSTR1	1.2	ADORA3	1.0	NPY2R	0.9	OXTR	0.8
DRD4	1.2	PK2	1.0	PK1	0.9	MRGPRX3	0.8
GPRC5C	1.2	TA1	1.0	CHRM1	0.9	HRH2	0.8
OXGR1	1.2	CNR1	1.0	GPRC6A	0.9	UTS2R	0.7
MRGPRX1	1.2	HRH1	1.0	GPR62	0.9	QRFP	0.7
FPR2	1.2	GPR182	1.0	GPR153	0.9	CCR10	0.7
HTR2C VNV	1.2	GPR101	1.0	GPR21	0.9	GPR162	0.7
HRH4	1.2	CCRL2	1.0	EDNRB	0.9	HTR1F	0.7
GAL3	1.2	AVPR2	1.0	GRM4	0.9	CNR2	0.7
P2RY11	1.2	APJ	1.0	NPY1R	0.9	TBXA2R	0.7
CXCR3	1.1	GPR158	1.0	GPRC5A	0.9	CXCR6	0.7
LPAR2	1.1	GPR82	1.0	GLP1R	0.9	NMUR2	0.7
GPR83	1.1	MC3Rb	1.0	GRM8	0.9	MAS1L	0.7
MRGPRG	1.1	S1PR4	1.0	GPR35	0.9	P2RY14	0.7
GPR56	1.1	ADRB1	1.0	LPA6	0.9	ADORA2A	0.7
CXCR1	1.1	GPR55	1.0	CXCR2	0.9	CALCRL	0.7
RXFP3	1.1	GPR37L1	1.0	GPR18	0.9	LPA4	0.7
CALCRb	1.1	CXCR5	1.0	VIPR1	0.9	GRM6	0.6
GPR116	1.1	PTGER1	1.0	HCA3	0.9	LTB4R	0.6
GPR31	1.1	MTNRI8	1.0	SSTR4	0.9	CCR6	0.6
CHRM4	1.1	P2RY1	1.0	PTGER2	0.9	GPR173	0.6
GRPR	1.1	HTR2CVGV	1.0	HTR1A	0.9	FSHR	0.6
NPBW1	1.1	OPN3	1.0	CCKAR	0.9	PTGFR	0.6
GAL1	1.1	F2RL2	1.0	GPR171	0.9	GPR126	0.5
CMKLR1	1.1	GNRHR	1.0	NMBR	0.9	MTNRI1A	0.5
DRD2	1.1	GPR152	1.0	GHSR	0.9	GPR75	0.5
GPR141	1.1	GPR45	1.0	F2RL3	0.9	TAAAR2	0.4
GPR148	1.1	P2RY2	1.0	P2RY13	0.9	GPR157	0.4
GPR84	1.1	GPR87	1.0	GPFR	0.9	BDKBR1	0.3
MCSR	1.1	NPY5R	1.0	GPR85	0.9		
PTGIR	1.1	GPR97	1.0	GPR37	0.9		

Table A.7: Results of the PDSP GPCR functional screen for candidate compound 5. Each receptor listed while the average percent of activation is list.

PDSP GPCR Results for Candidate 6

DNA	% Activation	DNA	% Activation	DNA	% Activation	DNA	% Activation
HRH3	2.7	P2RY14	1.2	GPR173	1.0	NPFF2	0.9
GPR135	2.1	GPR82	1.2	LTB4R	1.0	CYSLTR1	0.9
MC4R	2.1	SUCNR1	1.2	LPAR2	1.0	BDKBR2	0.9
QRFP	1.9	ADORA2B	1.2	GAL2	1.0	GPRC5D	0.9
MRGPRX1	1.9	GPR146	1.2	MAS1L	1.0	MCHR1R	0.9
GPR151	1.8	GNRHR	1.2	ELTD1	1.0	CASR	0.9
BB3	1.8	GPR26	1.2	GPR132	1.0	CXCR7	0.9
FFA1	1.8	NTSR1	1.2	GPR4	1.0	GPR125	0.9
NMUR1	1.7	CCR3	1.2	MCHR2R	1.0	P2RY4	0.9
S1PR2	1.7	GPR148	1.2	HCA1	1.0	P2RY12	0.9
HTR6	1.7	LPAR6	1.2	FFA3	1.0	GPR158	0.9
MRGPRX3	1.6	CXCR2	1.2	HTR2C VSV	1.0	PTH2R	0.9
P2RY6	1.6	HTR1E	1.2	OXER1	1.0	NPY2R	0.9
GPR88	1.6	CXCR1	1.2	OXTR	1.0	GPER	0.9
ADRA2A	1.6	ADRA1D	1.2	CNR1	1.0	CCR6	0.9
GPR6	1.6	P2RY10	1.2	GPR120	1.0	CCR10	0.9
TAAR5	1.6	AVPR2	1.2	GPR162	1.0	DRD2	0.9
CXCR4	1.6	MRGPRX2	1.2	CXCR6	1.0	NPY1R	0.9
HTR4	1.6	APJ	1.2	GPR27	1.0	GPR31	0.9
GPRC5B	1.6	GPR56	1.2	GRM7	1.0	AVPR1B	0.9
GPR156	1.5	GPR18	1.2	GPR115	1.0	CRHR1	0.8
MC1R	1.5	AVPR1A	1.2	PTGER4	1.0	GPR142	0.8
MRGPRD	1.5	GPR149	1.2	ADRA1B	1.0	RXFP2	0.8
GPR52	1.5	NPFF1	1.2	PTGER2	1.0	SSTR2	0.8
GPR141	1.5	GPR17	1.2	GPR1	1.0	KISSPEPTIN	0.8
GPR61	1.5	AGTR1	1.2	CHRM5	1.0	TAARB	0.8
FPR3	1.5	GRM8	1.1	GPR19	1.0	GPRC5A	0.8
SCTR	1.5	RXFP1	1.1	GPRC6A	1.0	F2RL3	0.8
PTGER1	1.4	MCSR	1.1	P2RY13	1.0	HTR2C INI	0.8
OPRD1	1.4	P2RY2	1.1	C3AR1	1.0	HTR2A	0.8
CKBR	1.4	PTGER3	1.1	CCRA	1.0	GIPR	0.8
LPAR1	1.4	HTR1B	1.1	BDKBR1	1.0	GPR143	0.8
GAL1	1.4	GPR171	1.1	HTR7	1.0	HTR2CVNV	0.8
HTR5	1.4	PK2	1.1	FPR1	1.0	CCR5	0.8
GPR85	1.4	CCR7	1.1	GPR97	1.0	GPR21	0.8
ADR83	1.4	GPR87	1.1	NPBW1	1.0	GPR111	0.8
GPR150	1.4	TACR1	1.1	GPR63	1.0	GPR124	0.8
RXFP3	1.4	MAS1	1.1	ADRA2C	1.0	PTAFR	0.8
OPN3	1.4	ADRA2B	1.1	GPR68	1.0	GRM1	0.8
DRD4	1.4	GMR2	1.1	GPR153	1.0	GLP1R	0.8
CYSLTR2	1.4	CHRM2	1.1	MGRPRG	1.0	GPR25	0.8
GPR182	1.4	P2RY1	1.1	EDNRA	1.0	GPR133	0.8
HRH1	1.4	PK1	1.1	PTH1R	1.0	GCGR	0.8
FFA2	1.4	HRH2	1.1	CHRM4	1.0	GPR37L1	0.8
GPR116	1.4	LTB4R2B	1.1	LPA4	1.0	CNR2	0.8
MRGPRE	1.4	GAL3	1.1	CCKAR	1.0	RXFP4	0.8
NPBW2	1.4	GPR160	1.1	GPR152	1.0	PTGFR	0.8
HTR1D	1.3	ADRA1A	1.1	GPR176	1.0	GPR126	0.8
MRGPRX4	1.3	CCR8	1.1	NPS	1.0	GPR37	0.7
GPR34	1.3	CCR2	1.1	F2R-L1	1.0	FPR2	0.7
MTNR1A	1.3	TACR3	1.1	GPR161	1.0	CRHR2	0.7
GPR183	1.3	GPR110	1.1	GPR45	1.0	P2RY11	0.7
MTNR1B	1.3	GPR35	1.1	HTR1A	1.0	GRM5	0.7
ADORA1	1.3	S1PR5	1.1	TAAR6	1.0	DRD5	0.7
GPBA	1.3	GPR119	1.1	CMKLR1	1.0	S1PR3	0.7
GPR3	1.3	GPR123	1.1	TAAR9	1.0	EDNRB	0.7
GPR84	1.3	GABBR1	1.1	NMUR2	1.0	GPR62	0.7
S1PR1	1.3	HCTR1	1.1	SSTR5	1.0	HCA3	0.7
GPR55	1.3	MGRPRF	1.1	HTR2B	0.9	CXCR3	0.7
ADORA2A	1.3	GPR113	1.1	GPR65	0.9	TBXA2R	0.7
GPR174	1.3	OXGR1	1.1	PTGIR	0.9	MC2R	0.7
GHSR	1.3	MLNR	1.1	ADRB2	0.9	TSHR	0.7
CXCR5	1.3	GPR83	1.1	GLP2R	0.9	ADCYAP1R1	0.7
CCRL2	1.3	OPN5	1.1	MC3Rb	0.9	GPR12	0.6
PTGDR	1.3	GPR22	1.1	LPAR5	0.9	GPR144	0.6
VIPR1	1.3	GPR77	1.1	GRPR	0.9	GPR75	0.6
S1PR4	1.3	HTR2CVGV	1.1	P2RY8	0.9	GPRC5C	0.6
GPR44	1.3	DRD1	1.1	TAI1	0.9	GRM4	0.6
HCTR2	1.3	OPRK1	1.1	PRR2	0.9	GPR50	0.6
GPR114	1.3	CALCR1	1.1	NTSR2	0.9	DRD3	0.6
GPR101	1.2	UTS2R	1.1	GPR15	0.9	CALCRb	0.6
OPRL1	1.2	GPR78	1.1	ADORA3	0.9	GHRHR	0.6
VIPR2	1.2	F2RL2	1.1	CSA	0.9	NPY4R	0.6
CD97	1.2	SSTR1	1.1	GPR39	0.9	GPR32	0.6
CHRM3	1.2	LHCGR	1.1	F2R	0.9	CX3CR1	0.5
ADRB1	1.2	OPRM1	1.1	GPR20	0.9	GPR157	0.4
SSTR4	1.2	HTR1F	1.1	GPR64	0.9	GRM6	0.4
AGTR2	1.2	TACR2	1.0	NMBR	0.9	TAAR2	0.3
CHRM1	1.2	HCA2	1.0	HRH4	0.9		
NPYSR	1.2	SSTR3	1.0	FSHR	0.9		

Table A.8: Results of the PDSP GPCR functional screen for candidate compound 6. Each receptor listed while the average percent of activation is list.

PDSP GPCR Results for Compound 7

DNA	% Activation	DNA	% Activation	DNA	% Activation	DNA	% Activation
HRH3	2.7	P2RY14	1.2	GPR173	1.0	NPFF2	0.9
GPR135	2.1	GPR82	1.2	LTB4R	1.0	CYSLTR1	0.9
MC4R	2.1	SUCNR1	1.2	LPAR2	1.0	BDKBR2	0.9
QRF1	1.9	ADORA2B	1.2	GAL2	1.0	GPRC5D	0.9
MARGPRX1	1.9	GPR146	1.2	MAS1L	1.0	MCHR1R	0.9
GPR151	1.8	GNRHR	1.2	ELTD1	1.0	CASR	0.9
BB3	1.8	GPR26	1.2	GPR132	1.0	CXCR7	0.9
FFA1	1.8	NTSR1	1.2	GPR4	1.0	GPR125	0.9
NMUR1	1.7	CCR3	1.2	MCHR2R	1.0	P2RY4	0.9
S1PR2	1.7	GPR148	1.2	HCA1	1.0	P2RY12	0.9
HTR6	1.7	LPAR6	1.2	FFA3	1.0	GPR158	0.9
MARGPRX3	1.6	CXCR2	1.2	HTR2C VSV	1.0	PTH2R	0.9
P2RY6	1.6	HTR1E	1.2	OXER1	1.0	NPY2R	0.9
GPR88	1.6	CXCR1	1.2	OXTR	1.0	GPER	0.9
ADRA2A	1.6	ADRA1D	1.2	CNR1	1.0	CCR6	0.9
GPR6	1.6	P2RY10	1.2	GPR120	1.0	CCR10	0.9
TAAR5	1.6	AVPR2	1.2	GPR162	1.0	DRD2	0.9
CXCR4	1.6	MARGPRX2	1.2	CXCR6	1.0	NPY1R	0.9
HTR4	1.6	APJ	1.2	GPR27	1.0	GPR31	0.9
GPRC5B	1.6	GPR56	1.2	GRM7	1.0	AVPR1B	0.9
GPR156	1.5	GPR18	1.2	GPR115	1.0	CRHR1	0.8
MC1R	1.5	AVPR1A	1.2	PTGER4	1.0	GPR142	0.8
MARGPRD	1.5	GPR149	1.2	ADRA1B	1.0	RXFP2	0.8
GPR52	1.5	NPFF1	1.2	PTGER2	1.0	SSTR2	0.8
GPR141	1.5	GPR17	1.2	GPR1	1.0	KISSPEPTIN	0.8
GPR61	1.5	AGTR1	1.2	CHRM5	1.0	TAAR8	0.8
FPR3	1.5	GRM8	1.1	GPR19	1.0	GPRC5A	0.8
SCTR	1.5	RXFP1	1.1	GPRC6A	1.0	F2RL3	0.8
PTGER1	1.4	MCSR	1.1	P2RY13	1.0	HTR2C INI	0.8
OPRD1	1.4	P2RY2	1.1	C3AR1	1.0	HTR2A	0.8
CKBR	1.4	PTGER3	1.1	CCR4	1.0	GIPR	0.8
LPAR1	1.4	HTR1B	1.1	BDKBR1	1.0	GPR143	0.8
GAL1	1.4	GPR171	1.1	HTR7	1.0	HTR2C VNV	0.8
HTR5	1.4	PK2	1.1	FPR1	1.0	CCR5	0.8
GPR85	1.4	CCR7	1.1	GPR97	1.0	GPR21	0.8
ADR83	1.4	GPR87	1.1	NPBW1	1.0	GPR111	0.8
GPR150	1.4	TACR1	1.1	GPR63	1.0	GPR124	0.8
RXFP3	1.4	MAS1	1.1	ADRA2C	1.0	PTAFR	0.8
OPN3	1.4	ADRA2B	1.1	GPR68	1.0	GRM1	0.8
DRD4	1.4	GMR2	1.1	GPR153	1.0	GLP1R	0.8
CYSLTR2	1.4	CHRM2	1.1	MARGPRG	1.0	GPR25	0.8
GPR182	1.4	P2RY1	1.1	EDNRA	1.0	GPR133	0.8
HRH1	1.4	PK1	1.1	PTH1R	1.0	GCGR	0.8
FFA2	1.4	HRH2	1.1	CHRM4	1.0	GPR37L1	0.8
GPR116	1.4	LTB4R2B	1.1	LPA4	1.0	CNR2	0.8
MARGPRE	1.4	GAL3	1.1	CCKAR	1.0	RXFP4	0.8
NPBW2	1.4	GPR160	1.1	GPR152	1.0	PTGFR	0.8
HTR1D	1.3	ADRA1A	1.1	GPR176	1.0	GPR126	0.8
MARGPRX4	1.3	CCR8	1.1	NPS	1.0	GPR37	0.7
GPR34	1.3	CCR2	1.1	F2R-L1	1.0	FPR2	0.7
MTNR1A	1.3	TACR3	1.1	GPR161	1.0	CRHR2	0.7
GPR183	1.3	GPR110	1.1	GPR45	1.0	P2RY11	0.7
MTNR1B	1.3	GPR35	1.1	HTR1A	1.0	GRM5	0.7
ADORA1	1.3	S1PR5	1.1	TAAR6	1.0	DRD5	0.7
GPBA	1.3	GPR119	1.1	CMKLR1	1.0	S1PR3	0.7
GPR3	1.3	GPR123	1.1	TAAR9	1.0	EDNRB	0.7
GPR84	1.3	GABBR1	1.1	NMUR2	1.0	GPR62	0.7
S1PR1	1.3	HCTR1	1.1	SSTR5	1.0	HCA3	0.7
GPR55	1.3	MARGPRF	1.1	HTR2B	0.9	CXCR3	0.7
ADORA2A	1.3	GPR113	1.1	GPR65	0.9	TBXA2R	0.7
GPR174	1.3	OXGR1	1.1	PTGIR	0.9	MC2R	0.7
GHSR	1.3	MLNR	1.1	ADRB2	0.9	TSHR	0.7
CXCR5	1.3	GPR83	1.1	GLP2R	0.9	ADCYAP1R1	0.7
CCRL2	1.3	OPN5	1.1	MC3Rb	0.9	GPR12	0.6
PTGDR	1.3	GPR22	1.1	LPAR5	0.9	GPR144	0.6
VIPR1	1.3	GPR77	1.1	GRPR	0.9	GPR75	0.6
S1PR4	1.3	HTR2CVGV	1.1	P2RY8	0.9	GPRC5C	0.6
GPR44	1.3	DRD1	1.1	TA1	0.9	GRM4	0.6
HCTR2	1.3	OPRK1	1.1	PRRP	0.9	GPR50	0.6
GPR114	1.3	CALCRL	1.1	NTSR2	0.9	DRD3	0.6
GPR101	1.2	UTS2R	1.1	GPR15	0.9	CALCRb	0.6
OPRL1	1.2	GPR78	1.1	ADORA3	0.9	GHRHR	0.6
VIPR2	1.2	F2RL2	1.1	CSA	0.9	NPY4R	0.6
CD97	1.2	SSTR1	1.1	GPR39	0.9	GPR32	0.6
CHRM3	1.2	LHCGR	1.1	F2R	0.9	CX3CR1	0.5
ADRB1	1.2	OPRM1	1.1	GPR20	0.9	GPR157	0.4
SSTR4	1.2	HTR1F	1.1	GPR64	0.9	GRM6	0.4
AGTR2	1.2	TACR2	1.0	NMBR	0.9	TAAR2	0.3
CHRM1	1.2	HCA2	1.0	HRH4	0.9		
NPY5R	1.2	SSTR3	1.0	FSHR	0.9		

Table A.9: Results of the PDSP GPCR functional screen for candidate compound 7. Each receptor listed while the average percent of activation is list.

PDSP GPCR Results for Compound 8

DNA	% Activation	DNA	% Activation	DNA	% Activation	DNA	% Activation
CXCR7	47.0	CCKBR	1.1	FPR2	0.9	PRRP	0.8
BB3	2.5	NTSR1	1.1	PTGIR	0.9	ADRA1D	0.8
CXCR6	2.4	GPR87	1.1	GPR62	0.9	C3AR1	0.8
GAL1	2.1	PTH2R	1.1	GCGR	0.9	OXER1	0.8
GPR150	1.9	CNR2	1.1	UTS2R	0.9	NPS	0.8
HRH1	1.9	GPR114	1.1	HCTR1	0.9	GPR64	0.8
CXCR3	1.8	GPR4	1.1	GPR148	0.9	OPN3	0.8
OPRD1	1.8	VIPR1	1.1	GRM7	0.9	TAAR9	0.8
CX3CR1	1.7	PTAFR	1.1	GPR176	0.9	EDNRB	0.8
GPR61	1.7	NPY4R	1.1	CSA	0.9	HTR1F	0.8
MTNR1B	1.7	QRFP	1.1	GPR183	0.9	AVPR1A	0.8
P2RY6	1.6	GPR173	1.1	F2RL2	0.9	MRGPRG	0.8
SSTR4	1.6	CALCR1	1.1	OPN5	0.9	ADRA1B	0.8
S1PR4	1.6	TACR2	1.1	CRHR2	0.9	P2RY8	0.8
FPR3	1.6	CXCR5	1.1	CXCR4	0.9	HTR2C INI	0.8
CCR6	1.6	ADRA2A	1.1	GPR146	0.9	GPR75	0.8
ADORA1	1.6	ADORA2B	1.1	HTR7	0.9	GPBA	0.8
GPR6	1.5	GPR45	1.1	RXF3	0.9	HTR4	0.8
MCCR4	1.5	CCR2	1.1	P2RY12	0.9	CYSLTR1	0.8
MRGPRX1	1.5	TACR1	1.1	GPR21	0.9	TSHR	0.8
HTR1B	1.5	MRGPRX4	1.1	HCA1	0.9	F2R-L1	0.8
GAL2	1.5	SCTR	1.1	GPR120	0.9	FFA3	0.8
GPR52	1.5	MTNR1A	1.1	CCKAR	0.9	SUCNR1	0.8
FAA1	1.4	GNRHR	1.1	GPRCA	0.9	PK2	0.8
GPR111	1.4	P2RY2	1.1	GPR26	0.9	GPR39	0.8
GPR151	1.4	GPR18	1.1	AGTR1	0.9	NTSR2	0.8
CHRM4	1.4	GMR2	1.1	ADRB3	0.9	CCR4	0.7
CCR3	1.4	HTR1E	1.1	GPR132	0.9	CCR5	0.7
CYSLTR2	1.4	TACR3	1.1	GPR63	0.9	CCR8	0.7
GPR119	1.4	SSTR2	1.1	MC2R	0.9	GRM1	0.7
GPRC5C	1.4	HRH3	1.1	GPR125	0.9	GRM5	0.7
ELTD1	1.4	RXF2	1.1	F2R	0.9	CALCRb	0.7
KISSPEPTIN	1.4	RXFP4	1.0	OPRL1	0.9	NMUR2	0.7
GPR34	1.4	GPR156	1.0	OXTR	0.9	ADRA2B	0.7
MRGPRE	1.4	LTB4R	1.0	GPR35	0.9	GPR124	0.7
GPR44	1.4	HTR2C VNV	1.0	GPR115	0.9	GPR158	0.7
DRD2	1.3	GPR144	1.0	GHRHR	0.9	PTGER2	0.7
GPR84	1.3	HTR5	1.0	NMUR1	0.9	HCA3	0.7
GPRC5B	1.3	GPR78	1.0	GPR12	0.9	GRM4	0.7
RXF1	1.3	P2RY10	1.0	CHRM5	0.9	NPY1R	0.7
GPR110	1.3	NPBW1	1.0	LPA6	0.9	PTGER4	0.7
MCSR	1.3	LPA1	1.0	CHRM2	0.9	DRD1	0.7
GPR20	1.3	GPR17	1.0	HTR1A	0.9	GRPR	0.7
GPR50	1.3	GPR56	1.0	SSTR5	0.9	FSHR	0.7
GPR27	1.3	CXCR2	1.0	GPR174	0.9	LTB4R2B	0.7
ADCYAP1R1	1.3	HTR6	1.0	HTR2A	0.9	TBXA2R	0.7
MCHR1R	1.3	LHCGR	1.0	CNR1	0.9	MRGPRX3	0.7
CHRM3	1.3	GPR22	1.0	MRGPRD	0.9	CCR7	0.7
HRH4	1.3	ADRA1A	1.0	PTGDR	0.9	GPRC5D	0.7
MAS1	1.3	P2RY4	1.0	NPY2R	0.9	NPFF2	0.7
GPR1	1.3	GPR182	1.0	DRD5	0.9	DRD4	0.7
SSTR3	1.3	PTGFR	1.0	LPA5	0.9	TAAR5	0.7
AVPR2	1.2	GPR82	1.0	GPR19	0.9	LPA2	0.7
GPR88	1.2	MCHR2R	1.0	ADORA2A	0.9	GPR97	0.7
MAS1L	1.2	GPR101	1.0	P2RY13	0.9	CRHR1	0.7
OPRM1	1.2	HCA2	1.0	GIPR	0.9	GLP1R	0.7
GHSR	1.2	CD97	1.0	GPR68	0.8	F2RL3	0.7
HRH2	1.2	S1PR1	1.0	GRM8	0.8	GPR113	0.6
CHRM1	1.2	PTGER1	1.0	ADORA3	0.8	ADRB2	0.6
GPR116	1.2	MLNR	1.0	GPR149	0.8	GPR126	0.6
GPR32	1.2	TAAR6	1.0	S1PR5	0.8	DRD3	0.6
GPR77	1.2	PTGER3	1.0	CMKLR1	0.8	GAL3	0.6
FAA2	1.2	HTR2C VSV	1.0	CCR10	0.8	GLP2R	0.6
AGTR2	1.2	GPR123	1.0	NPFF1	0.8	PTH1R	0.6
P2RY1	1.2	GPR31	1.0	FPR1	0.8	AVPR1B	0.6
GPR85	1.2	GPR160	1.0	MC3Rb	0.8	VIPR2	0.6
NPBW2	1.2	HTR2B	1.0	GPR133	0.8	GPR142	0.6
ADRA2C	1.2	EDNRA	1.0	GABBR1	0.8	TAAR8	0.6
GPR25	1.2	P2RY14	1.0	GPR153	0.8	S1PR3	0.6
GPER	1.2	LPA4	1.0	GPR162	0.8	GPR143	0.6
ADRB1	1.2	GPR171	1.0	OPRK1	0.8	GPR37L1	0.5
GPR141	1.2	HTR1D	1.0	S1PR2	0.8	NMBR	0.5
SSTR1	1.2	CCRL2	1.0	PK1	0.8	GPR37	0.5
GPR55	1.2	MRGPRF	1.0	GPRCA	0.8	HTR2CVGV	0.5
GPR3	1.2	GPR83	1.0	BDKBR2	0.8	GPR157	0.5
OXGR1	1.2	TA1	1.0	GPR152	0.8	GRM6	0.5
APJ	1.2	GPR65	1.0	BDKBR1	0.8	GPR15	0.5
HCTR2	1.1	GPR135	0.9	MC1R	0.8	TAAR2	0.4
P2RY11	1.1	GPR161	0.9	CASR	0.8		
NPYSR	1.1	MRGPRX2	0.9	CXCR1	0.8		

Table A.10: Results of the PDSP GPCR functional screen for candidate compound 8. Each receptor listed while the average percent of activation is list.

PDSP GPCR Results for Compound 9

DNA	% Activation	DNA	% Activation	DNA	% Activation	DNA	% Activation
HRH3	2.7	P2RY14	1.2	GPR173	1.0	NPFF2	0.9
GPR135	2.1	GPR82	1.2	LTBR4	1.0	CYSLTR1	0.9
MCAR	2.1	SUCNR1	1.2	LPAR2	1.0	BDKBR2	0.9
QRFP	1.9	ADORA2B	1.2	GAL2	1.0	GPRC5D	0.9
MRGPRX1	1.9	GPR146	1.2	MAS1L	1.0	MCHR1R	0.9
GPR151	1.8	GNRHR	1.2	ELTD1	1.0	CASR	0.9
BB3	1.8	GPR26	1.2	GPR132	1.0	CXCR7	0.9
FFA1	1.8	NTSR1	1.2	GPR4	1.0	GPR125	0.9
NMUR1	1.7	CCR3	1.2	MCHR2R	1.0	P2RY4	0.9
S1PR2	1.7	GPR148	1.2	HCA1	1.0	P2RY12	0.9
HTR6	1.7	LPAR6	1.2	FFA3	1.0	GPR158	0.9
MRGPRX3	1.6	CXCR2	1.2	HTR2C VSV	1.0	PTH2R	0.9
P2RY6	1.6	HTR1E	1.2	OXER1	1.0	NPY2R	0.9
GPR88	1.6	CXCR1	1.2	OXTR	1.0	GPFR	0.9
ADRA2A	1.6	ADRA1D	1.2	CNR1	1.0	CCR6	0.9
GPR6	1.6	P2RY10	1.2	GPR120	1.0	CCR10	0.9
TAAR5	1.6	AVPR2	1.2	GPR162	1.0	DRD2	0.9
CXCR4	1.6	MRGPRX2	1.2	CXCR6	1.0	NPY1R	0.9
HTR4	1.6	APJ	1.2	GPR27	1.0	GPR31	0.9
GPRC5B	1.6	GPR56	1.2	GRM7	1.0	AVPR1B	0.9
GPR156	1.5	GPR18	1.2	GPR115	1.0	CRHR1	0.8
MCLR	1.5	AVPR1A	1.2	PTGER4	1.0	GPR142	0.8
MRGPRD	1.5	GPR149	1.2	ADRA1B	1.0	RXFP2	0.8
GPR52	1.5	NPFF1	1.2	PTGER2	1.0	SSTR2	0.8
GPR141	1.5	GPR17	1.2	GPR1	1.0	KISSPEPTIN	0.8
GPR61	1.5	AGTR1	1.2	CHRM5	1.0	TAAR8	0.8
FPR3	1.5	GRM8	1.1	GPR19	1.0	GPRC5A	0.8
SCTR	1.5	RXFP1	1.1	GPRC6A	1.0	F2RL3	0.8
PTGER1	1.4	MCSR	1.1	P2RY13	1.0	HTR2C INI	0.8
OPRD1	1.4	P2RY2	1.1	C3AR1	1.0	HTR2A	0.8
CCKBR	1.4	PTGER3	1.1	CCR4	1.0	GIPR	0.8
LPAR1	1.4	HTR1B	1.1	BDKBR1	1.0	GPR143	0.8
GAL1	1.4	GPR171	1.1	HTR7	1.0	HTR2C VNV	0.8
HTR5	1.4	PK2	1.1	FPR1	1.0	CCR5	0.8
GPR85	1.4	CCR7	1.1	GPR97	1.0	GPR21	0.8
ADR83	1.4	GPR87	1.1	NPBW1	1.0	GPR111	0.8
GPR150	1.4	TACR1	1.1	GPR63	1.0	GPR124	0.8
RXFP3	1.4	MAS1	1.1	ADRA2C	1.0	PTAFR	0.8
OPN3	1.4	ADRA2B	1.1	GPR68	1.0	GRM1	0.8
DRD4	1.4	GMR2	1.1	GPR153	1.0	GLP1R	0.8
CYSLTR2	1.4	CHRM2	1.1	MRGPRG	1.0	GPR25	0.8
GPR182	1.4	P2RY1	1.1	EDNRA	1.0	GPR133	0.8
HRH1	1.4	PK1	1.1	PTH1R	1.0	GCCR	0.8
FFA2	1.4	HRH2	1.1	CHRM4	1.0	GPR37L1	0.8
GPR116	1.4	LTBR4R2B	1.1	LPA4	1.0	CNR2	0.8
MRGPRE	1.4	GAL3	1.1	CCKAR	1.0	RXFP4	0.8
NPBW2	1.4	GPR160	1.1	GPR152	1.0	PTGFR	0.8
HTR1D	1.3	ADRA1A	1.1	GPR176	1.0	GPR126	0.8
MRGPRX4	1.3	CCR8	1.1	NPS	1.0	GPR37	0.7
GPR34	1.3	CCR2	1.1	F2R-L1	1.0	FPR2	0.7
MTNR1A	1.3	TACR3	1.1	GPR161	1.0	CRHR2	0.7
GPR183	1.3	GPR110	1.1	GPR45	1.0	P2RY11	0.7
MTNR1B	1.3	GPR35	1.1	HTR1A	1.0	GRM5	0.7
ADORA1	1.3	S1PR5	1.1	TAAR6	1.0	DRD5	0.7
GPBA	1.3	GPR119	1.1	CMKLR1	1.0	S1PR3	0.7
GPR3	1.3	GPR123	1.1	TAAR9	1.0	EDNRB	0.7
GPR84	1.3	GABBR1	1.1	NMUR2	1.0	GPR62	0.7
S1PR1	1.3	HCTR1	1.1	SSTR5	1.0	HCA3	0.7
GPR55	1.3	MRGPRF	1.1	HTR2B	0.9	CXCR3	0.7
ADORA2A	1.3	GPR113	1.1	GPR65	0.9	TBXA2R	0.7
GPR174	1.3	OXGR1	1.1	PTGIR	0.9	MC2R	0.7
GHSR	1.3	MLNR	1.1	ADR2	0.9	TSHR	0.7
CXCR5	1.3	GPR83	1.1	GLP2R	0.9	ADCYAP1R1	0.7
CCRL2	1.3	OPN5	1.1	MC3Rb	0.9	GPR12	0.6
PTGDR	1.3	GPR22	1.1	LPAR5	0.9	GPR144	0.6
VIPR1	1.3	GPR77	1.1	GRPR	0.9	GPR75	0.6
S1PR4	1.3	HTR2CVGV	1.1	P2RY8	0.9	GPRC5C	0.6
GPR44	1.3	DRD1	1.1	TA1	0.9	GRM4	0.6
HCTR2	1.3	OPRK1	1.1	PRRP	0.9	GPR50	0.6
GPR114	1.3	CALCR1	1.1	NTSR2	0.9	DRD3	0.6
GPR101	1.2	UTS2R	1.1	GPR15	0.9	CALCRb	0.6
OPRL1	1.2	GPR78	1.1	ADORA3	0.9	GHRHR	0.6
VIPR2	1.2	F2RL2	1.1	CSA	0.9	NPY4R	0.6
CD97	1.2	SSTR1	1.1	GPR39	0.9	GPR32	0.6
CHRM3	1.2	LHCGR	1.1	F2R	0.9	CX3CR1	0.5
ADRB1	1.2	OPRM1	1.1	GPR20	0.9	GPR157	0.4
SSTR4	1.2	HTR1F	1.1	GPR64	0.9	GRM6	0.4
AGTR2	1.2	TACR2	1.0	NMBR	0.9	TAAR2	0.3
CHRM1	1.2	HCA2	1.0	HRH4	0.9		
NPYSR	1.2	SSTR3	1.0	FSHR	0.9		

Table A.11: Results of the PDSP GPCR functional screen for candidate compound 9. Each receptor listed while the average percent of activation is list.

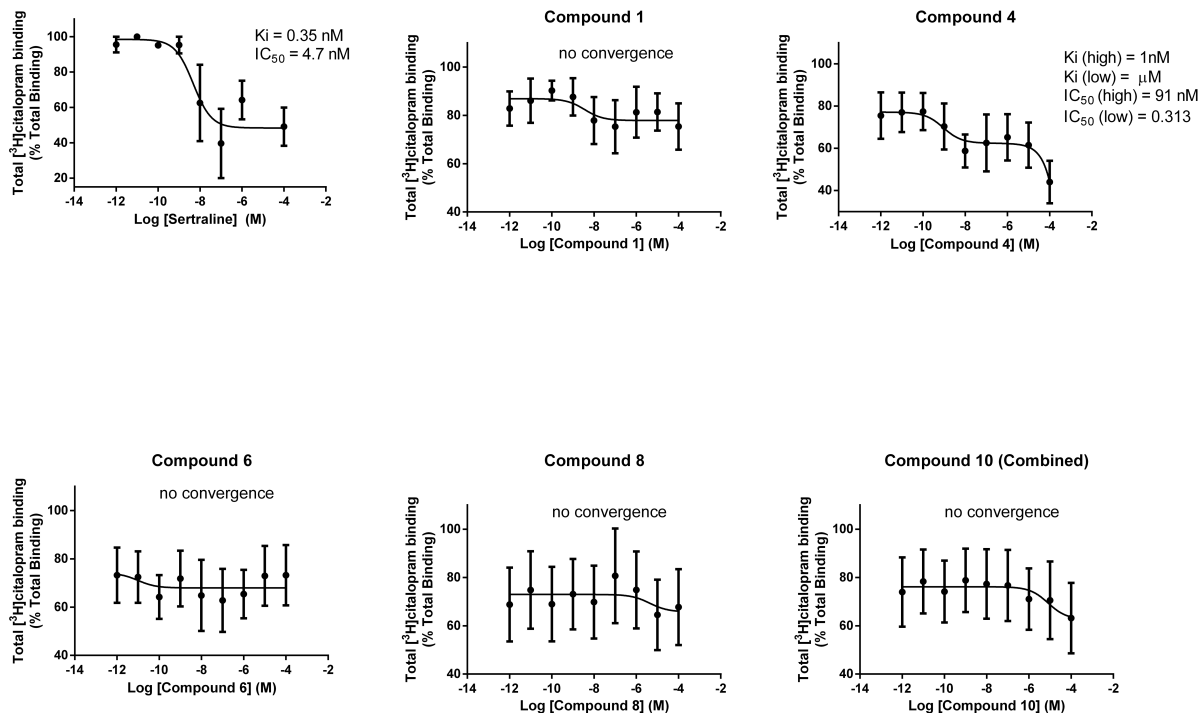


Figure A.1: Competition of Sertraline for [³H]-Citalopram Binding to SERT. The affinity of sertraline, compound 1, compound 4, compound 6, compound 8, and compound 10 (1pM-100mM) for SERT was assessed by competition binding using the radioligand [³H]-citalopram. A composite binding curve was constructed from individual curves. Composite affinity (IC₅₀, K_i) values were derived by GraphPad Prism non-linear regression analyses least squares fit. Each data point represents the mean +/- (SD) of two to four independent experiments performed in duplicate.